

# Deep Learning in CT Image Formation

Marc Kachelrieß

[marc.kachelriess@dkfz.de](mailto:marc.kachelriess@dkfz.de)

German Cancer Research Center (DKFZ)

Heidelberg, Germany

[www.dkfz.de/ct](http://www.dkfz.de/ct)

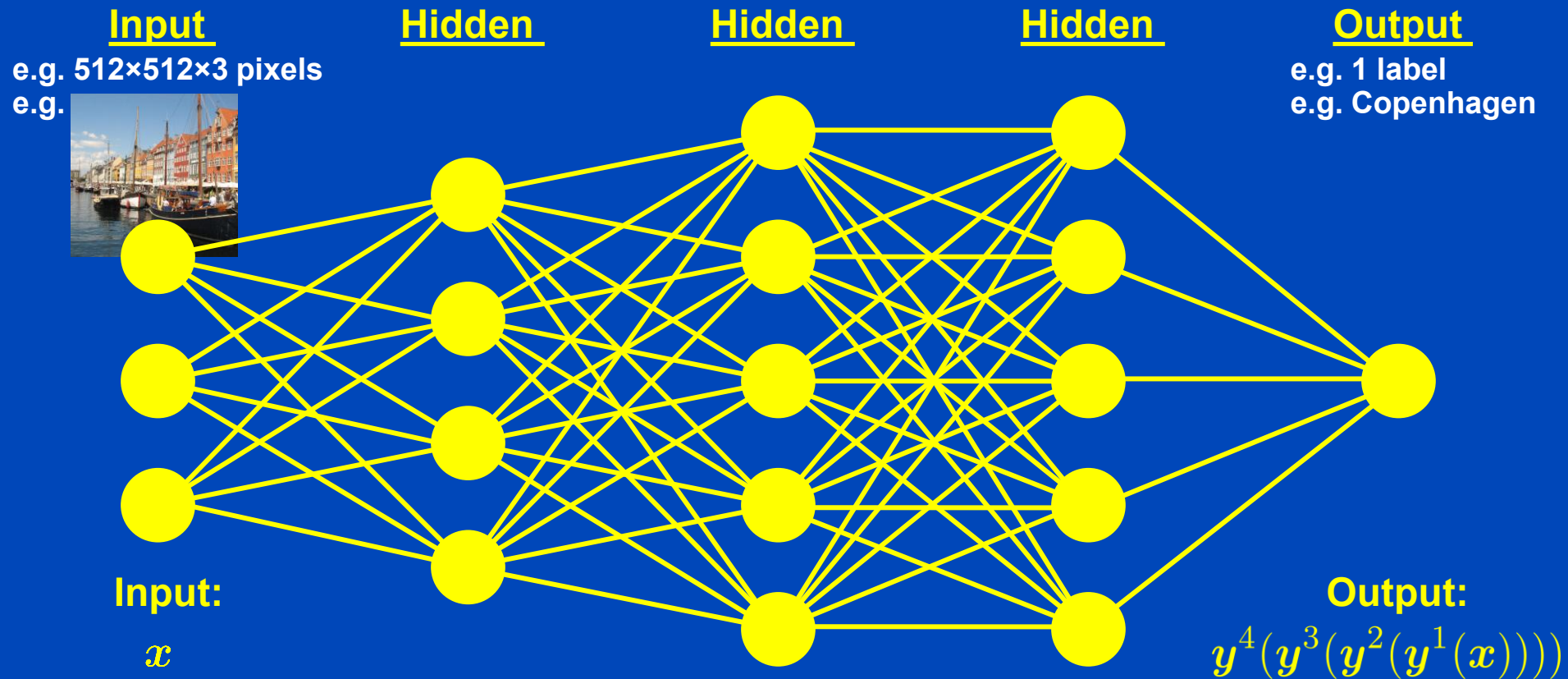


DEUTSCHES  
KREBSFORSCHUNGSZENTRUM  
IN DER HELMHOLTZ-GEMEINSCHAFT

# REALLY SHORT BASICS

# Fully-Connected Neural Network

- Each layer fully connects to previous layer
- Difficult to train (many parameters in  $W$  and  $b$ )
- Spatial relations not necessarily preserved



$y(x) = f(W \cdot x + b)$  with  $f(x) = (f(x_1), f(x_2), \dots)$  point-wise scalar, e.g.  $f(x) = x \vee 0 = \text{ReLU}$

# Universal Approximation Theorem<sup>1</sup>

- A fully-connected network with at least three layers is also called a multi layer perceptron (MLP).

*If  $\sigma$  is continuous, bounded and nonconstant, then  $\mathfrak{R}_M(\sigma)$  is dense in the subset  $\mathcal{C}$  of continuous and compact functions of  $\mathbb{R}^M$ .*

$$\begin{aligned}\mathfrak{R}_M(\sigma) &= \bigcup_N \mathfrak{R}_M^{(N)}(\sigma) \\ &= \bigcup_N \left\{ g : \mathbb{R}^M \rightarrow \mathbb{R} \mid \overbrace{g(x) = \sum_{j=0}^N w_{k,j}^{(3)} \sigma \left( \sum_{i=0}^M w_{j,i}^{(2)} x_i \right)}^{3\text{-layer MLP with final activation linear and } N \text{ hidden neurons}} \right\}\end{aligned}$$

- For any function  $h(x) \in \mathcal{C} \in \mathbb{R}^M$  we can find a function  $g(x) \in \mathfrak{R}_M(\sigma)$  for which  $\|h(x) - g(x)\|_p < \epsilon$ .
- Any 3-layer MLP with appropriately chosen layer sizes and activation function, e.g. the sigmoid function, is a universal function approximator.
- **This theorem does not provide any insight into how to find the unknowns!**

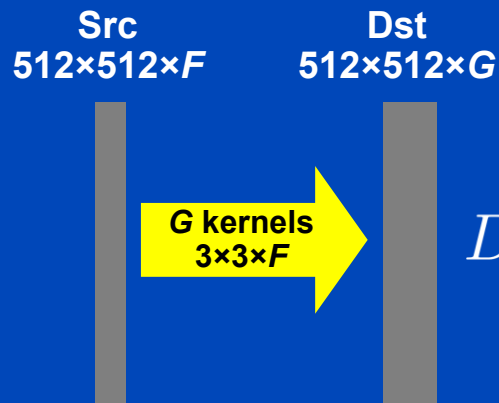
<sup>1</sup>Hornik, Kurt; Stinchcombe, Maxwell; White, Halbert (1989). Multilayer Feedforward Networks are Universal Approximators. Neural Networks. Vol. 2. Pergamon Press. pp. 359–366; Theorem 2

# Convolutional Neural Network (CNN)

- Replace dense  $W$  in  $y(x) = f(W \cdot x + b)$  by a sparse matrix  $W$  with sparsity being of convolutional type (band diagonal of Toeplitz type).
- CNNs consist (mainly) of convolutional layers.
- Convolutional layers are not fully connected.
- Convolutional layers are small, say  $3 \times 3$ , convolution kernels whose entries need to be found by training.
- CNNs preserve spatial relations to some extent.

$$W_{1D} = \begin{pmatrix} 1 & 8 & 0 & 0 & 0 & 0 \\ 2 & 1 & 8 & 0 & 0 & 0 \\ 0 & 2 & 1 & 8 & 0 & 0 \\ 0 & 0 & 2 & 1 & 8 & 0 \\ 0 & 0 & 0 & 2 & 1 & 8 \\ 0 & 0 & 0 & 0 & 2 & 1 \end{pmatrix}$$

*Only three unknowns!*



$$D_{i,j,g} = \sum_f S_{i,j,f} * K_{i,j,f}^g = \sum_{a,b,f} S_{i-a,j-b,f} K_{a,b,f}^g$$

=  $3 \times 3 \times F \times I \times J \times G$  madd operations

**Attention: No convolution in depth direction!**

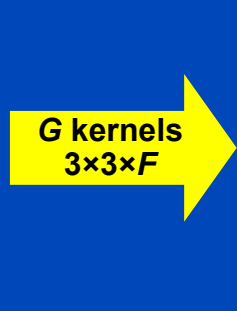
Here, a 2D example is shown. Conv layers also exist in 3D and higher dimensions.

# Convolution Layers

- Input layer  $S$ 
  - vector of size  $I$  with  $F$  features:  $I \times F$
  - image of size  $I$  by  $J$  with  $F$  features:  $I \times J \times F$
  - volume of size  $I$  by  $J$  by  $K$  with  $F$  features:  $I \times J \times K \times F$
  - ...
- Convolution kernel  $K$ 
  - $G$  kernels of size  $(2A+1) \times (2B+1) \times F$  with or without padding\*
- Output layer  $D$ 
  - same spatial dimensions as input layer\*
  - $G$  features (depth  $G$ )

Src  
 $512 \times 512 \times F$

Dst  
 $512 \times 512 \times G$



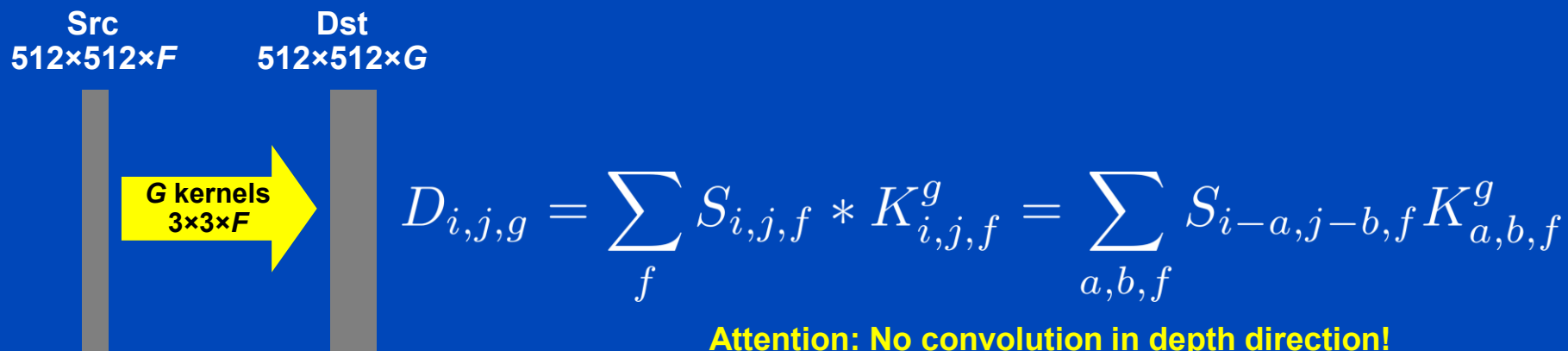
$$D_{i,j,g} = \sum_f S_{i,j,f} * K_{i,j,f}^g = \sum_{a,b,f} S_{i-a,j-b,f} K_{a,b,f}^g$$

**Attention: No convolution in depth direction!**

\*Convolution may include a stride (step size)  $> 1$ . Similar to convolution with stride 1 followed by pooling.

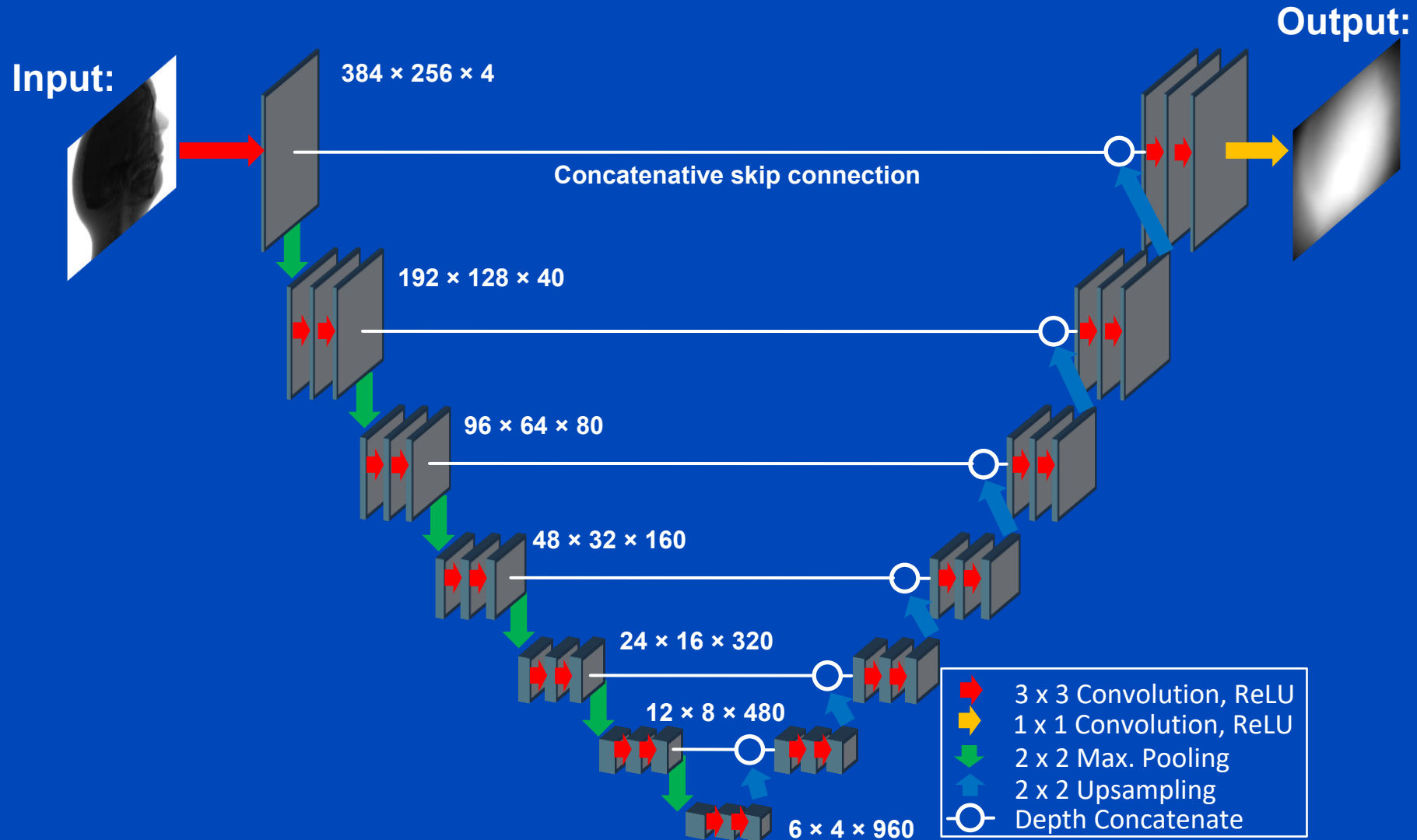
# Convolution Layers

- Convolution in spatial domain (1D, 2D, 3D, ...)
- Full connectivity in depth
- Filter size, number of filters, receptive field
- Learns filter kernels
- Far less parameters than fully connected layers
- Respects properties of many imaging systems



**Attention: No convolution in depth direction!**

# U-Net<sup>1</sup>



<sup>1</sup>O. Ronneberger, P. Fischer, and T. Brox. U-net: Convolutional networks for biomedical image segmentation. Proc. MICCAI:234-241, 2015.

# Loss Function

- The neural network coefficients (weights and biases)  $\mathbf{c}$  are chosen by minimizing a loss function (cost function)

$$\mathbf{c} = \arg \min_{\mathbf{c}} \sum_{n=1}^N L(\mathbf{c}, \mathbf{x}_n, \mathbf{y}_n)$$

with  $\mathbf{x}_n$  being the training data input,  $\mathbf{y}(\mathbf{c}, \mathbf{x}_n)$  being the network output, and  $\mathbf{y}_n$  being the so-called labels, i.e. the training target, and  $N$  being the number of training samples.

- An example for such a loss function is the MSE loss

$$L(\mathbf{c}, \mathbf{x}_n, \mathbf{y}_n) = \left( \mathbf{y}(\mathbf{c}, \mathbf{x}_n) - \mathbf{y}_n \right)^2$$

# Toy Example

Nested scalar functions  $f(c, x)$  with unknown coefficients  $c$

Loss  
Function

$$L(c_3, c_2, c_1, x) = (f_3(c_3, f_2(c_2, f_1(c_1, x))) - y)^2$$

last layer output  
2<sup>nd</sup> layer output  
1<sup>st</sup> layer output  
input  
training target

Intermediate  
Values

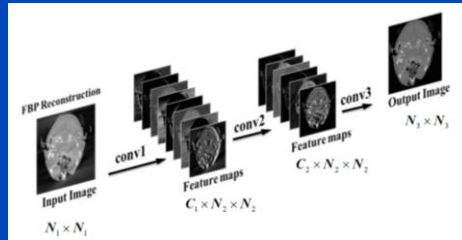
$$\begin{aligned} L_3 &= \frac{dL}{df_3} = 2(f_3 - y) \\ L_2 &= \frac{dL}{df_2} = \frac{dL}{df_3} \frac{df_3}{df_2} = L_3 \frac{df_3}{df_2} \\ &\dots \\ L_n &= \frac{dL}{df_n} = L_{n+1} \frac{df_{n+1}}{df_n} \end{aligned}$$

Desired  
Gradients

$$\begin{aligned} \frac{dL}{dc_3} &= \frac{dL}{df_3} \frac{df_3}{dc_3} = L_3 \frac{df_3}{dc_3} \\ \frac{dL}{dc_2} &= \frac{dL}{df_3} \frac{df_3}{df_2} \frac{df_2}{dc_2} = L_2 \frac{df_2}{dc_2} \\ &\dots \\ \frac{dL}{dc_n} &= L_n \frac{df_n}{dc_n} \end{aligned}$$

# MAKING UP DATA

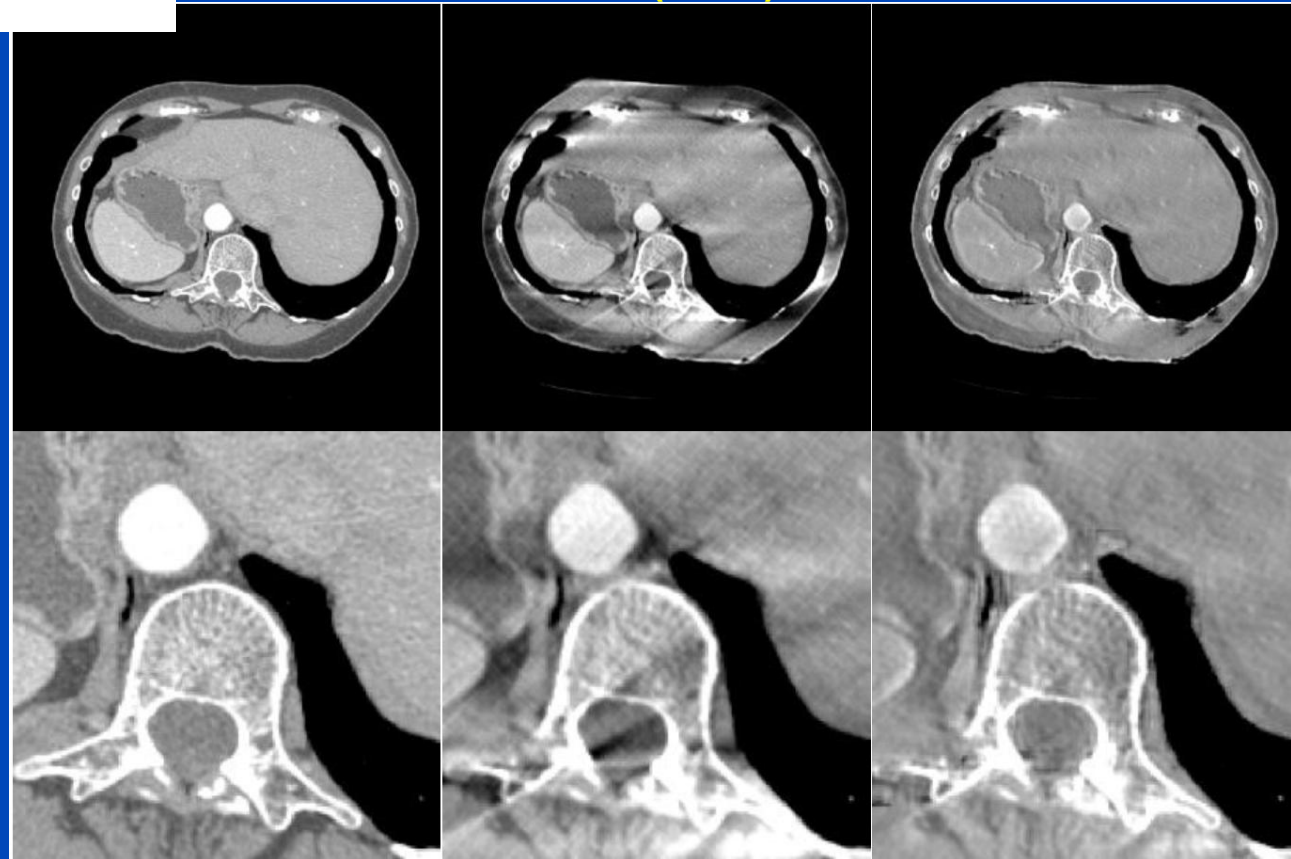
# Limited Angle Example



**GT**

**FBP (150°)**

**CNN**



# Deep MAR Examples

### Reducing Metal Streak Artifacts in CT Images via Deep Learning: Pilot Results

Lei Guo, Qingyuan Tang, Yan-Yu, Binbin Chen, Tianxin Gu, Binbin Guo, Guo-Wei

- Takes 32x32 input patch from NMAR image and produces 20x20 output patch
- Very basic CNN

### Gjesteby, 2017

- Same network as in previous work
- Detail image is the high-pass filtered original image
- Detail image and NMAR image are both put as inputs in 2 streams that converge later in the CNN
- Network uses residual error and cost function is a combination of MSE and perceptual loss

### Deep Neural Network for CT Metal Artifact Reduction with a Perceptual Loss Function

Lei Guo, Qingyuan Tang, Yan-Yu, Binbin Chen, Tianxin Gu, Binbin Guo, Guo-Wei

### Gjesteby, 2018

- Inputs for the network are the NMAR image and the high-pass filtered original image
- Corrects streaks after NMAR
- Loss function is MSE or perceptual loss (from VGG network)
- MSE shows over-smoothing
- Trained on simulated data
- Each residual unit learns residual error

### Gjesteby, 2018

### A dual-stream deep convolutional network for reducing metal streak artifacts in CT images

Lei Guo, Qingyuan Tang, Yan-Yu, Binbin Chen, Tianxin Gu, Binbin Guo, Guo-Wei

### Gjesteby, 2019

### Gjesteby, 2019

### Gjesteby, 2019

### Metal artifact reduction for practical dental computed tomography by improving interpolation-based reconstruction with deep learning

Kunlun Liang, Li Zhang, and Qingyuan Tang

### Xing, 2019

- Perform initial LIMAR to obtain images with interpolation artifacts
- Apply U-Net to pre-corrected images to reduce artifacts
- Network minimizes L2-norm loss outside of the metal regions

### Xing, 2019

### Metal artifact reduction on cervical CT images by deep residual learning

Yu Huang<sup>1,2</sup>, Jian Wang<sup>1,2</sup>, Fan Tang<sup>1,2</sup>, Tai Zhong<sup>1,2</sup> and Yu Zhang<sup>1,2</sup>

### Zhang, 2018

### Zhang, 2018

- Metal is placed in real CT images. Artifacts are created by forward and back-projecting soft tissue, bone, and metal
- Network input is patch of artifact image  $I$  and output is the residual, i.e.  $R = I - G^T$
- Loss function is MSE of the residual
- Learning the residual is found to be better than learning the artifact-free image (no images)

### Convolutional Neural Network Based Metal Artifact Reduction in X-Ray Computed Tomography

Wei Zhang<sup>1</sup>, Senior Member, IEEE, and Hongping Yu<sup>1</sup>, Senior Member, IEEE

### Yu, 2018

### Yu, 2018

- Training data are generated from clinical data with metal artifacts added afterwards through polychromatic forward- & back-projection
- Cost function is MSE
- CNN gets patches from the artifact BHC corrected, and LI corrected image as input, produces corrected patches
- Prior image is generated from CNN result by segmenting water and setting it to the average value of all water pixels and leaving bone intact
- Metal trace in the uncorrected sinogram is replaced with values from the prior image
- Having different types of MAR as input improves results

### Metal-Artifact Reduction Using Deep-Learning Based Sinogram Completion: Initial Results

Reinhold E. H. Chen, Yuesha He, Luca A. Scudiero, Guo-Wei, Binbin Guo

### Claus, 2017

- Trained and evaluated on simulated data with metal circle in the center (no other positions tested)
- Data are heavily simplified (random ellipses)
- Inputs are 2 81x21 sized patches from the sinogram next to metal patch. Won't work for complex metals
- Relatively small network (4 layers)

### Deep Learning Based Metal inpainting in the Projection Domain: Initial Results

Thomas M. Gottschalk<sup>1,2,3,4</sup>, Björn W. Kubler<sup>1</sup>, Holger Köster<sup>1</sup>, and Andreas Högl<sup>1</sup>

### Gottschalk, 2019

- Corrects C-Arm projection data
- Data were obtained by placing metal on top of human knee cadavers
- Loss function is MSE
- Networks are based on U-Net with additional skip connection from original image to output
- Basic network can be used to implicitly segment the metal for the Mask-MAR-Net
- Providing a metal mask significantly improves results
- Results are blurred slightly

### Gottschalk, 2019

### Deep Learning based Metal Inpainting in the Projection Domain using additional Neighboring Projection Information

Thomas M. Gottschalk, Björn W. Kubler and Andreas Högl

### Gottschalk, 2020

- U-Net corrects CBCT projections
- Has metal mask and 10 neighbouring projections as additional input channels

### Gottschalk, 2020

### Fast Enhanced CT Metal Artifact Reduction using Data Domain Deep Learning

Mohammad Oussou Ghani, W. Chen, Karl, Felton, IEEE

### Ghani, 2019

- Metal trace is replaced via a CGAN
- Uses transfer learning from training data to real data; not described in depth
- Not applied to medical images

### Ghani, 2019

### Generative Mask Pyramid Network for CT/CBCT Metal Artifact Reduction with Joint Projection-Sinogram Correction

Benli Liu<sup>1,2</sup>, Wei-An Liu<sup>1</sup>, Zhiliang Han<sup>1</sup>, Leren Vongphimol<sup>1</sup>, William J. Siskin<sup>3</sup>, Si-Kwon Zhou<sup>3</sup>, and Jiebo Luo<sup>1</sup>

### Liao, 2019

### Liao, 2019

- First replaces metal trace in the projections (i.e. fixed angle but varying  $\xi$  and  $z$ )
- Then transforms the projections into sinograms and uses a second network to improve those
- Both networks are GANs with a U-Net generator and CNN discriminator
- Uses a Mask Pyramid to ensure the metal mask is seen by all stages of the U-Net
- Data are regular CT scans with metal traces from other patients imposed on them

### DuoNet: Dual Network for CT Metal Artifact Reduction

Wei-An Liu<sup>1</sup>, Benli Liu<sup>1</sup>, Cheng Peng<sup>1</sup>, Xiaohang Tang<sup>1</sup>, Jinglai Zhang<sup>1</sup>, Jiebo Luo<sup>1</sup>, Renee Chellappa<sup>2</sup>, Shaohua Kevin Zhou<sup>2</sup>

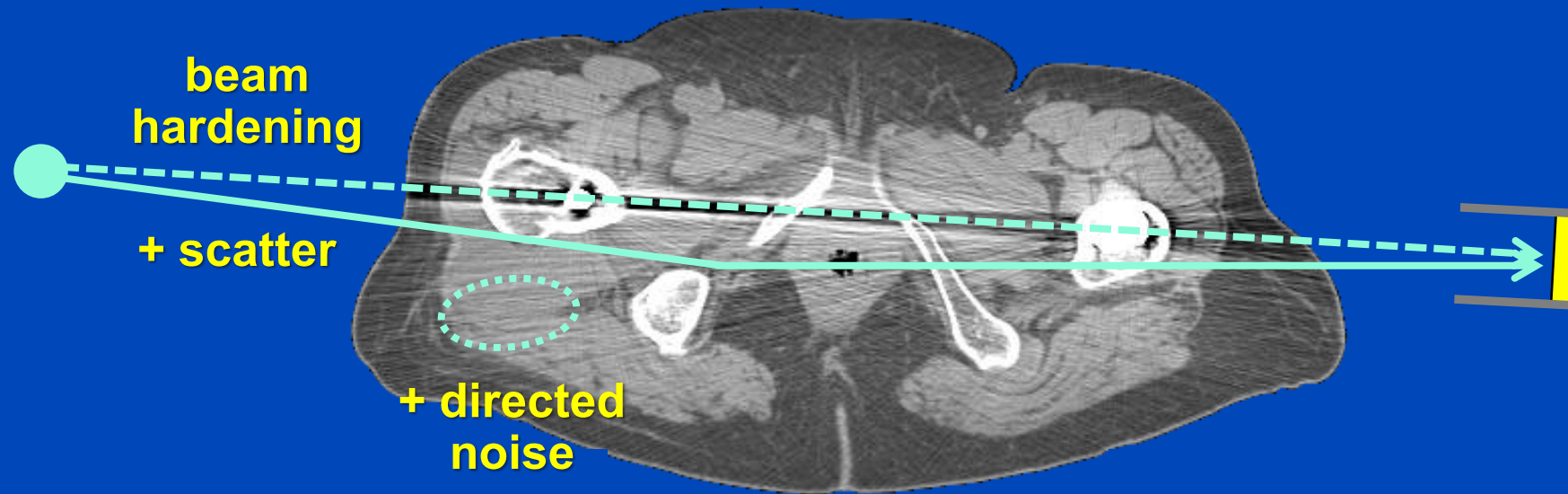
### Lin, 2019

### Lin, 2019

- Input are LI pre-corrected sinograms/images
- First improves the sinograms through a U-Net with mask pyramid (so all parts of the U-Net see the mask)
- Then applies FBP (Radon Inversion Layer) and uses the result as input for a second U-Net, which improves it in image domain
- Unclear how the LI and CNN results are combined



# Metal artifacts are



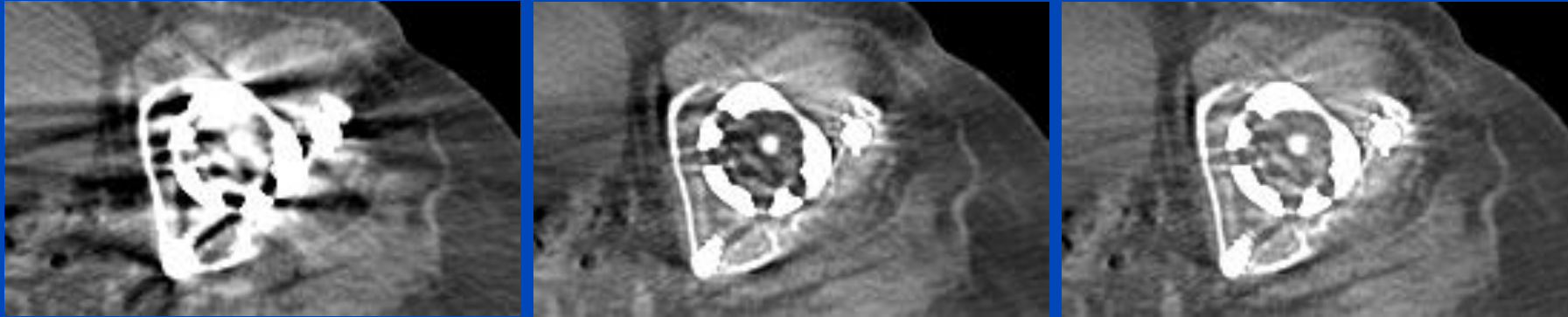
+ increased susceptibility to sampling artifacts and motion.

# MAR without Machine Learning is a Good Alternative: Frequency Split Normalized MAR<sup>1,2</sup>

Uncorrected

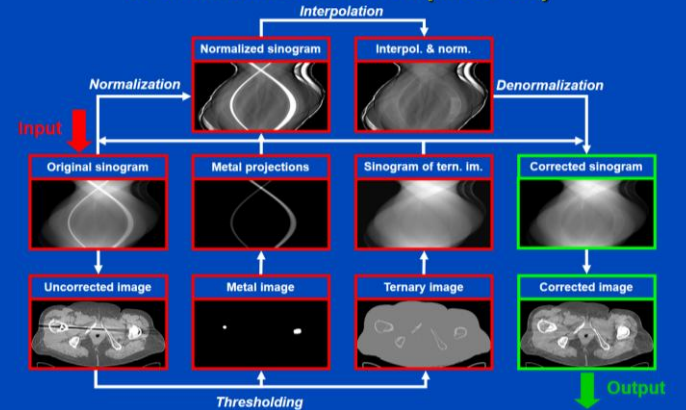
FSLIMAR

FSNMAR

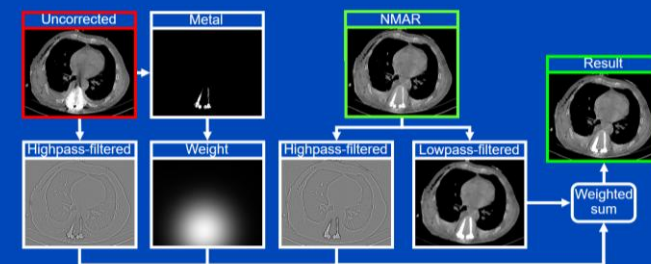


Patient with bilateral hip prosthesis, Somatom Definition Flash, (C=40/W=500).

## Normalized MAR (NMAR)

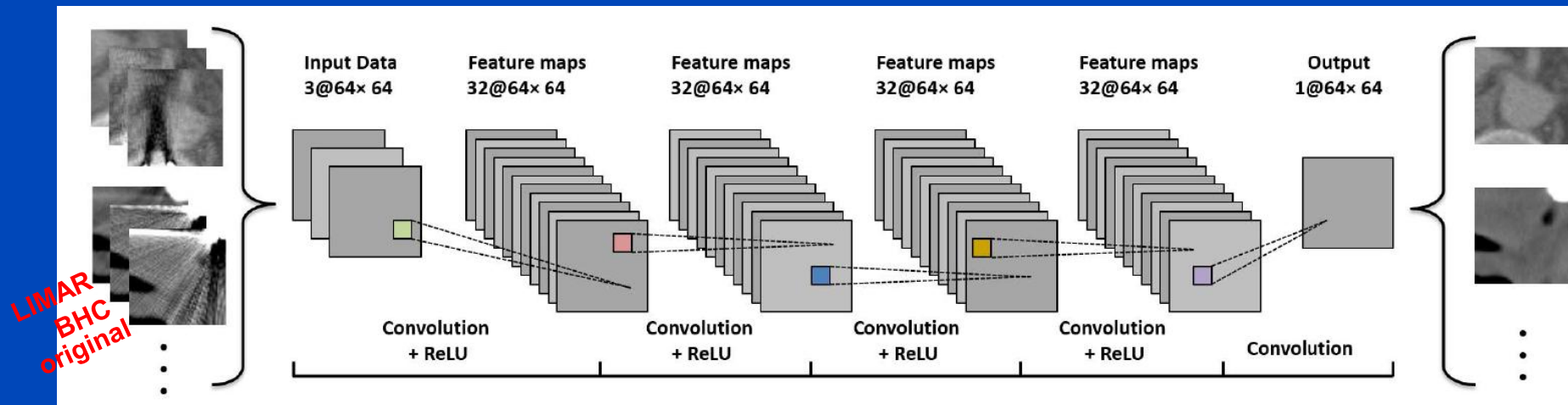


## FSMAR: Scheme

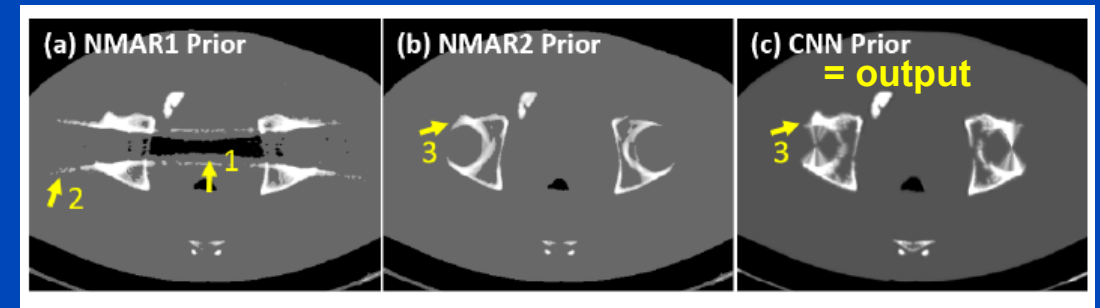
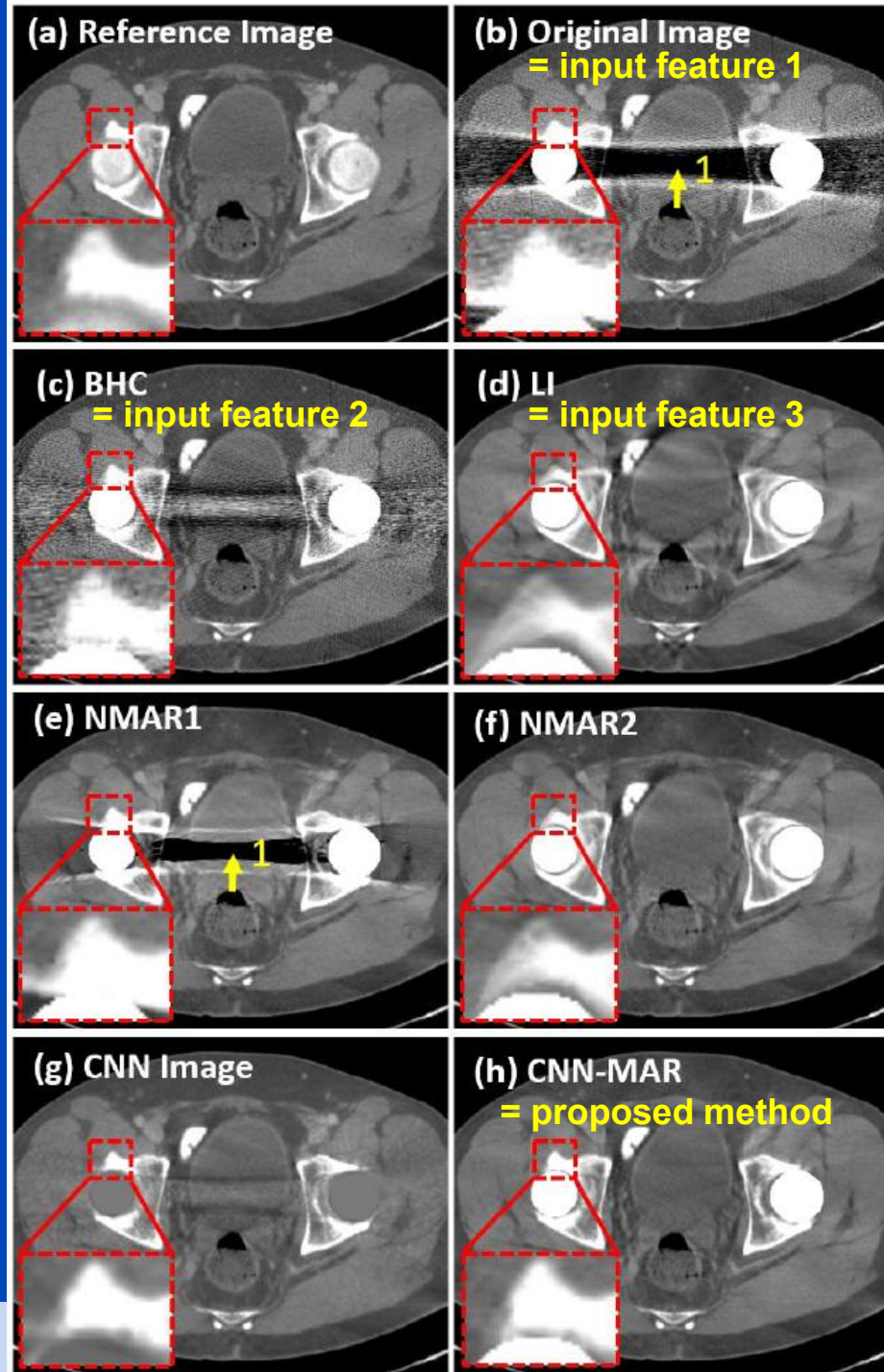


# MAR Example

- Deep CNN-driven patch-based combination of the advantages of several MAR methods trained on simulated artifacts

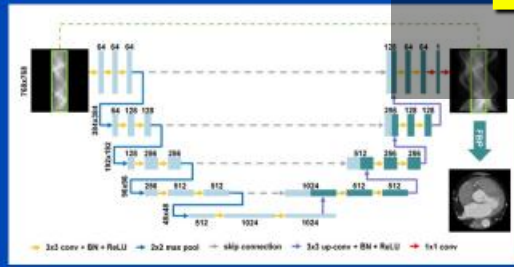


- followed by segmentation into tissue classes
- followed by forward projection of the CNN prior and replacement of metal areas of the original sinogram
- followed by reconstruction



## Deep learning -based sinogram extension method for interior computed tomography

Juuso H. J. Ketola<sup>1\*</sup>, Helmi Heino<sup>1\*</sup>, Mikael A. K. Juntunen<sup>1,2,3</sup>, Mikko T. Nieminen<sup>1,2,3,4</sup>, and Satu I. Jakonen<sup>1</sup>  
<sup>1</sup>Research Unit of Medical Imaging, Physics and Technology, University of Oulu, Oulu, Finland  
<sup>2</sup>The South Savo Health Care Authority, Mikkeli Central Hospital, Oulu, Finland  
<sup>3</sup>Department of Diagnostic Radiology, Oulu University Hospital, Oulu, Finland  
<sup>4</sup>Medical Research Center Oulu, Oulu University Hospital and University of Oulu, Oulu, Finland



Ketola, Juuso H., et al. "Deep learning-based sinogram extension method for interior computed tomography." *Medical Imaging 2021: Physics of Medical Imaging*, Vol. 11095. International Society for Optics and Photonics, 2021. **dkfz.**

# Deep Detruncation

## Results

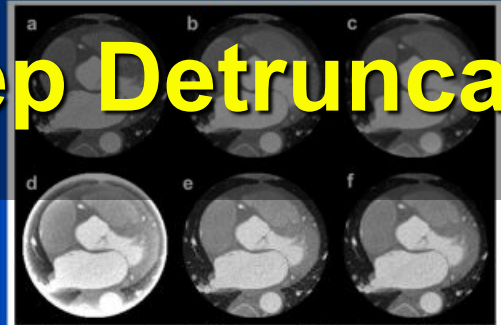
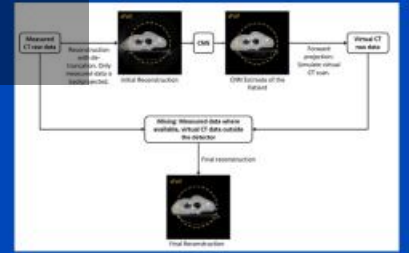


Figure 3. Example reconstructions. a. Original data from center. b. Adaptive detruncation followed by filtered backprojection. c. Total variation regularization. d. Filtered backprojection. e. FBP-CapNet. f. Our Method. Reconstructions have been masked to visualize the region-of-interest.

Ketola, Juuso H., et al. "Deep learning-based sinogram extension method for interior computed tomography." *Medical Imaging 2021: Physics of Medical Imaging*, Vol. 11095. International Society for Optics and Photonics, 2021. **dkfz.**

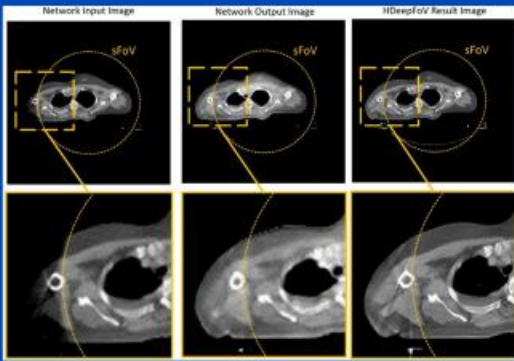
## Evaluation of novel AI-based extended field-of-view CT reconstructions

Gabriel Paiva Fonseca<sup>1,2</sup>  
<sup>1</sup>Department of Radiation Oncology (MAASTRO), GROW School for Oncology and Developmental Biology, Maastricht University Medical Center+, Maastricht 6200 ET, The Netherlands  
<sup>2</sup>Mathias Baer-Beck<sup>1</sup>, Eric Fournie and Christian Hofmann  
<sup>3</sup>Seneca Healthcare GmbH, Fürth/Main, Germany  
 Barla Rinaldi, Michel C. Ours, Wouter J.C. van Elmpt and Frank Verhaegen  
<sup>4</sup>Department of Radiation Oncology (MAASTRO), GROW School for Oncology and Developmental Biology, Maastricht University Medical Center+, Maastricht 6200 ET, The Netherlands  
 Received 28 February 2021; revised 27 April 2021; accepted for publication 30 April 2021; published 31 May 2021



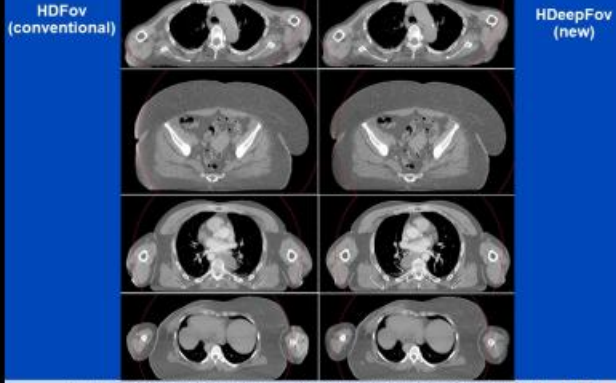
Fonseca, Gabriel Paiva, et al. "Evaluation of novel AI-based extended field-of-view CT reconstructions." *Medical Physics* (2021). **dkfz.**

## Results



Fonseca, Gabriel Paiva, et al. "Evaluation of novel AI-based extended field-of-view CT reconstructions." *Medical Physics* (2021). **dkfz.**

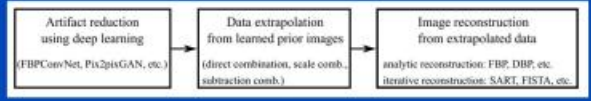
## Results



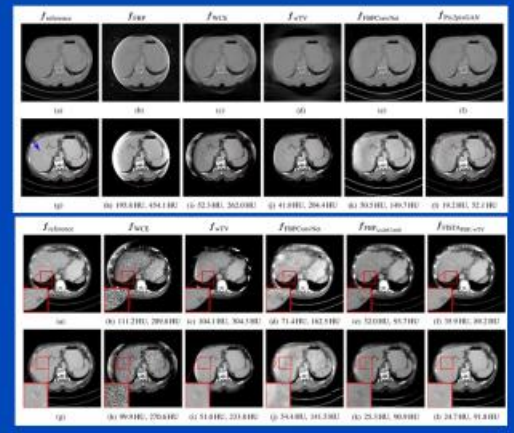
Fonseca, Gabriel Paiva, et al. "Evaluation of novel AI-based extended field-of-view CT reconstructions." *Medical Physics* (2021). **dkfz.**

## Data Extrapolation From Learned Prior Images for Truncation Correction in Computed Tomography

Yixing Huang<sup>1</sup>, Alexander Preuß<sup>2</sup>, Michael Manhart<sup>3</sup>, Guenter Lauritsch<sup>4</sup>, and Andreas Maier<sup>1</sup>, Senior Member, IEEE



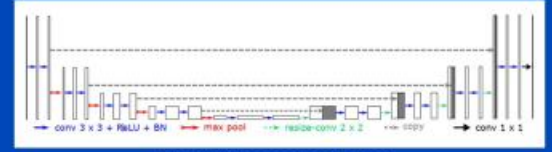
Huang, Yixing, et al. "Data Extrapolation From Learned Prior Images for Truncation Correction in Computed Tomography." *IEEE Transactions on Medical Imaging* (2021). **dkfz.**



Huang, Yixing, et al. "Data Extrapolation from Learned Prior Images for Truncation Correction in Computed Tomography." *IEEE Transactions on Medical Imaging* (2021). **dkfz.**

## Data Consistent CT Reconstruction from Insufficient Data with Learned Prior Images

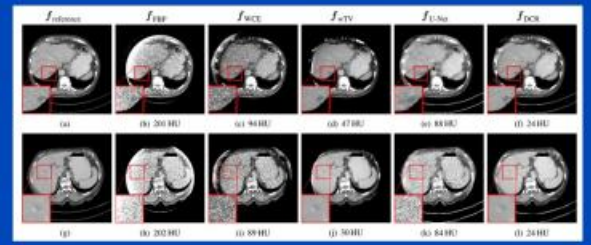
Yixing Huang, Alexander Preuß, Michael Manhart, Guenter Lauritsch, Andreas Maier



Input: WCE-porrected Image  
 Output: corrected image  
 Corrected image is then forward-projected and the projections are combined with the original raw data. Finally, the combined data are reconstructed iteratively.

Huang, Yixing, et al. "Data consistent CT reconstruction from insufficient data with learned prior images." *arXiv preprint arXiv:2005.10034* (2020). **dkfz.**

## Results



Huang, Yixing, et al. "Data consistent CT reconstruction from insufficient data with learned prior images." *arXiv preprint arXiv:2005.10034* (2020). **dkfz.**

## Deep Detruncation

### Classification of DL-based reconstruction methods

1) Sinogram domain learning

2) Image domain learning

3) Dual-domain learning

- S: Sinogram domain network
- I: Image domain network
- P: Projection operation
- R: Reconstruction operation
- F: Dual-domain information fusion operation

**1) Wang, et al., A Review of Deep Learning CT Reconstructions from Incomplete Projection Data. IEEE Transactions on Radiation and Plasma Medical Sciences, doi: 10.1109/TRPMS.2022.3274549 (2022)**

## Deep learning-based sinogram extension method for interior computed tomography

Jusuo H. J. Ketola<sup>1</sup>, Heikki Heino<sup>1</sup>, Mikael A. K. Juntunen<sup>1</sup>, Mika T Nieminen<sup>1,2</sup>, and Sora I. Jakonić<sup>1</sup>

<sup>1</sup>Research Unit of Medical Imaging, Physics and Technology, University of Oulu, Oulu, Finland  
<sup>2</sup>The South Savo Health Care Authority, Mikkeli Central Hospital, Oulu, Finland  
<sup>3</sup>Department of Diagnostic Radiology, Oulu University Hospital, Oulu, Finland  
<sup>4</sup>Health Center Oulu, Oulu University Hospital and University of Oulu, Oulu, Finland

**1) H.J. Ketola, et al., Deep learning-based sinogram extension method for interior computed tomography. Medical Imaging: Physics of Medical Imaging, doi: 10.1186/1098-1336-1336-1336 (2021)**

## Results

**1) H.J. Ketola, et al., Deep learning-based sinogram extension method for interior computed tomography. Medical Imaging: Physics of Medical Imaging, doi: 10.1186/1098-1336-1336-1336 (2021)**

## Deep Detruncation

### Classification of DL-based reconstruction methods

1) Sinogram domain learning

2) Image domain learning

3) Dual-domain learning

- S: Sinogram domain network
- I: Image domain network
- P: Projection operation
- R: Reconstruction operation
- F: Dual-domain information fusion operation

**1) Wang, et al., A Review of Deep Learning CT Reconstructions from Incomplete Projection Data. IEEE Transactions on Radiation and Plasma Medical Sciences, doi: 10.1109/TRPMS.2022.3274549 (2022)**

## Evaluation of novel AI-based extended field-of-view CT reconstructions

Gabriel Peña Ponce<sup>1</sup>

<sup>1</sup>Department of Radiation Therapy (MALT/RT), GROW School for Oncology and Developmental Biology, Maastricht University Medical Center, Maastricht 6229 XZ, The Netherlands

Mathias Beer-Beck<sup>1</sup>, Eric Fournie and Christian Hofmann  
 Simon Rothbarth, Michael C. Olsen, Wouter J.C. van Erp and Frank Verhaagen  
 Department of Radiation Therapy (MALT/RT), GROW School for Oncology and Developmental Biology, Maastricht University Medical Center, Maastricht 6229 XZ, The Netherlands

(Received 29 February 2021; revised 27 April 2021; accepted for publication 30 April 2021; published 11 May 2021)

**1) P. Ponce, et al., Evaluation of novel AI-based extended field-of-view CT reconstructions. Med Phys, doi:10.1088/1361-6560/ab8121 (2021)**

## Results

**1) P. Ponce, et al., Evaluation of novel AI-based extended field-of-view CT reconstructions. Med Phys, doi:10.1088/1361-6560/ab8121 (2021)**

## Results

**1) P. Ponce, et al., Evaluation of novel AI-based extended field-of-view CT reconstructions. Med Phys, doi:10.1088/1361-6560/ab8121 (2021)**

## Evaluation of novel AI-based extended field-of-view CT reconstructions

Gabriel Peña Ponce<sup>1</sup>

<sup>1</sup>Department of Radiation Therapy (MALT/RT), GROW School for Oncology and Developmental Biology, Maastricht University Medical Center, Maastricht 6229 XZ, The Netherlands

Mathias Beer-Beck<sup>1</sup>, Eric Fournie and Christian Hofmann  
 Simon Rothbarth, Michael C. Olsen, Wouter J.C. van Erp and Frank Verhaagen  
 Department of Radiation Therapy (MALT/RT), GROW School for Oncology and Developmental Biology, Maastricht University Medical Center, Maastricht 6229 XZ, The Netherlands

(Received 29 February 2021; revised 27 April 2021; accepted for publication 30 April 2021; published 11 May 2021)

**1) P. Ponce, et al., Evaluation of novel AI-based extended field-of-view CT reconstructions. Med Phys, doi:10.1088/1361-6560/ab8121 (2021)**

## Data Extrapolation From Learned Prior Images for Truncation Correction in Computed Tomography

Yiying Huang<sup>1</sup>, Alexander Priebe<sup>1</sup>, Michael Marban<sup>1</sup>, Guenter Lantisch<sup>1</sup>, and Andreas Maier<sup>1</sup>, Senior Member, IEEE

**1) Huang, et al., Data Extrapolation from Learned Prior Images for Truncation Correction in Computed Tomography. IEEE Transactions on Medical Imaging (2021)**

## Results

**1) Huang, et al., Data Extrapolation from Learned Prior Images for Truncation Correction in Computed Tomography. IEEE Transactions on Medical Imaging (2021)**

## Data Consistent CT Reconstruction from Insufficient Data with Learned Prior Images

Yiying Huang, Alexander Priebe, Michael Marban, Guenter Lantisch, Andreas Maier

**1) Huang, et al., Data consistent CT reconstruction from insufficient data with learned prior images. arXiv preprint arXiv:2004.10024 (2020)**

## Data Extrapolation From Learned Prior Images for Truncation Correction in Computed Tomography

Yiying Huang<sup>1</sup>, Alexander Priebe<sup>1</sup>, Michael Marban<sup>1</sup>, Guenter Lantisch<sup>1</sup>, and Andreas Maier<sup>1</sup>, Senior Member, IEEE

**1) Huang, et al., Data Extrapolation from Learned Prior Images for Truncation Correction in Computed Tomography. IEEE Transactions on Medical Imaging (2021)**

## Results

**1) Huang, et al., Data consistent CT reconstruction from insufficient data with learned prior images. arXiv preprint arXiv:2004.10024 (2020)**

## Generative adversarial networks improve interior computed tomography angiography reconstruction

Jusuo H J Ketola<sup>1</sup>, Heikki Heino<sup>1</sup>, Mikael A K Juntunen<sup>1</sup>, Mika T Nieminen<sup>1,2</sup>, Samuli Siltanen<sup>3</sup> and Sora I Jakonić<sup>1</sup>

- 1) Input: truncated sinogram
- 2) Extended with sinogram extension GAN
- 3) Superimpose original measured data
- 4) reconstruction post-processing GAN is used to yield an improved reconstruction
- 5) original data is superimposed in the sinogram before final filtered backprojection

**1) H.J. Ketola, et al., Generative adversarial networks improve interior computed tomography angiography reconstruction. Biomed. Phys. Eng. Express 7, 065001 (2021)**

## Results

**1) H.J. Ketola, et al., Generative adversarial networks improve interior computed tomography angiography reconstruction. Biomed. Phys. Eng. Express 7, 065001 (2021)**

## Results

**1) Huang, et al., Data consistent CT reconstruction from insufficient data with learned prior images. arXiv preprint arXiv:2004.10024 (2020)**

# Evaluation of novel AI-based extended field-of-view CT reconstructions

Gabriel Paiva Fonseca<sup>a)\*</sup>

*Department of Radiation Oncology (MAASTRO), GROW School for Oncology and Developmental Biology, Maastricht University Medical Centre+, Maastricht 6229 ET, The Netherlands*

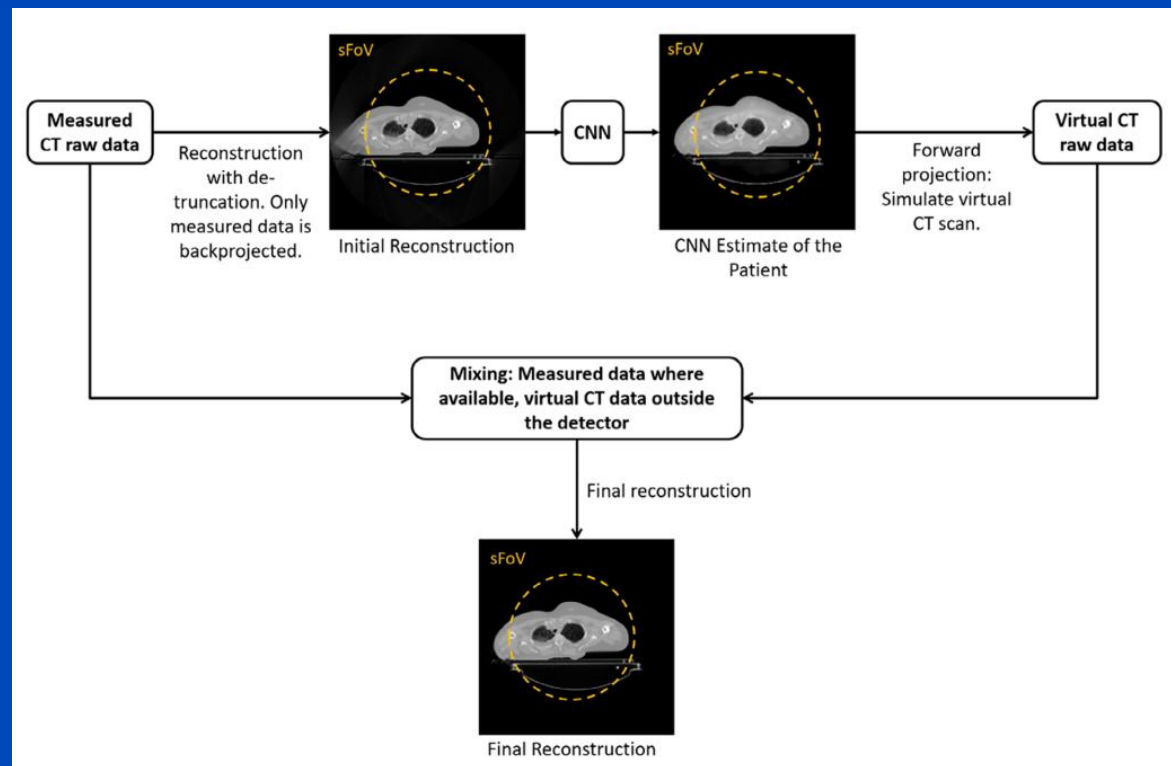
Matthias Baer-Beck\* Eric Fournie and Christian Hofmann

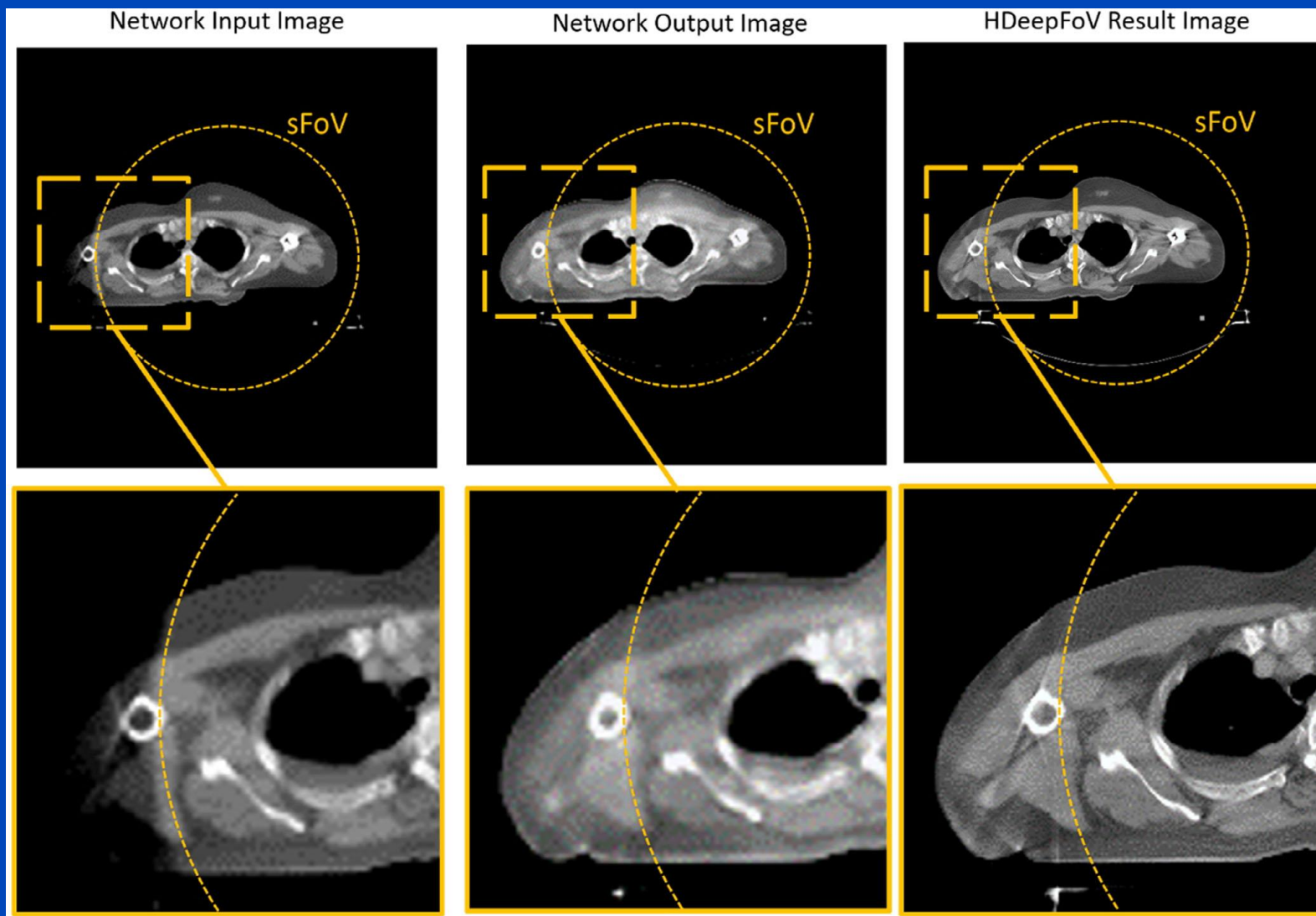
*Siemens Healthcare GmbH, Forchheim, Germany*

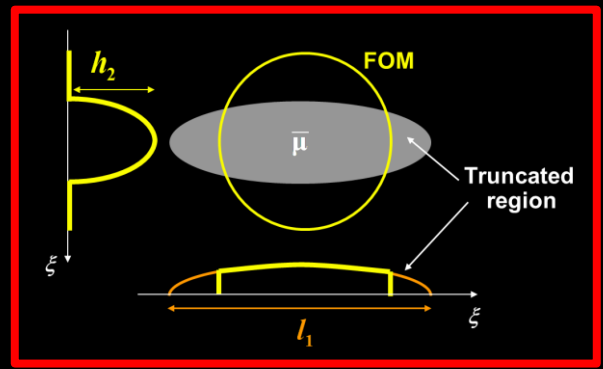
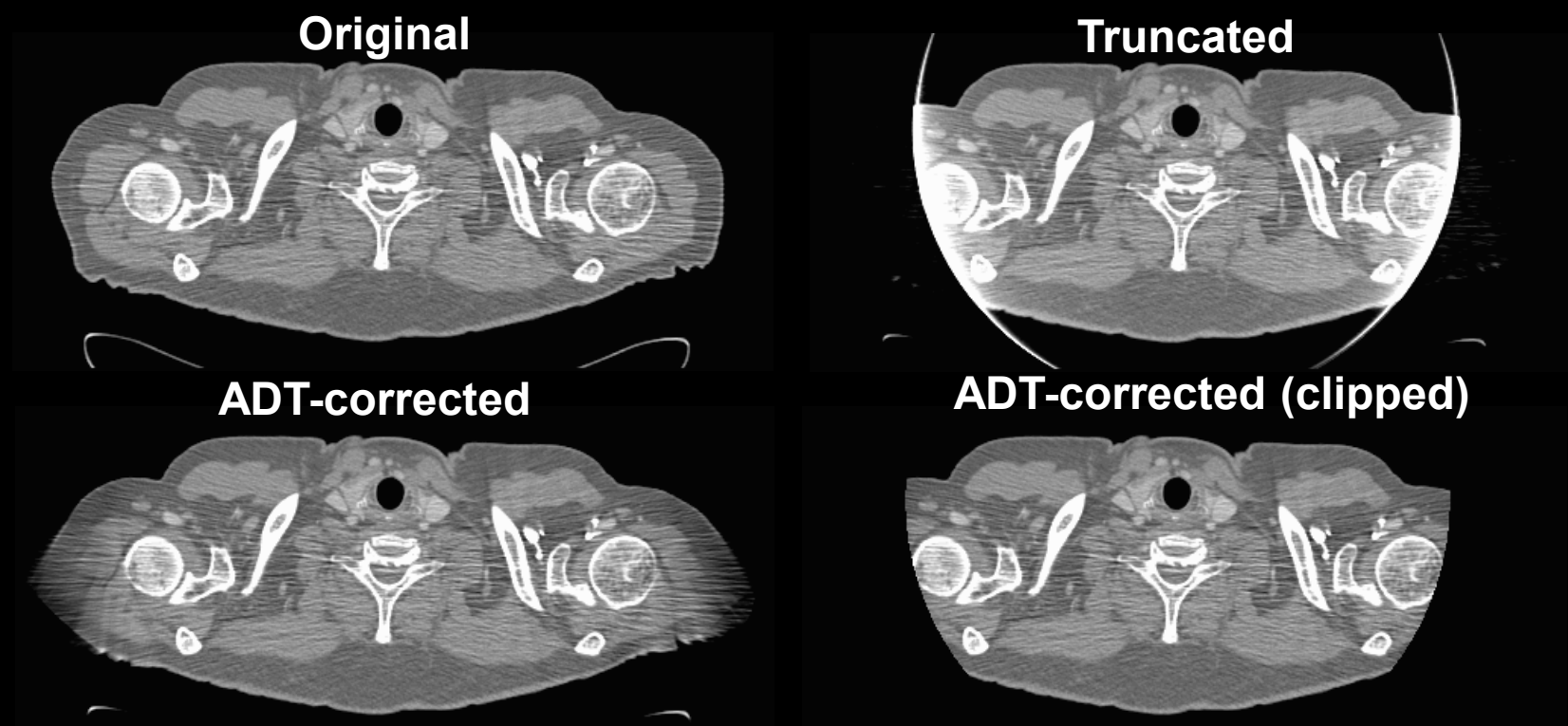
Ilaria Rinaldi, Michel C Ollers, Wouter J.C. van Elmpt and Frank Verhaegen

*Department of Radiation Oncology (MAASTRO), GROW School for Oncology and Developmental Biology, Maastricht University Medical Centre+, Maastricht 6229 ET, The Netherlands*

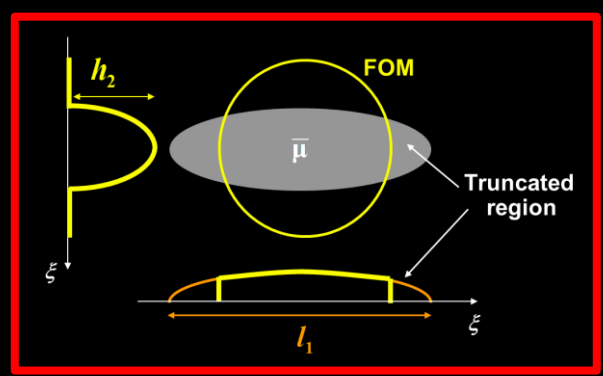
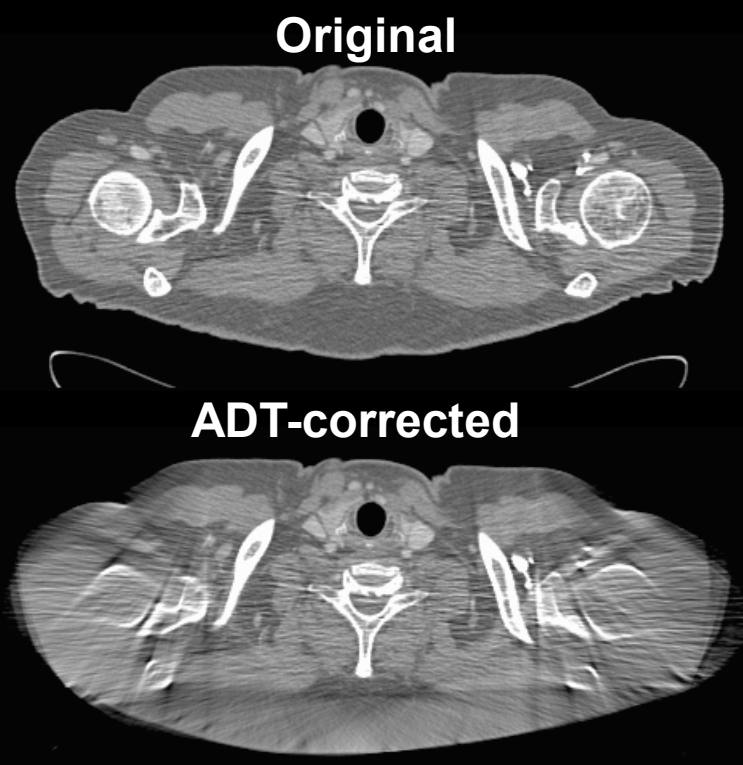
(Received 28 February 2021; revised 27 April 2021; accepted for publication 30 April 2021; published 31 May 2021)







$C = 0 \text{ HU}, W = 1000 \text{ HU}$



**C = 0 HU, W = 1000 HU**

**RESEARCH ARTICLE**

## MEDICAL PHYSICS

# Latent space reconstruction for missing data problems in CT e.g. for metal inpainting, detruncation, limited angle extrapolation, ...

Anton Kabelac<sup>1,2</sup> | Elias Eulig<sup>1,2</sup> | Joscha Maier<sup>1</sup> | Maximilian Hammermann<sup>1,2</sup> |  
Michael Knaup<sup>1</sup> | Marc Kachelrieß<sup>1,3</sup>

<sup>1</sup>Division of X-Ray Imaging and Computed Tomography, German Cancer Research Center (DKFZ), Heidelberg, Germany

<sup>2</sup>Faculty of Physics and Astronomy, Heidelberg University, Heidelberg, Germany

<sup>3</sup>Medical Faculty Heidelberg, Heidelberg University, Heidelberg, Germany

**Correspondence**

Anton Kabelac, Division of X-Ray Imaging and Computed Tomography, German Cancer Research Center (DKFZ), Heidelberg, Germany.  
Email: [anton.kabelac@dkfz.de](mailto:anton.kabelac@dkfz.de)

**Abstract**

**Background:** The reconstruction of a computed tomography (CT) image can be compromised by artifacts, which, in many cases, reduce the diagnostic value of the image. These artifacts often result from missing or corrupt regions in the projection data, for example, by truncation, metal, or limited angle acquisitions.

**Purpose:** In this work, we introduce a novel deep learning-based framework, latent space reconstruction (LSR), which enables correction of various types of artifacts arising from missing or corrupted data.

**Methods:** First, we train a generative neural network on uncorrupted CT images. After training, we iteratively search for the point in the latent space of this network that best matches the compromised projection data we measured. Once an optimal point is found, forward-projection of the generated CT image can be used to inpaint the corrupted or incomplete regions of the measured raw data.

# Image Domain Experiment

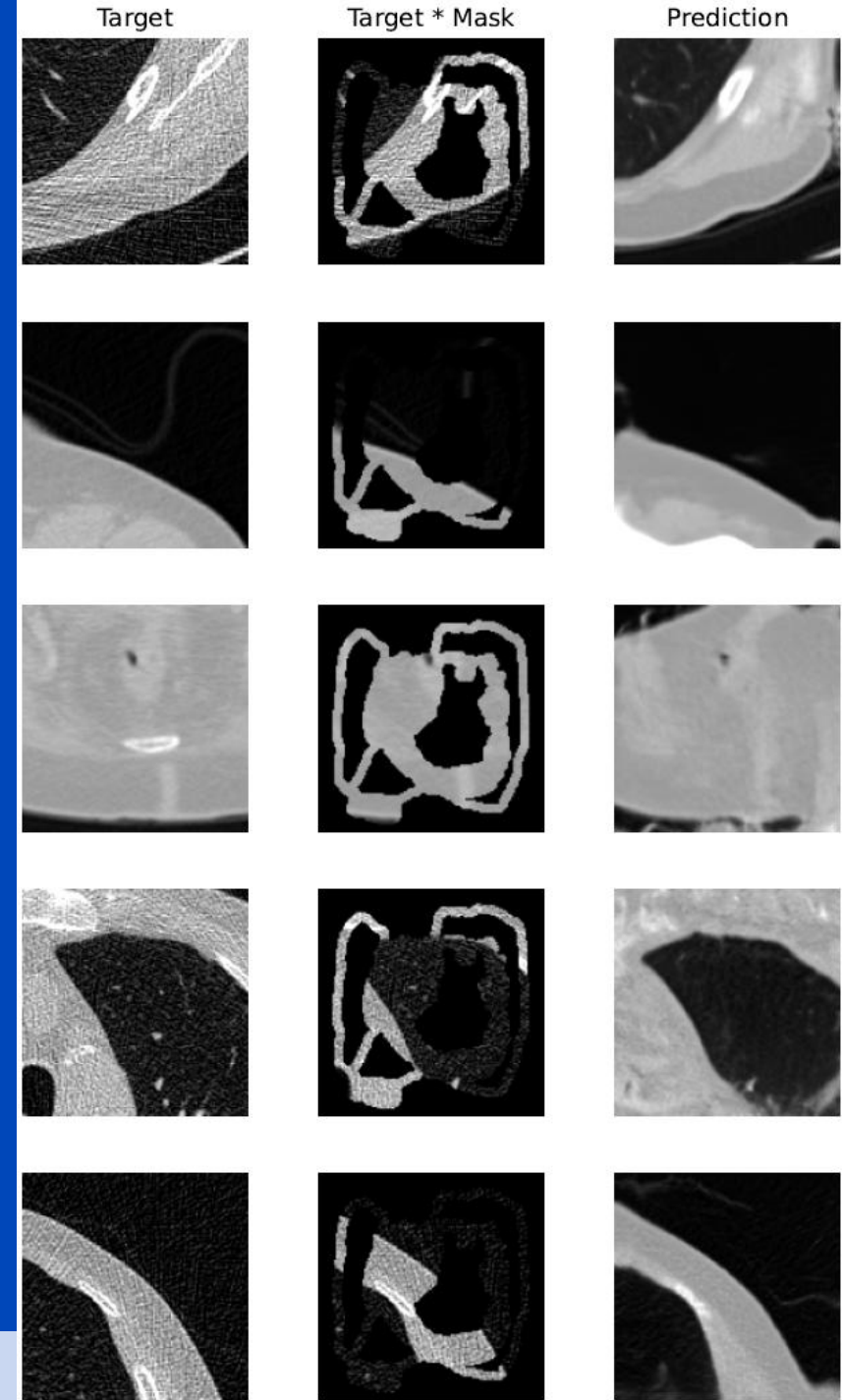
- Purely image domain
- Hand-crafted mask



- Minimizing

$$z = \arg \min_z \|D(z) - M(\mathbf{r})f(\mathbf{r})\|$$

- Results see rhs.

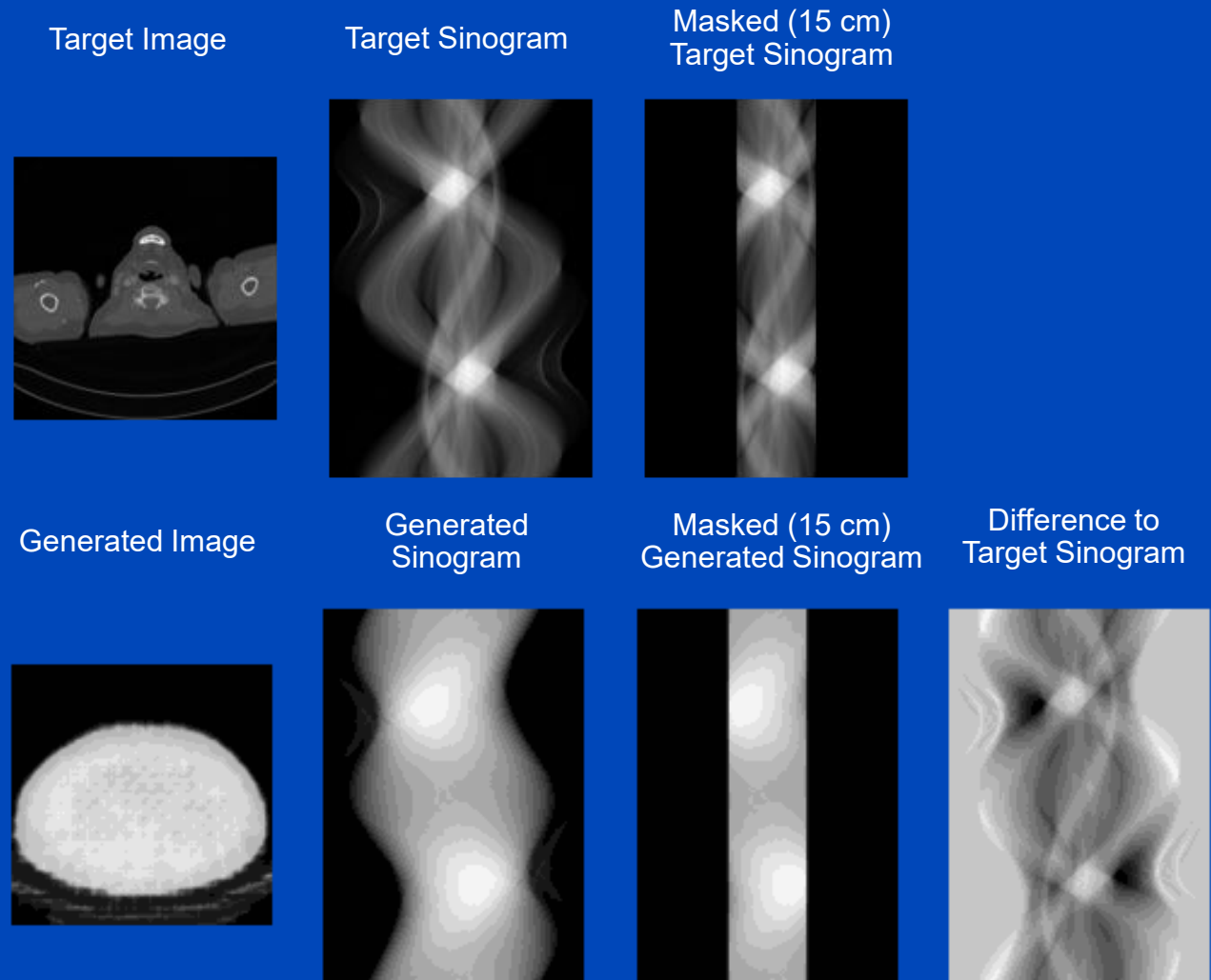
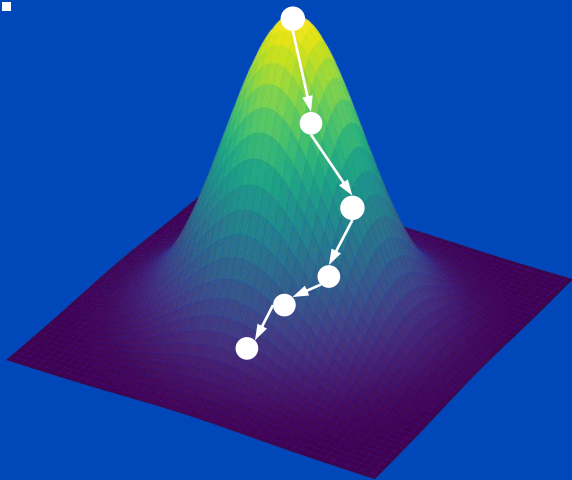


# Search in Latent Space

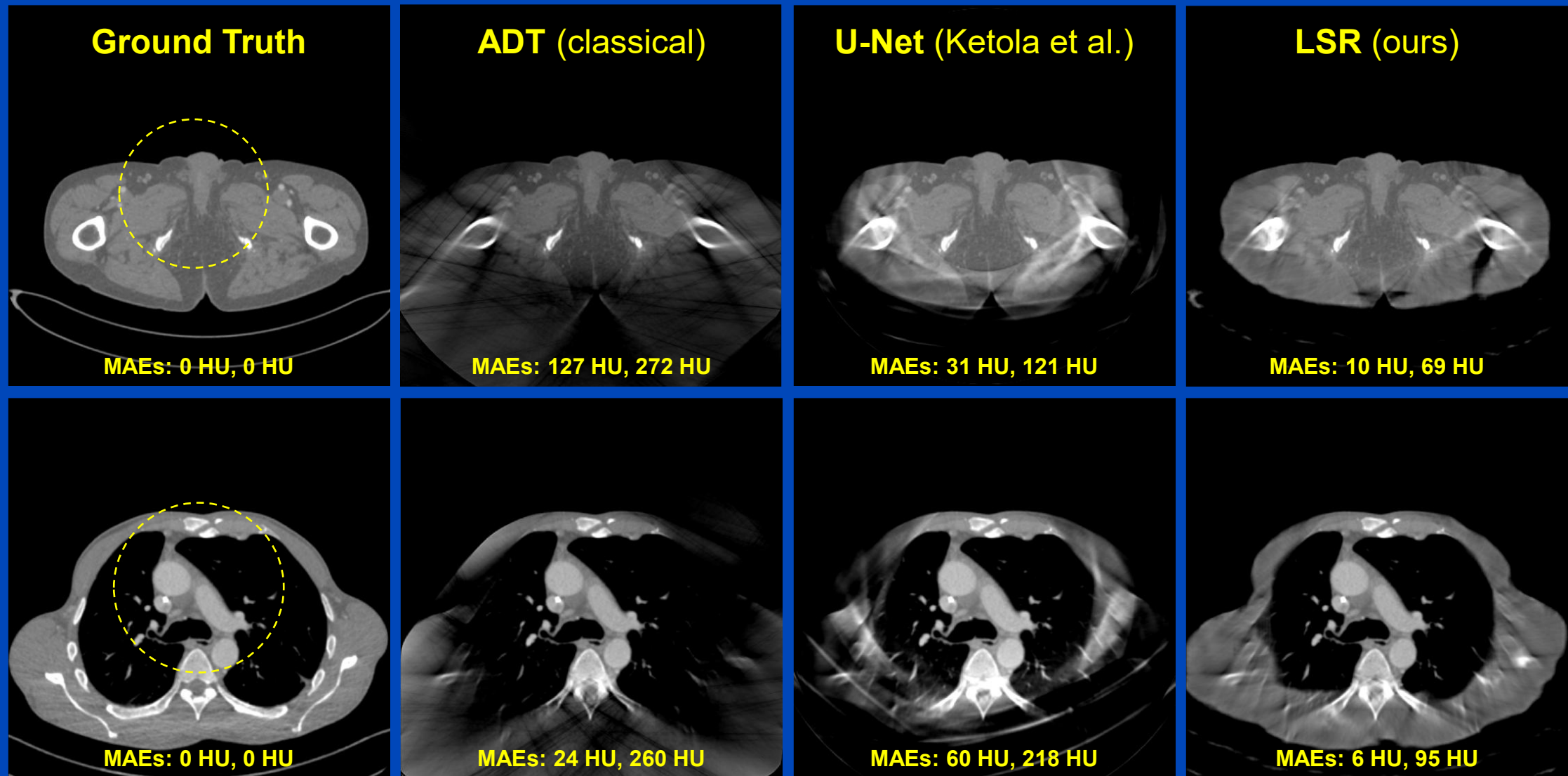
- Optimization of latent space vector in projection domain

$$z = \arg \min_z \|XD(z) - p\|_{15 \text{ cm}}$$

- Video showing intermediate images of selected iteration steps.



# Results



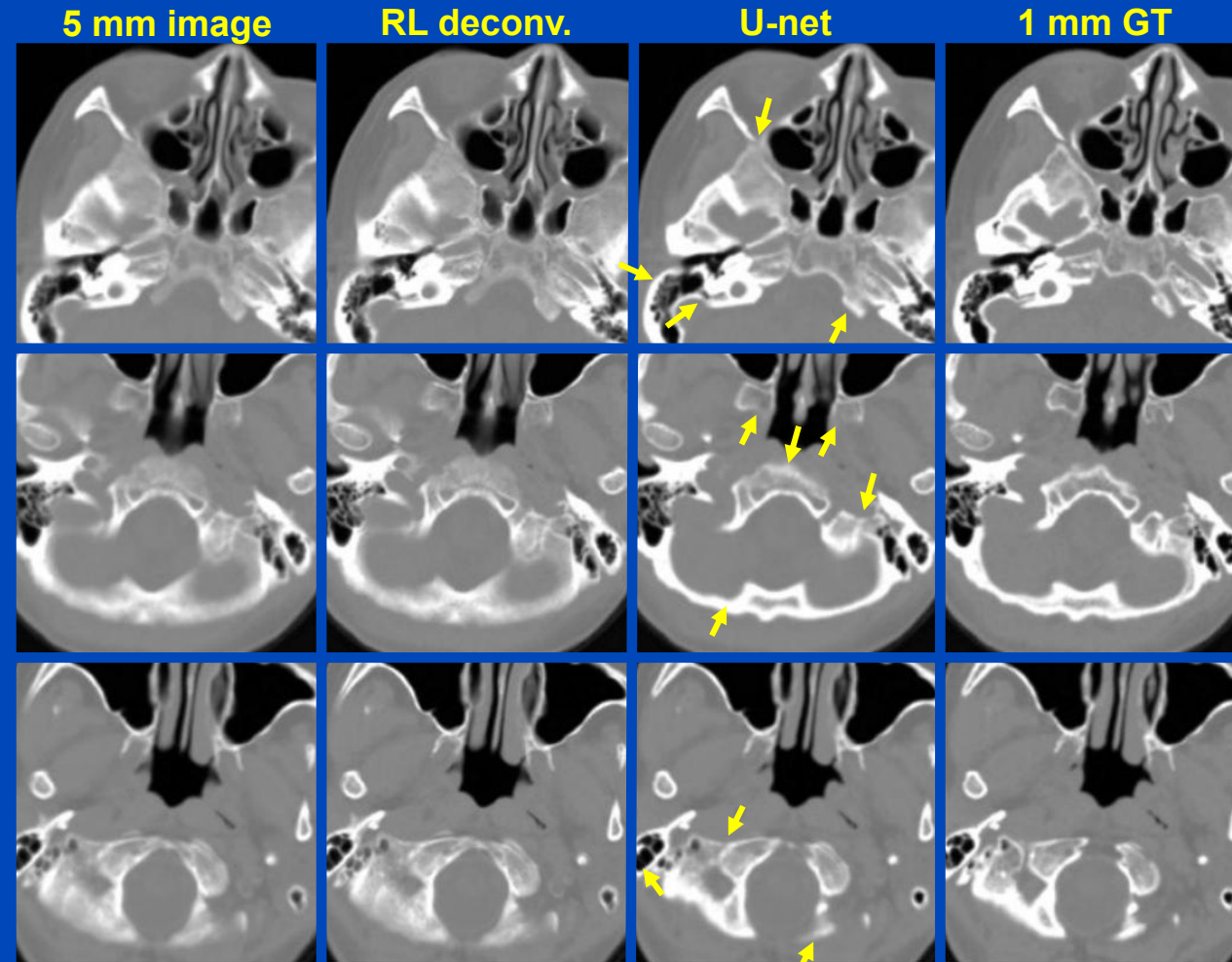
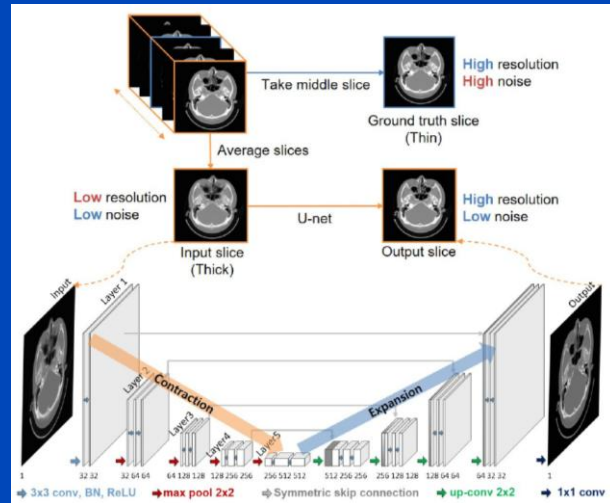
C = 50 HU, W = 1200 HU

Super resolution does not add new information.

**SPATIAL RESOLUTION IMPROVEMENT**

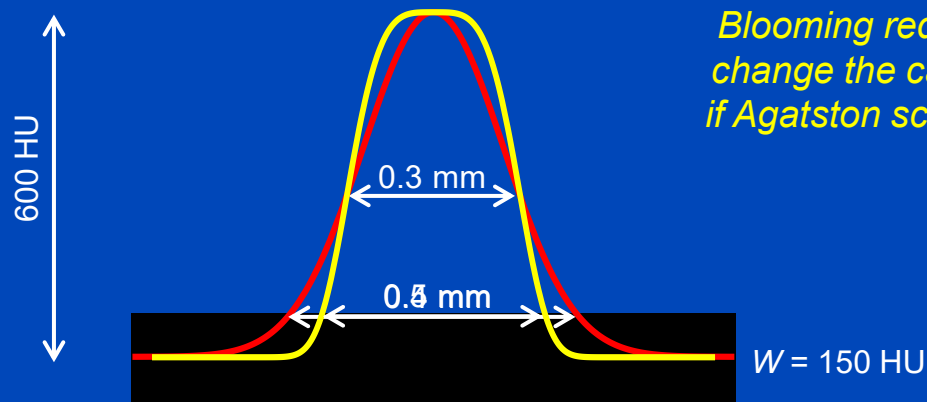
# Resolution Improvement Example

- 2D U-net to converts 5 mm thick images into 1 mm ones.
- E.g. to “replace a scanning protocol for a 1 mm slice with a 5 mm protocol”.

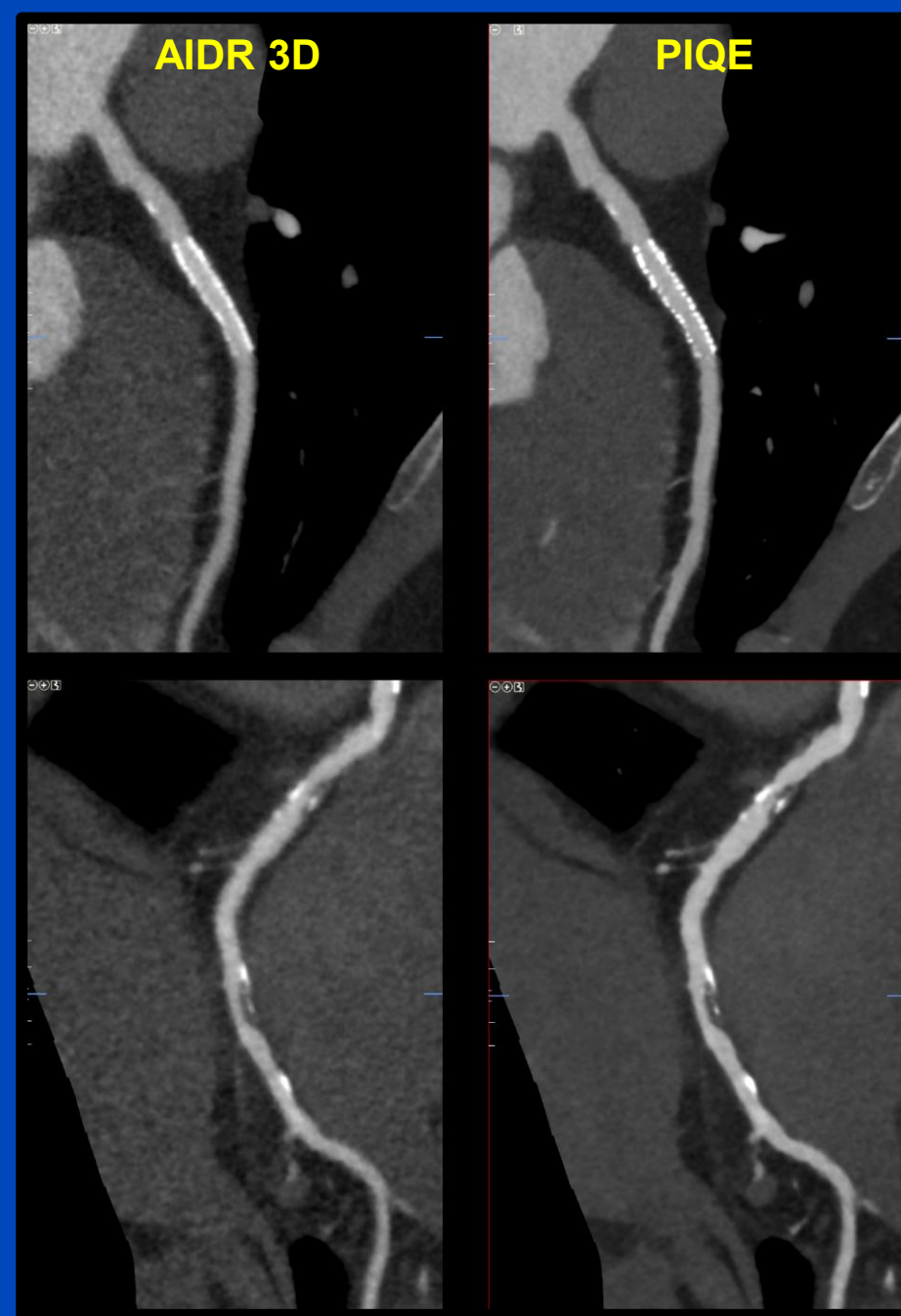


# Canon PIQE

- Precise IQ Engine (PIQE).
- Trained on data from Canon's Precision high spatial resolution CT
- Converts images from Canon's standard spatial resolution scanners (e.g. Aquilion ONE / PRISM edition) to look like high spatial resolution images.

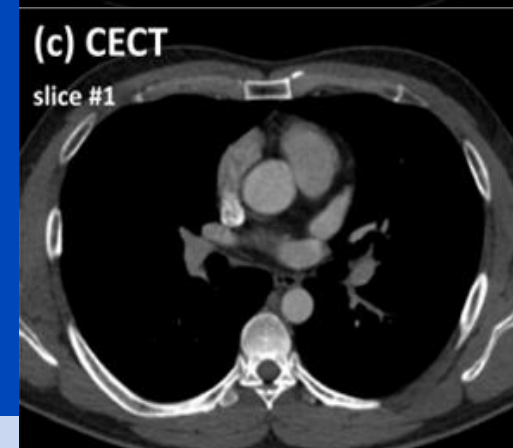
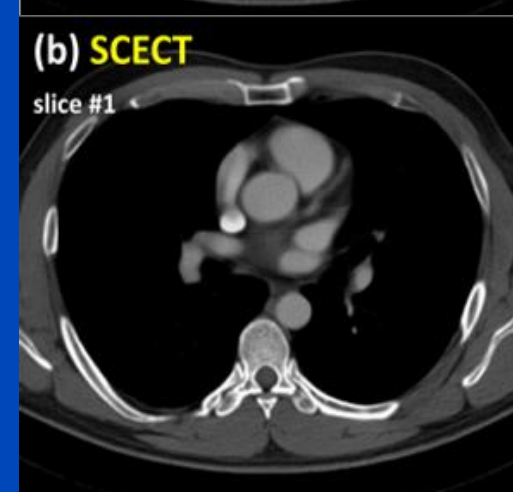
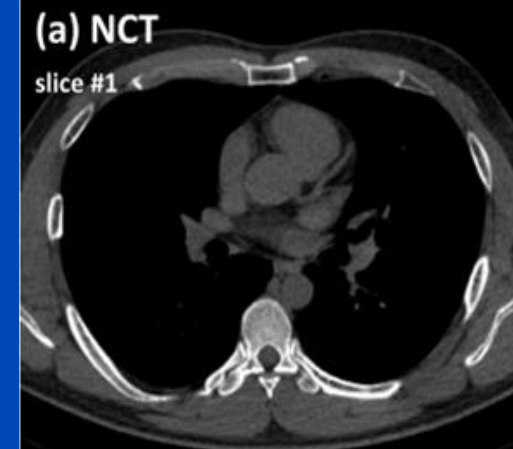


*Warning:  
Blooming reduction might  
change the calcium score,  
if Agatston scoring is used.*



# Fake Contrast Enhancement

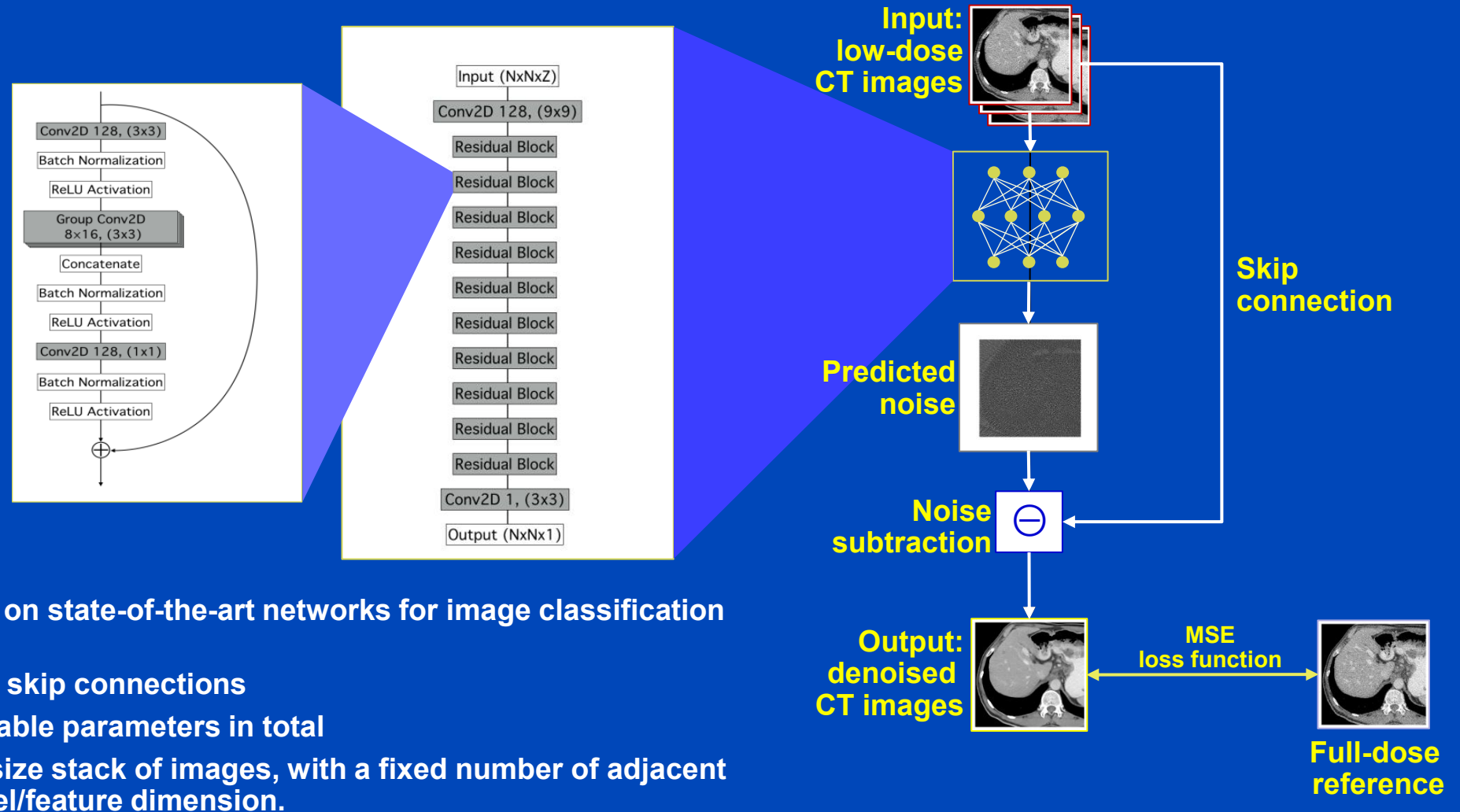
- [1] G. Santini, L. M. Zumbo, N. Martini, G. Valvano, A. Leo, A. Ripoli, F. Avogliero, D. Chiappino, D. D. Latta, “**Synthetic contrast enhancement** in cardiac CT with deep learning,” arXiv 1807:01779, 2018.
- [2] J. Liu, Y. Tian, A. M. Ağildere, K. M. Haberal, M. Coşkun, C. Duzgol, and O. Akin, “DyeFreeNet: Deep virtual **contrast CT synthesis**,” Lecture Notes in Computer Science. Springer International Publishing, pp. 80–89, 2020.
- [3] A. Chandrashekar, A. Handa, N. Shivakumar, P. Lapolla, V. Grau, R. Lee, “A deep learning approach to generate contrast-enhanced computerised tomography **Angiography without the use of intravenous contrast agents**,” arXiv 2003.01223, 2020.
- [4] J. W. Choi, Y. J. Cho, J. Y. Ha, S. B. Lee, S. Lee, Y. H. Choi, J.-E. Cheon, and W. S. Kim, “Generating **synthetic contrast enhancement from non-contrast** chest computed tomography using a generative adversarial network,” Scientific Reports, vol. 11, no. 1, 2021.
- [5] S. W. Kim, J. H. Kim, S. Kwak, M. Seo, C. Ryoo, C.-I. Shin, S. Jang, J. Cho, Y.-H. Kim, and K. Jeon, “The feasibility of deep learning-based **synthetic contrast-enhanced CT from non-enhanced CT** in emergency department patients with acute abdominal pain,” Scientific Reports, vol. 11, 2021.
- [6] J. Chun, J. S. Chang, C. Oh, I. Park, M. S. Choi, C.-S. Hong, H. Kim, G. Yang, J. Y. Moon, S. Y. Chung, Y. J. Suh, and J. S. Kim, “**Synthetic contrast-enhanced** computed tomography generation using a deep convolutional neural network for cardiac substructure delineation in breast cancer radiation therapy: a feasibility study,” Radiation Oncology, vol. 17, no. 1, 2022.
- [7] Y. Gao, H. Xie, C. Chang, J. Peng, S. Pan, R. L. J. Qiu, T. Wang, B. Ghavidel, J. Roper, J. Zhou, and X. Yang, “CT-based **synthetic iodine map** generation using conditional denoising diffusion probabilistic model,” Medical Physics, vol. 51, no. 9, pp. 6246–6258, 2024.
- [8] S. Han, J.-M. Kim, J. Park, S. W. Kim, S. Park, J. Cho, S.-J. Park, H.-J. Chung, S.-M. Ham, S. J. Park, and J. H. Kim, “Clinical feasibility of deep learning based **synthetic contrast-enhanced** abdominal CT in patients undergoing **non-enhanced** CT scans,” Scientific Reports, vol. 14, no. 1, 2024.



From [4]

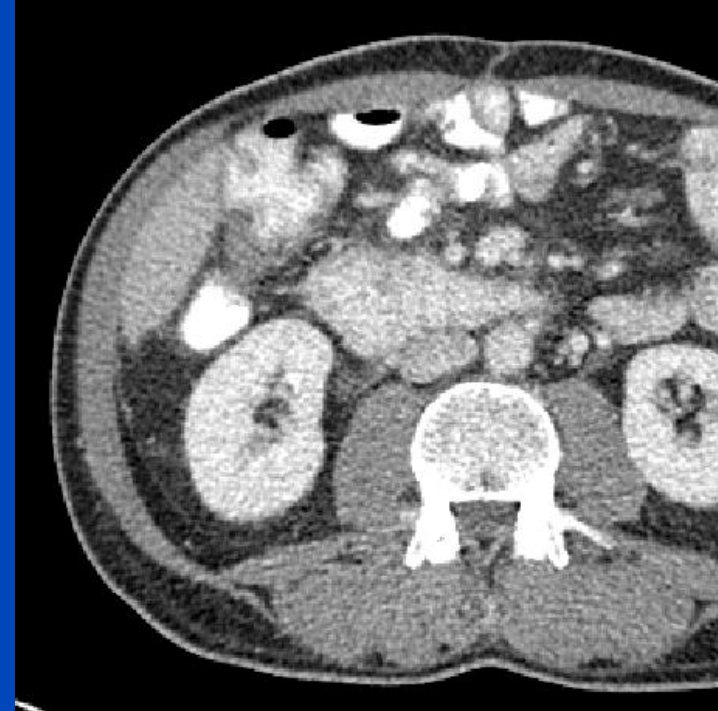
# NOISE REDUCTION

# Noise Removal Example 2



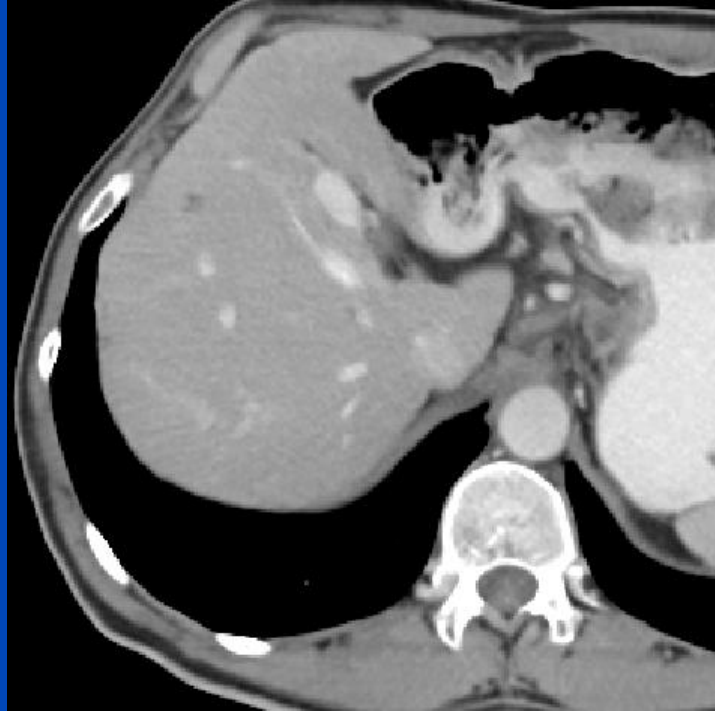
- Architecture based on state-of-the-art networks for image classification (ResNet).
- 32 conv layers with skip connections
- About 2 million tunable parameters in total
- Input is arbitrarily-size stack of images, with a fixed number of adjacent slices in the channel/feature dimension.

# Noise Removal Example 2



Low dose images (1/4 of full dose)

# Noise Removal Example 2



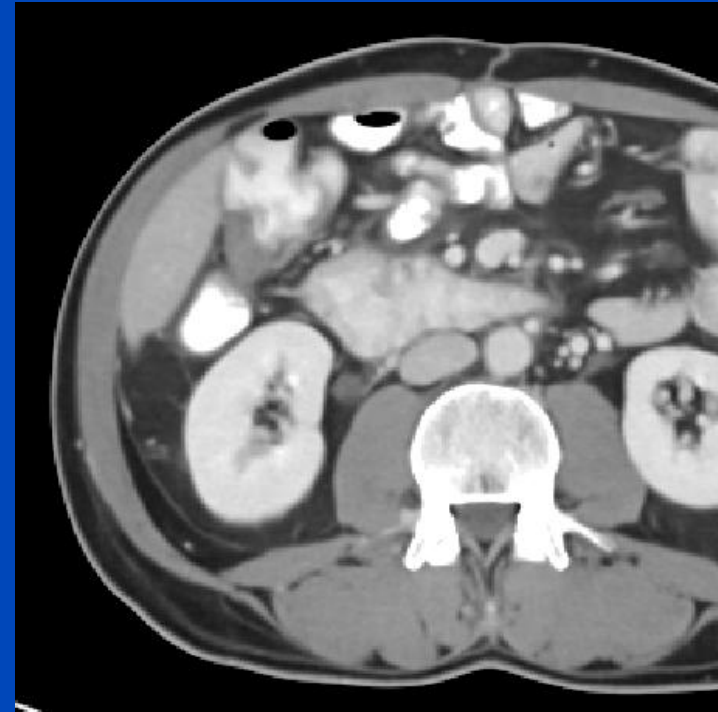
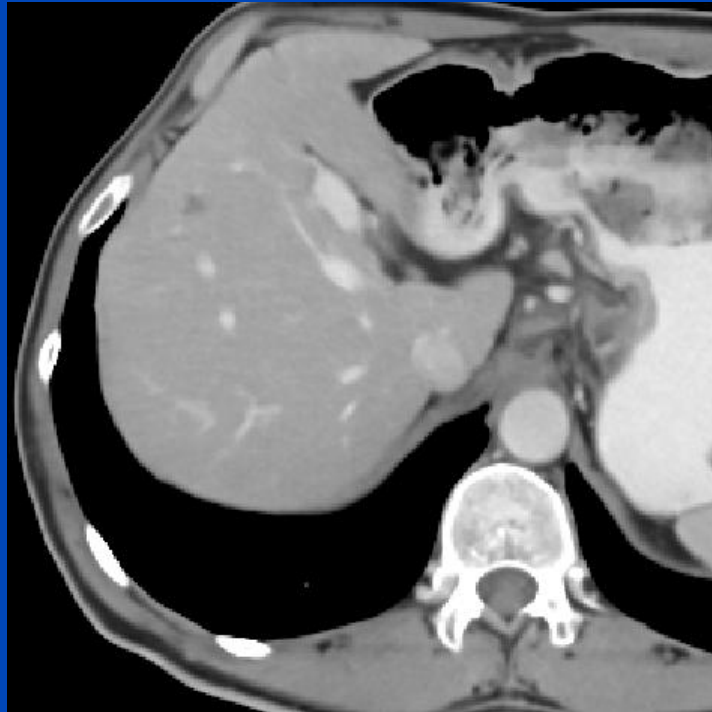
Denoised low dose

# Noise Removal Example 2



Full dose

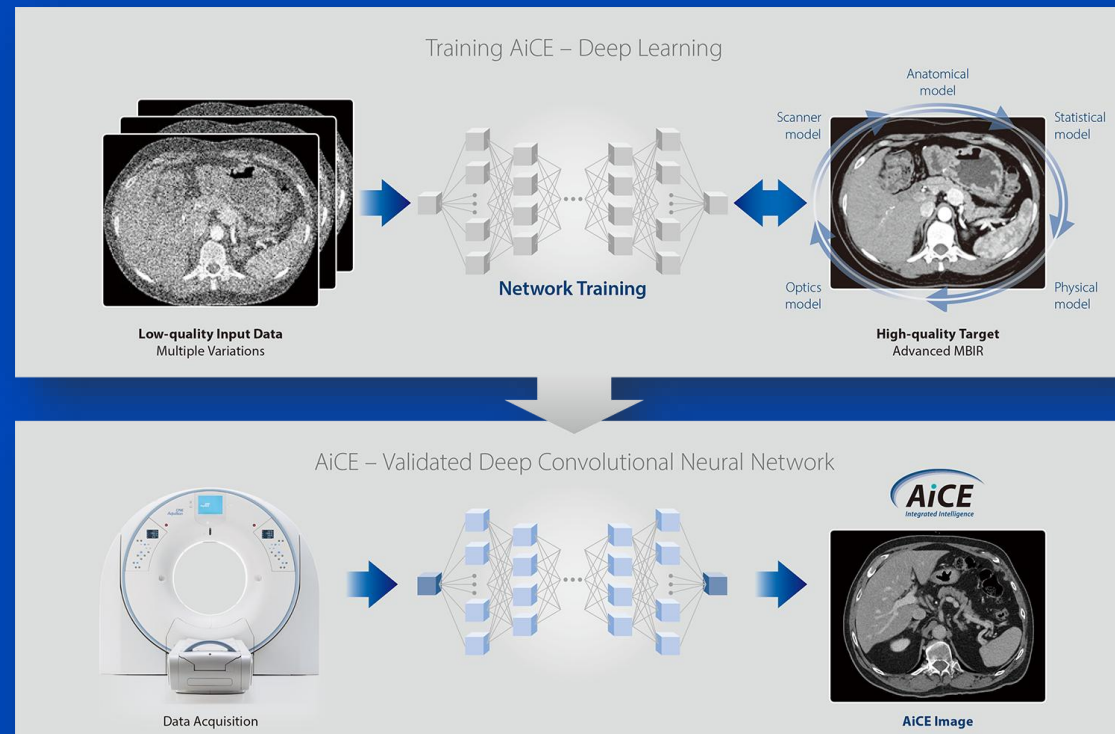
# Noise Removal Example 2



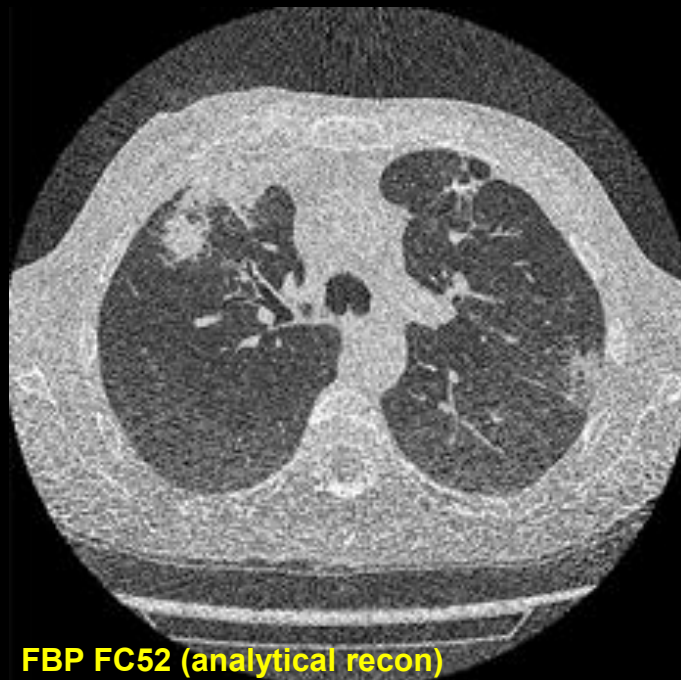
Denoised full dose

# Noise Removal: Canon's AiCE

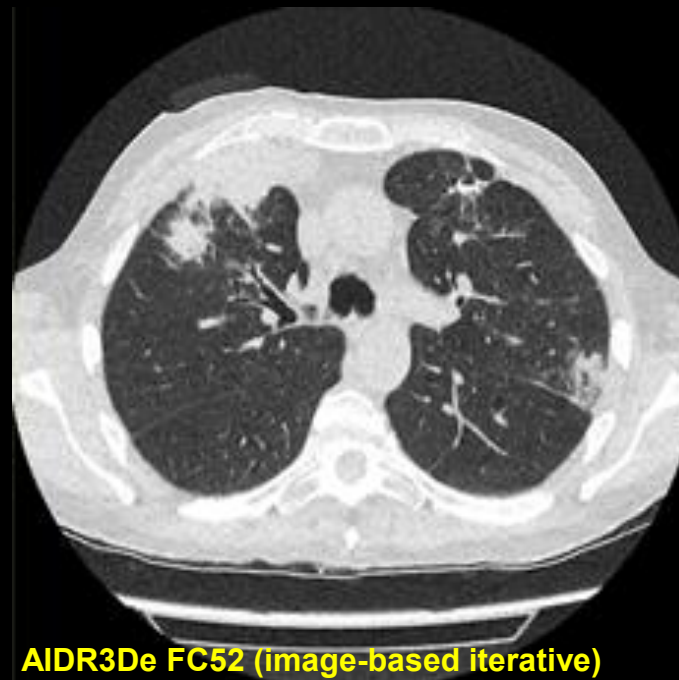
- Advanced intelligent Clear-IQ Engine (AiCE)
- Trained to restore low-dose CT data to match the properties of FIRST, the model-based IR of Canon.
- FIRST is applied to high-dose CT images to obtain a high fidelity training target



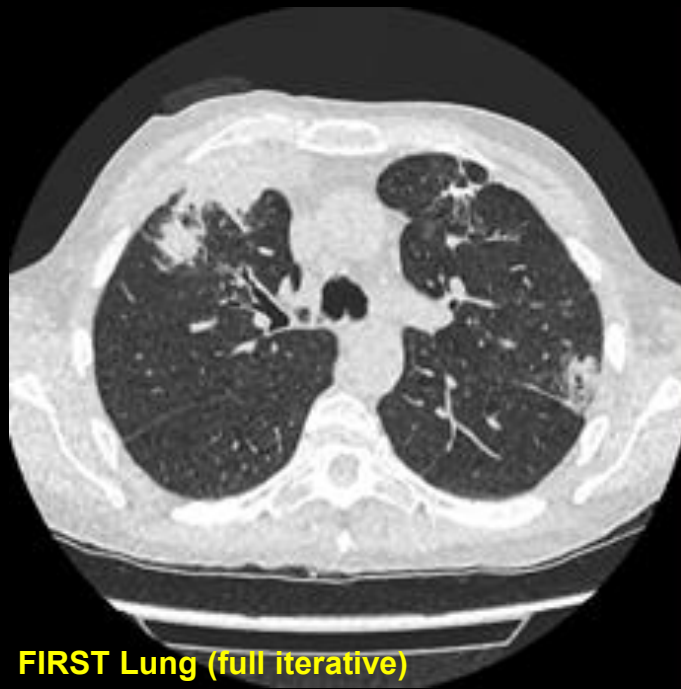
U = 100 kV  
CTDI = 0.6 mGy  
DLP = 24.7 mGy·cm  
D<sub>eff</sub> = 0.35 mSv



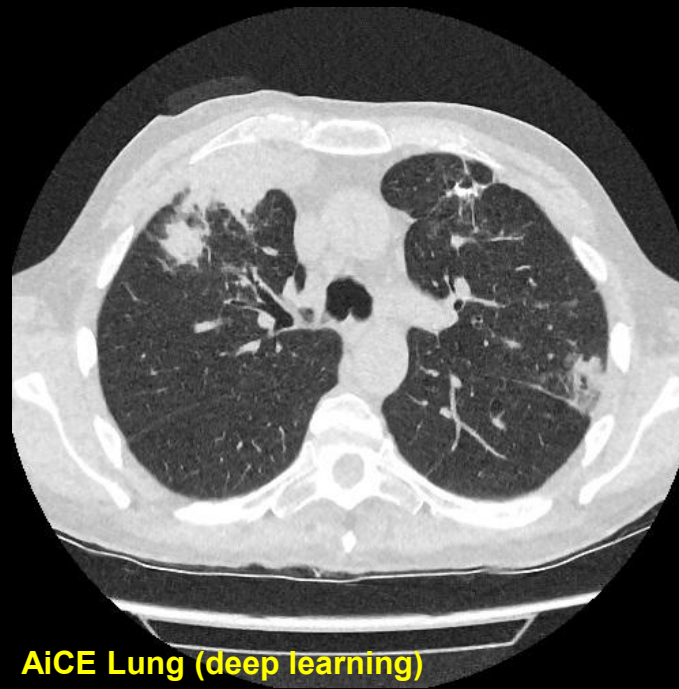
FBP FC52 (analytical recon)



AIDR3De FC52 (image-based iterative)



FIRST Lung (full iterative)



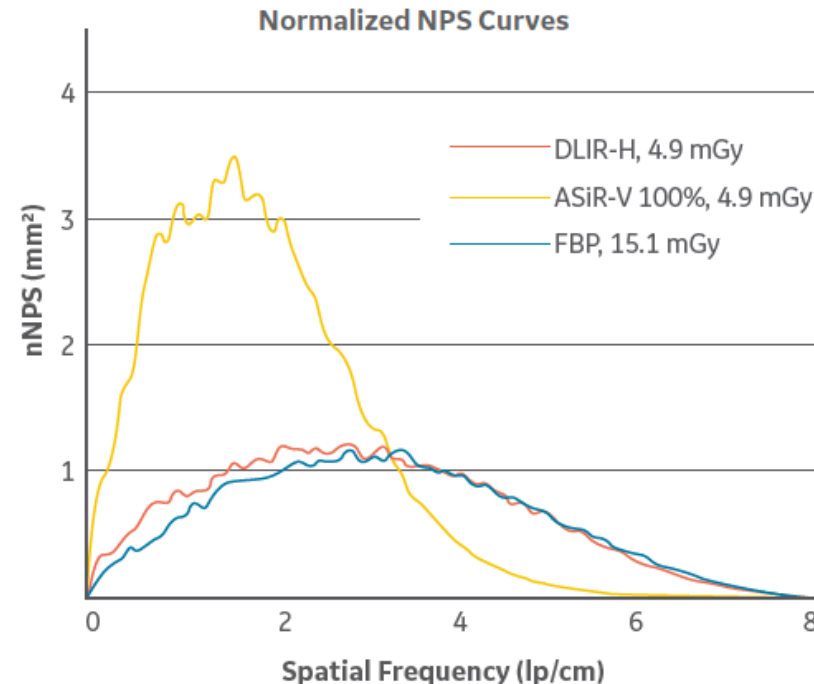
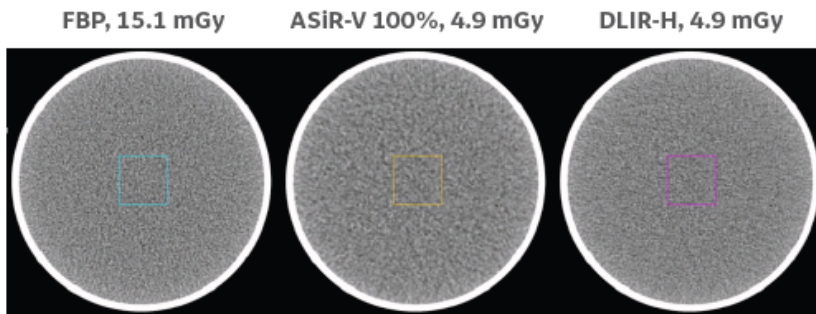
AiCE Lung (deep learning)

Courtesy of  
Radboudumc,  
the Netherlands

# Noise Reduction: GE's True Fidelity

- Based on a deep CNN
- Trained to restore low-dose CT data to match the properties of high quality FBP datasets.
- Said to preserve noise texture and NPS

The 20 cm water phantom (GE Healthcare, WI, US) was scanned on Revolution CT with two CTDIvol levels: 4.9mGy and 15.1mGy, and 2.5 mm thick images were reconstructed using FBP, ASiR-V 100% and DLIR-H (Fig. 11a). ASiR-V 100% and DLIR-H were selected for the highest potential visible change in image texture relative to the FBP reference at higher dose, for a challenging setup to compare the impact of the iterative reconstruction and deep-learning technologies on image appearance. The normalized NPS curves (Fig. 11b) show that images of low-dose DLIR have the same NPS characteristics as the images of high-dose FBP, whereas iterative reconstruction produces results that are clearly different.





**FBP**

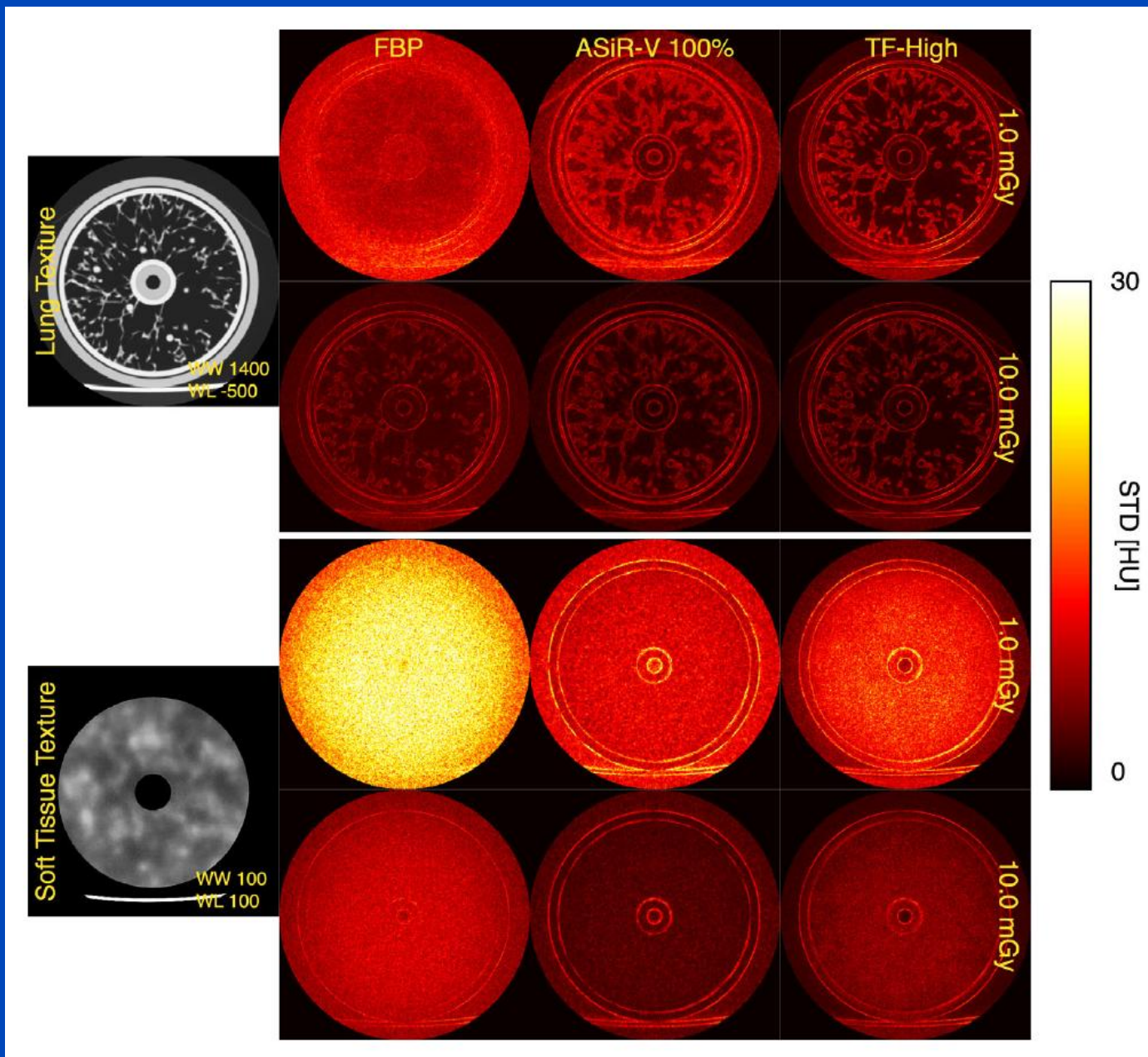


**ASIR V 50%**



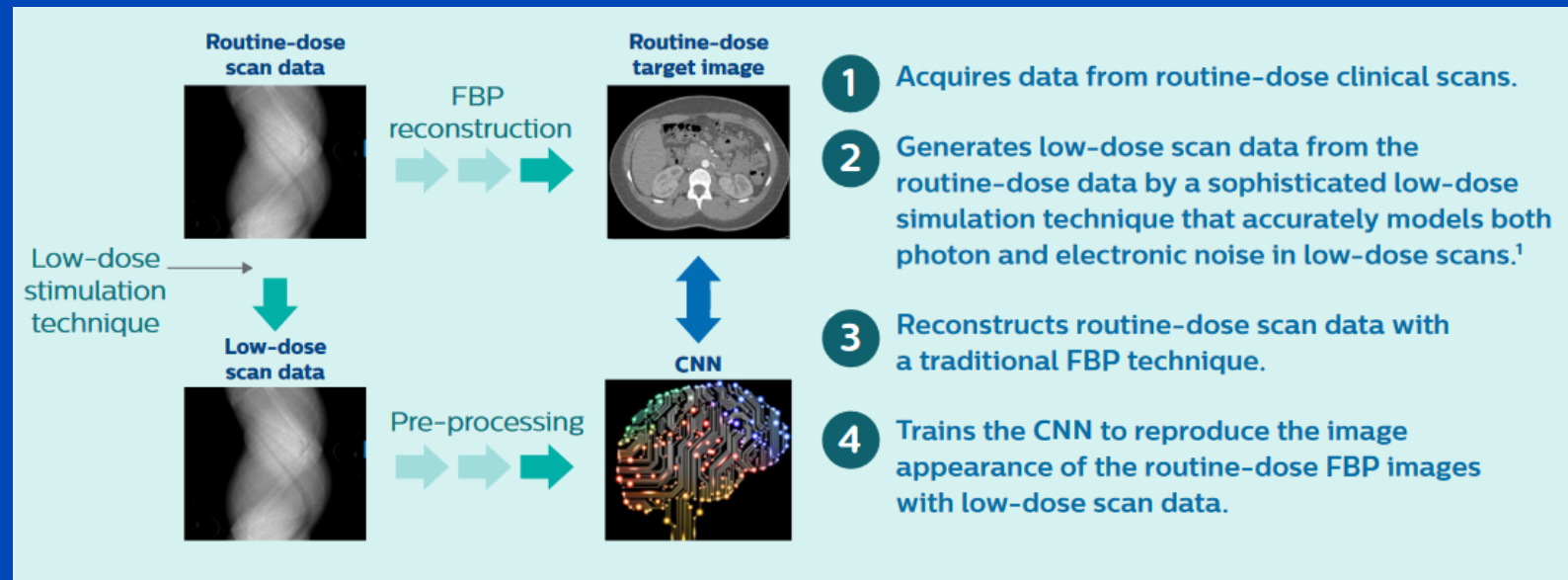
**True Fidelity**

Courtesy of GE Healthcare



# Noise Removal: Philips' Precise Image

- Noise-injected data serve as low dose examples while their original reconstructions are the labels. A CNN learns how to denoise the low dose images.





iDose<sup>4</sup> 1.4 mSv



Precise Image 0.7 mSv



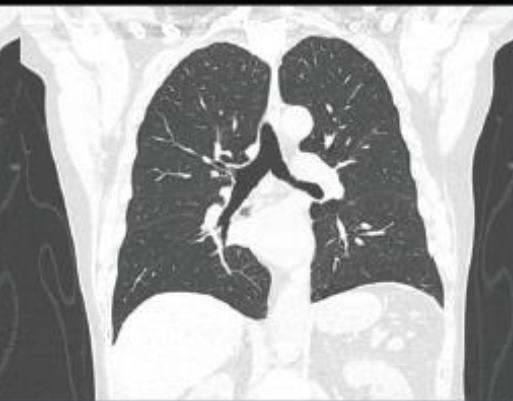
iDose<sup>4</sup> 5.1 mSv



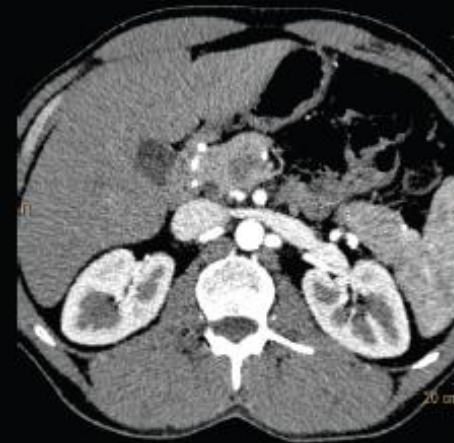
Precise Image 2.6 mSv



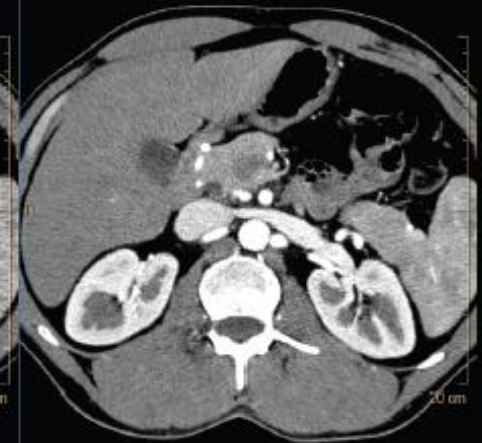
iDose<sup>4</sup> 1.5 mSv



Precise Image 0.75 mSv



iDose<sup>4</sup> 5.4 mSv



Precise Image 2.6 mSv

Study	Topic	Dose Reduction	Assessment	Reconstruction	Vendor
Beregi et al., 2022	low-dose abdomen phantom	79%	objective	AiCE	Canon
Hirai et al., 2022a	low-dose multiphase hepatic	52%	objective, subjective	AiCE	Canon
Hirai et al., 2022b	low-dose pediatric 80 kV	54%	objective, subjective	AiCE	Canon
Jin et al., 2022	low-dose interstitial lung disease	62%	objective, subjective	AiCE	Canon
Loffroy et al., 2022	low-dose head & neck	43%	objective, subjective	AiCE	Canon
Sun et al., 2022	ultra-low-dose urolithiasis	75%	objective, subjective	AiCE	Canon
Yoshioka et al., 2022	low-dose contrast abdomen	40%	objective, subjective	AiCE	Canon
Awai et al., 2021	low-dose abdominal UHR	30%	objective, subjective	AiCE	Canon
Dillman et al., 2021	pediatric detectability	52%	objective, subjective	AiCE	Canon
Loffroy et al., 2021	cardiac CTA stroke	40%	objective, subjective	AiCE	Canon
Kalra et al., 2020	low-dose lesion detection	83%	subjective	AiCE	Canon
Song et al., 2024	low-dose chest, lung parenchyma	86%	objective, subjective	AiCE	Canon
Othmann et al., 2023	ultra-high-resolution Head and Neck	30%	objective, subjective	AiCE	Canon
Willeminck et al., 2023	principles & prospects	71%	mixed	meta	many
Strigari et al., 2023	image quality phantom	96%	objective	Precise Image	Philips
Noel et al., 2024	lung phantom	25%-67%	objective	Precise Image	Philips
Deng et al., 2022	ultra-low-dose pulmonary nodules phantom	72%	objective, subjective	TrueFidelity	GE
Lee et al., 2021	pediatric chest & abdomen	63%	objective, subjective	TrueFidelity	GE
Funama et al., 2024	preoperative transcatheter aortic valve implantation	30%	objective, subjective	TrueFidelity	GE
Xi et al., 2024	colorectal cancer	75%	objective, subjective	AIIR	United

# REPLACEMENT OF LENGTHY COMPUTATIONS, FAST PHYSICS

# Deep Scatter Estimation (DSE)



TOP DOWNLOADED PAPER 2018-2019

CONGRATULATIONS TO

**Marc Kachelrieß**

whose paper has been recognized as  
one of the most read in

Medical Physics

This work received the  
**Behnken-Berger Award**  
at the DGMP annual meeting 2021

BEHNKEN-BERGER  STIFTUNG

WILEY

MEDICAL PHYSICS

The International Journal of Medical Physics Research and Practice

Congratulations — your work was one of the top  
downloaded in recent publication history!

Dear MARC,

We are excited to share that your research, published in [Medical Physics](#), is  
among the top 10% most downloaded papers!

- [Real-time scatter estimation for medical CT using the deep scatter estimation: Method and robustness analysis with respect to different anatomies, dose levels, tube voltages, and data truncation](#)

TOP DOWNLOADED PAPER 2018-2019

CONGRATULATIONS TO

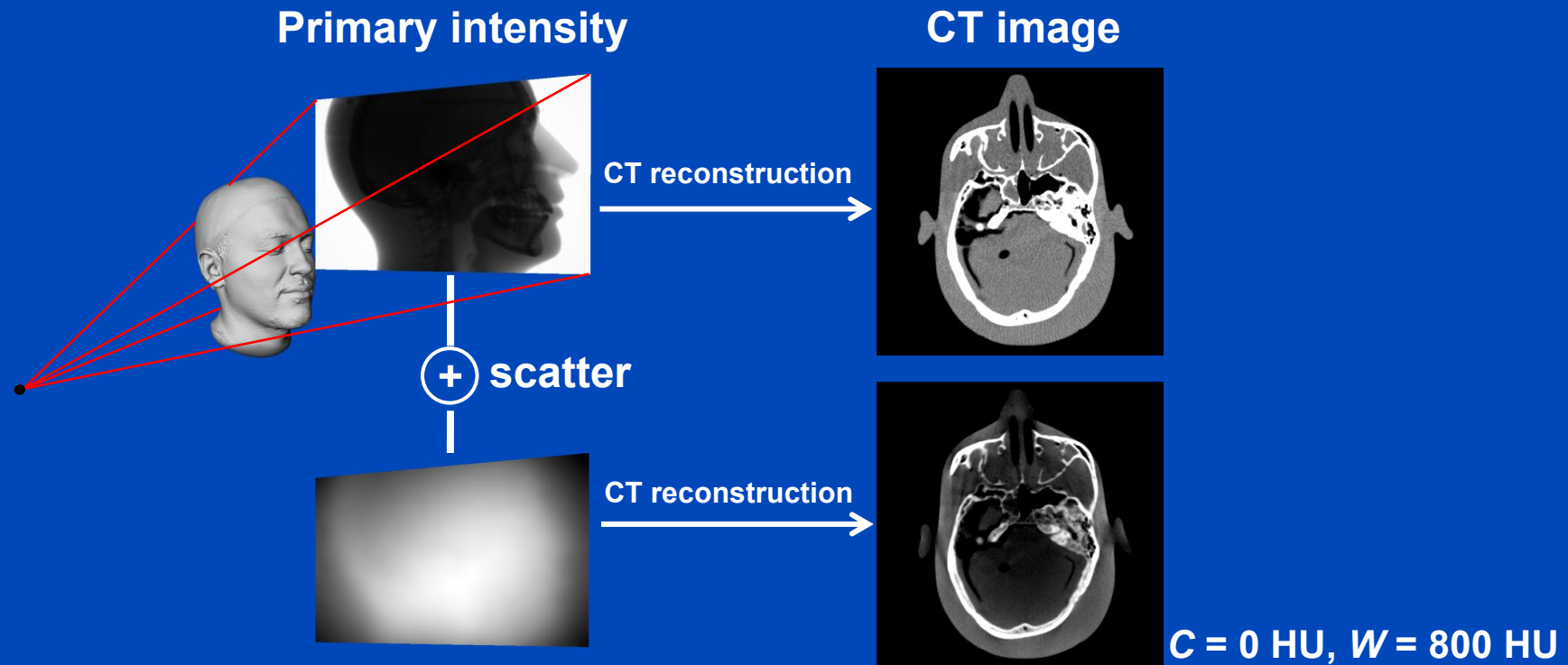
**Joscha Maier**

whose paper has been recognized as  
one of the most read in

Medical Physics

# Motivation

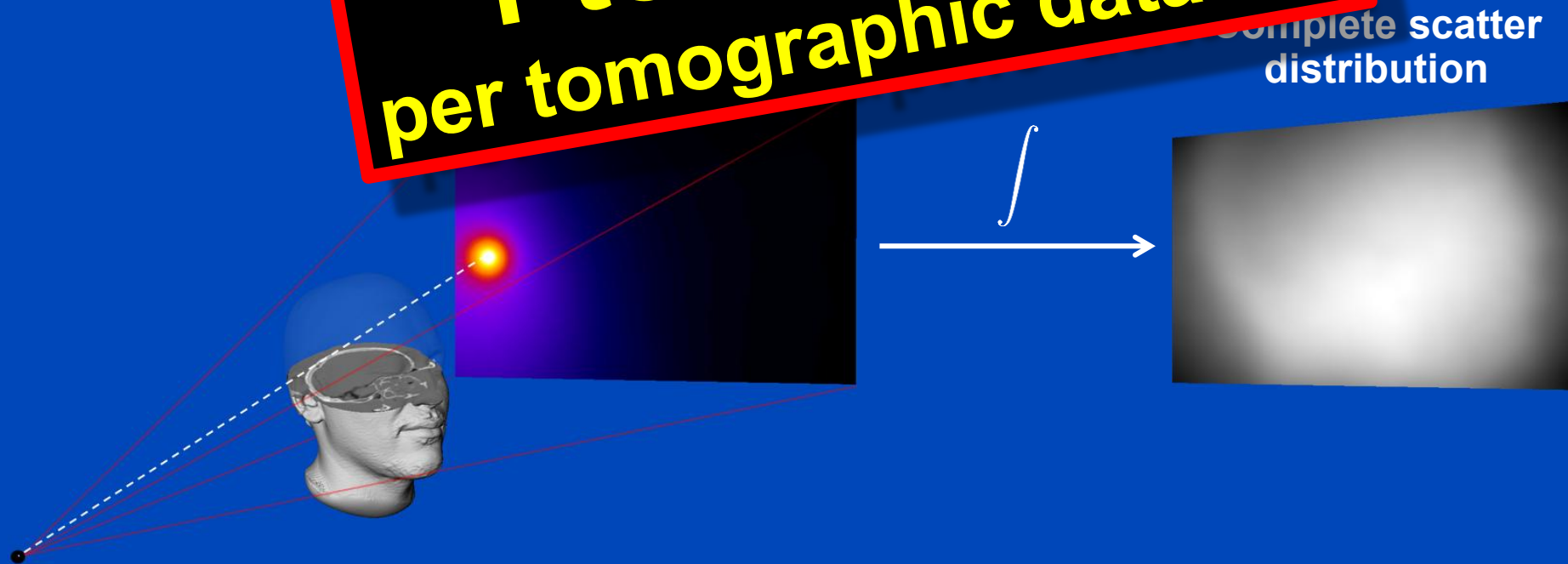
- X-ray scatter is a major cause of artifacts in CT and CBCT.
- Appropriate scatter correction is crucial to maintain the diagnostic value of the CT examination.



# Monte Carlo Scatter Estimation

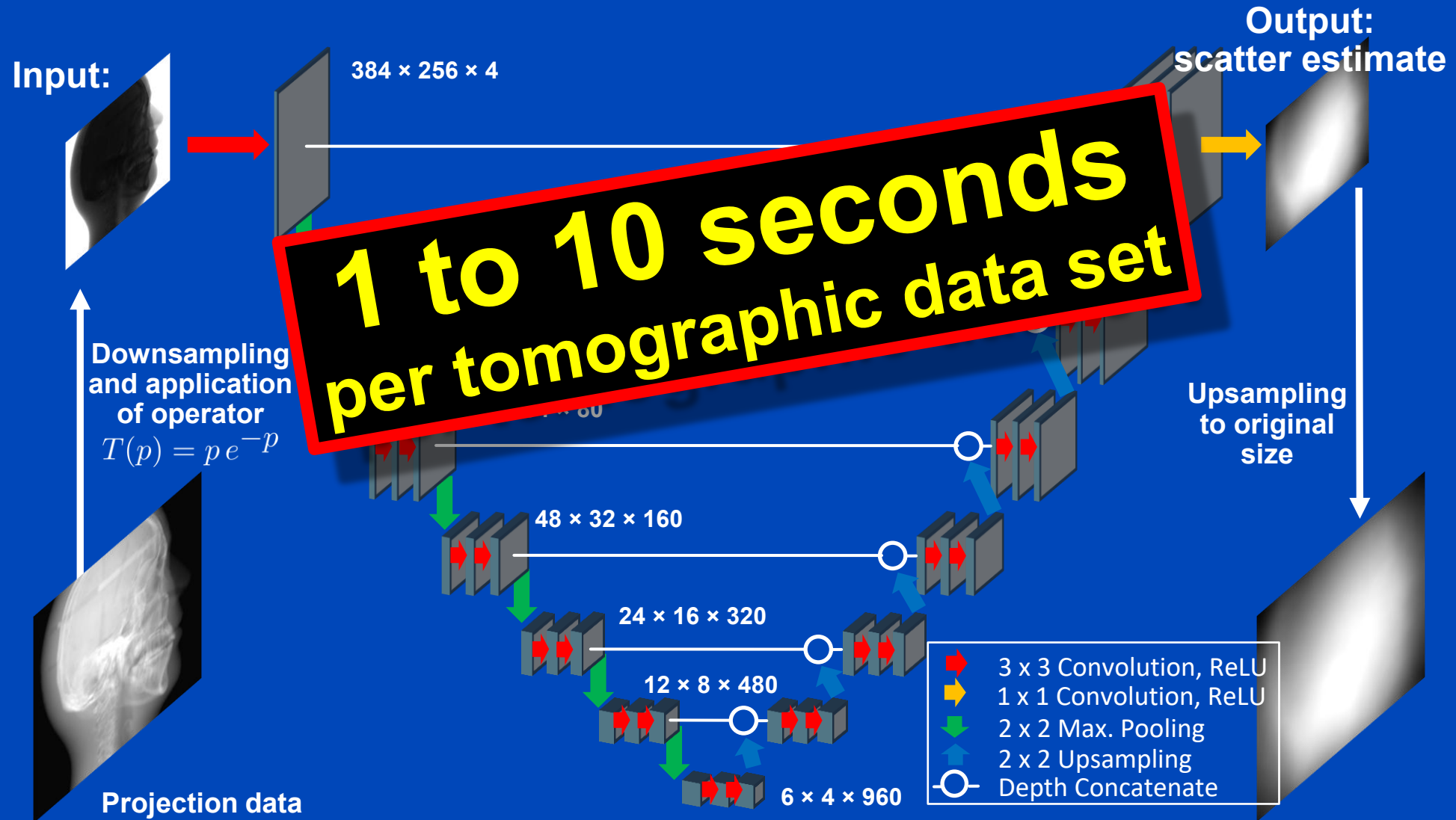
- Simulation of photon trajectories according to physical interaction probabilities.
- Simulating a large number of photons  $N$  approximates the actual scatter distribution.

**1 to 10 hours  
per tomographic data set**

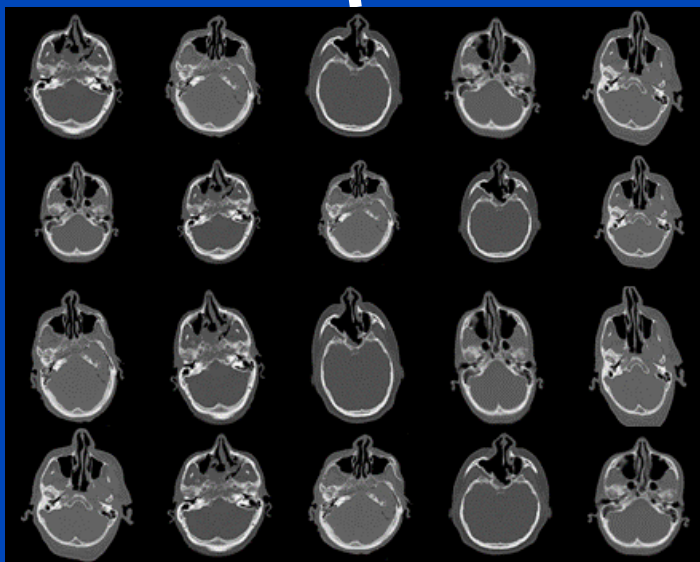
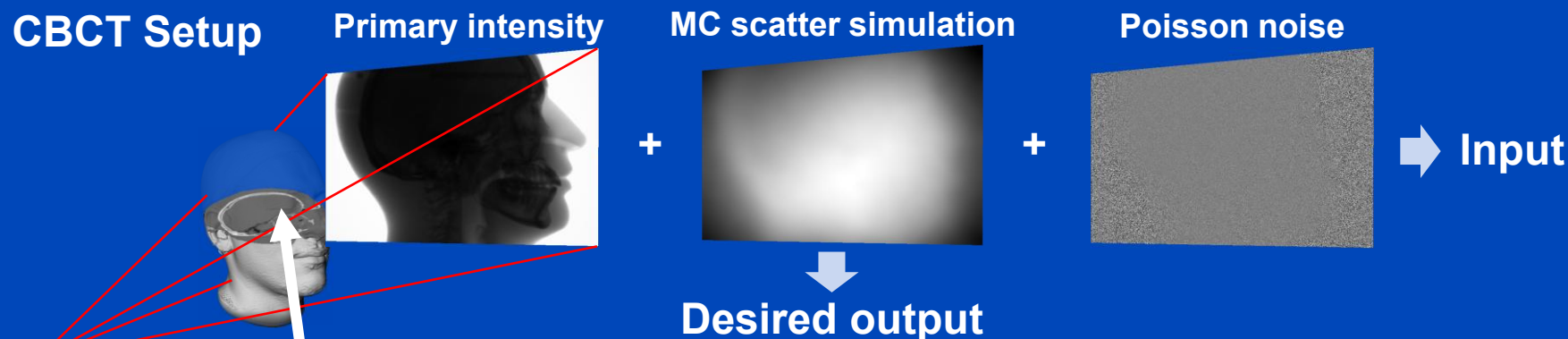


# Deep Scatter Estimation

## Network architecture & scatter estimation framework

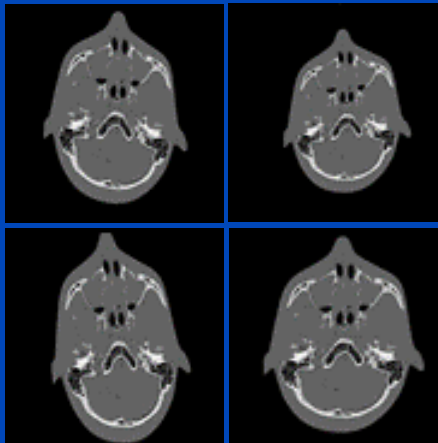
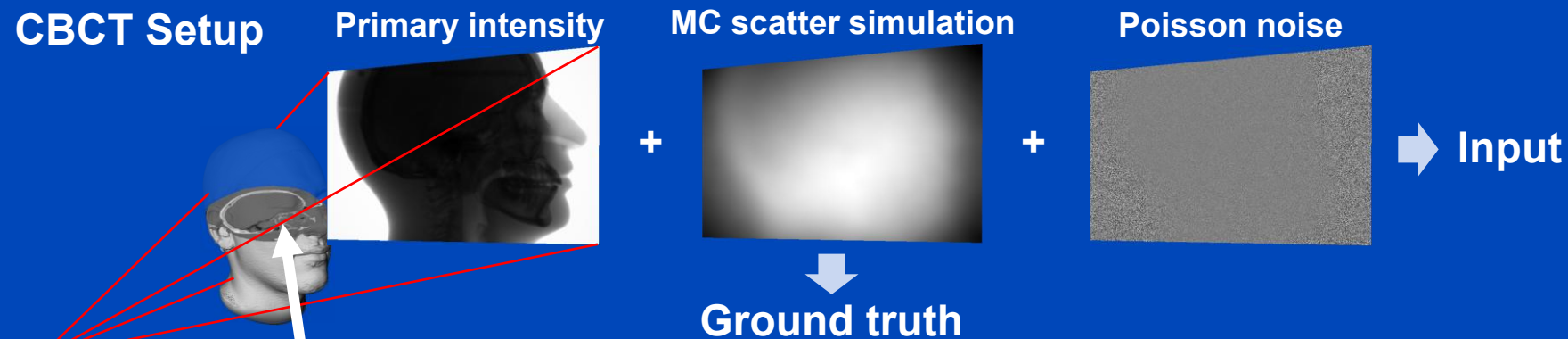


# Training the DSE Network



- **Simulation of 6000 projections using different heads and acquisition parameters (80 kV, ..., 140 kV in steps of 20 kV).**
- **Splitting into 80% training and 20% validation data.**
- **Mean  $S/P = 0.9$**
- **90<sup>th</sup> percentile  $S/P = 1.32$**
- **Training minimizes MSE pixel-wise loss on a GeForce GTX 1080 for 80 epochs.**

# Testing of the DSE Network for Simulated Data (at 120 kV)



- Application of the DSE network to predict scatter for simulated data of a head (different from training data).

# Results on Simulated Projection Data

	Primary intensity	Scatter ground truth (GT)	(Kernel - GT) / GT	(Hybrid - GT) / GT	(DSE - GT) / GT
View #1			<b>14.1%</b> mean absolute percentage error over all projections	<b>7.2%</b> mean absolute percentage error over all projections	<b>1.2%</b> mean absolute percentage error over all projections
View #2			<b>14.1%</b> mean absolute percentage error over all projections	<b>7.2%</b> mean absolute percentage error over all projections	<b>1.2%</b> mean absolute percentage error over all projections
View #3			<b>14.1%</b> mean absolute percentage error over all projections	<b>7.2%</b> mean absolute percentage error over all projections	<b>1.2%</b> mean absolute percentage error over all projections
View #4			<b>14.1%</b> mean absolute percentage error over all projections	<b>7.2%</b> mean absolute percentage error over all projections	<b>1.2%</b> mean absolute percentage error over all projections
View #5			<b>14.1%</b> mean absolute percentage error over all projections	<b>7.2%</b> mean absolute percentage error over all projections	<b>1.2%</b> mean absolute percentage error over all projections
	<b>C = 0.5, W = 1.0</b>	<b>C = 0.04, W = 0.04</b>	<b>C = 0%, W = 50%</b>	<b>C = 0%, W = 50%</b>	<b>C = 0%, W = 50%</b>

DSE trained to estimate scatter from **primary plus scatter**: High accuracy

# Results on Simulated Projection Data

	Primary intensity	Scatter ground truth (GT)	(Kernel - GT) / GT	(Hybrid - GT) / GT	(DSE - GT) / GT
View #1			<b>14.1%</b> mean absolute percentage error over all projections	<b>7.2%</b> mean absolute percentage error over all projections	<b>6.4%</b> mean absolute percentage error over all projections
View #2					
View #3					
View #4					
View #5					

**DSE, in its present form, needs to see scatter in its input data!**

**C = 0.5, W = 1.0**    **C = 0.04, W = 0.04**    **C = 0%, W = 50%**    **C = 0%, W = 50%**    **C = 0%, W = 50%**

DSE trained to estimate scatter from **primary only**: Low accuracy

# Results on Simulated Projection Data

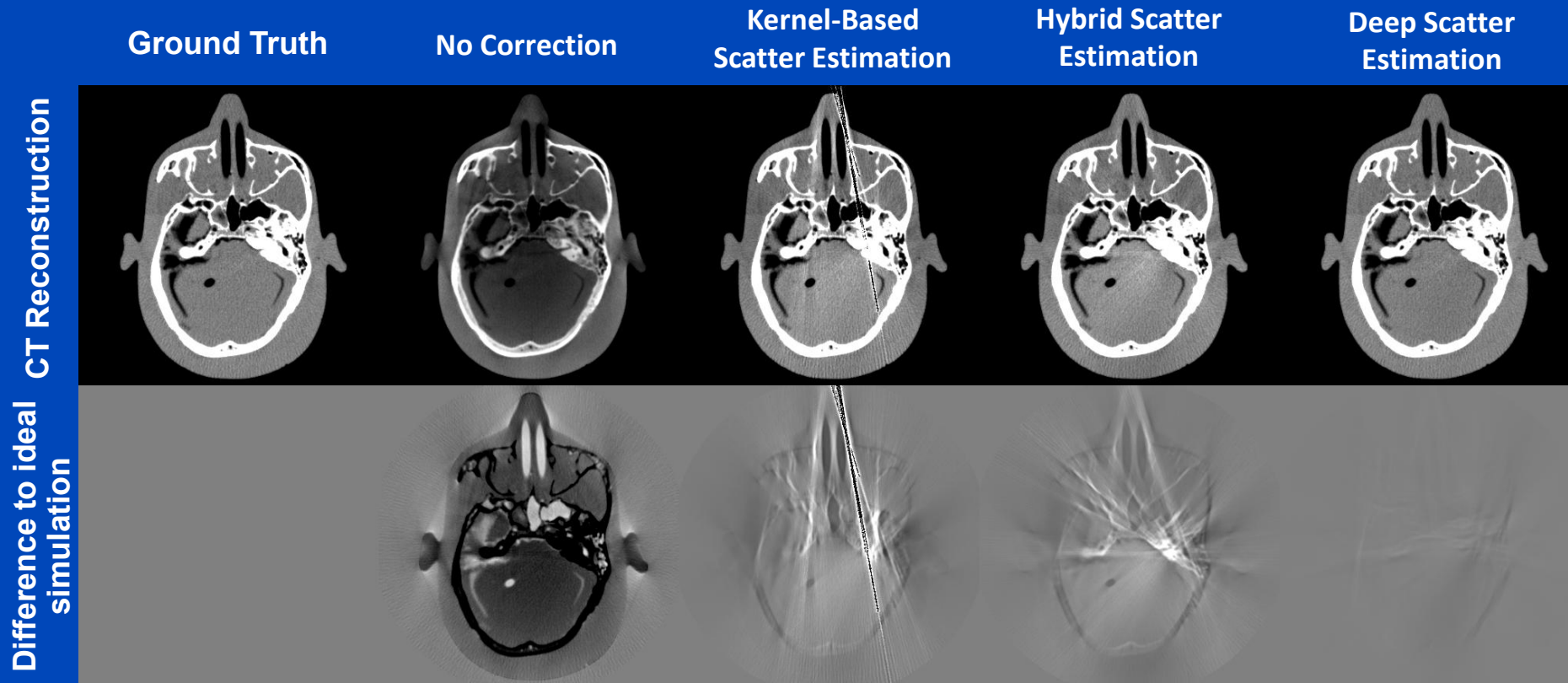
	Primary intensity	Scatter ground truth (GT)	(Kernel - GT) / GT	(Hybrid - GT) / GT	(DSE - GT) / GT
View #1			<b>14.1%</b> mean absolute percentage error over all projections	<b>7.2%</b> mean absolute percentage error over all projections	<b>1.2%</b> mean absolute percentage error over all projections
View #2					
View #3					
View #4					
View #5					

**DSE, in its present form, needs to see scatter in its input data!**

**C = 0.5, W = 1.0**    **C = 0.04, W = 0.04**    **C = 0%, W = 50%**    **C = 0%, W = 50%**    **C = 0%, W = 50%**

DSE trained to estimate scatter from **primary plus scatter**: High accuracy

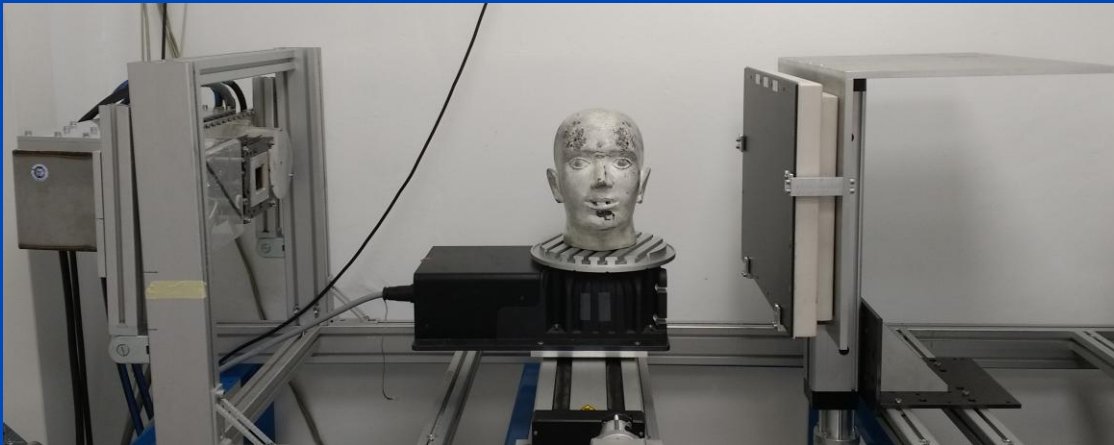
# Reconstructions of Simulated Data



$C = 0 \text{ HU}, W = 1000 \text{ HU}$

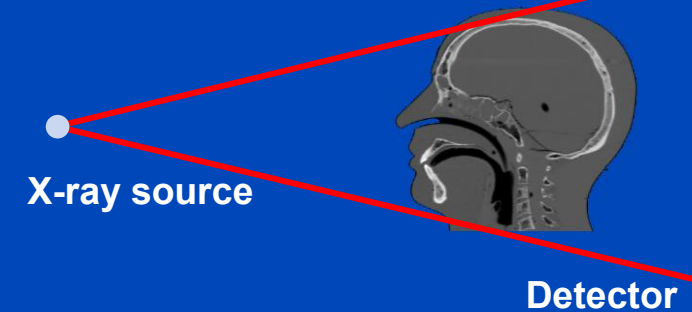
# Testing of the DSE Network for Measured Data (120 kV)

DKFZ table-top CT

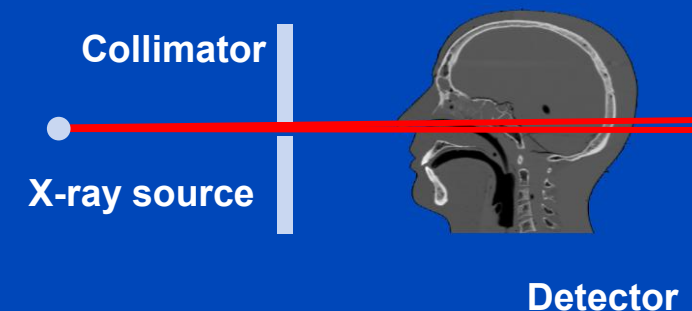


- Measurement of a head phantom at our in-house table-top CT.
- Slit scan measurement serves as ground truth.

Measurement to be corrected

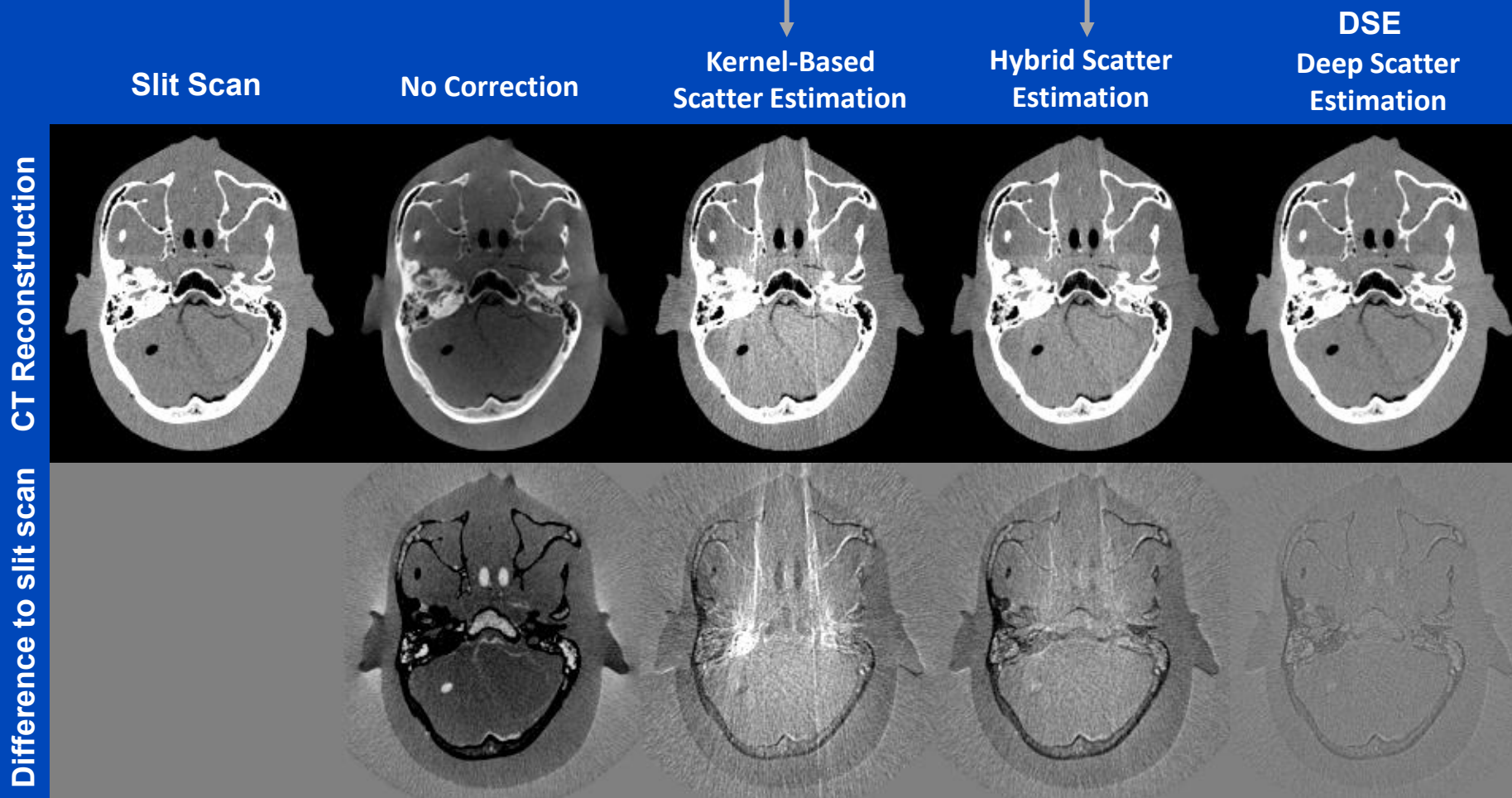


Ground truth: slit scan



# Reconstructions of Measured Data

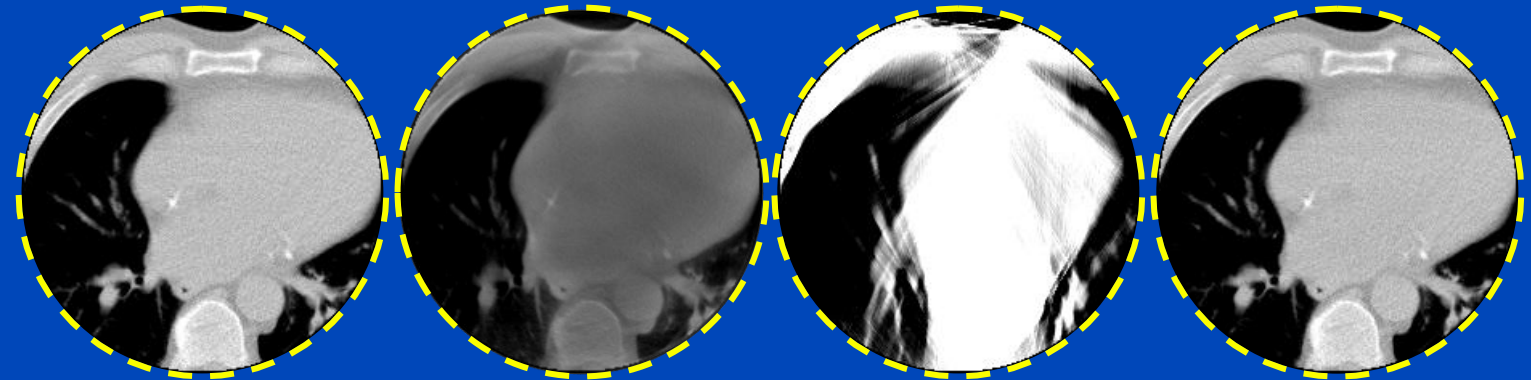
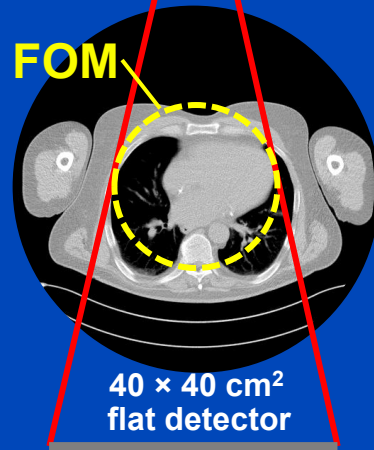
Parameters of the two comparison methods trained in the same way as those of DSE: same data, same loss function, same optimization algorithm.



$C = 0 \text{ HU}$ ,  $W = 1000 \text{ HU}$

A simple detruncation was applied to the rawdata before reconstruction. Images were clipped to the FOM before display.  $C = -200$  HU,  $W = 1000$  HU.

# Truncated DSE

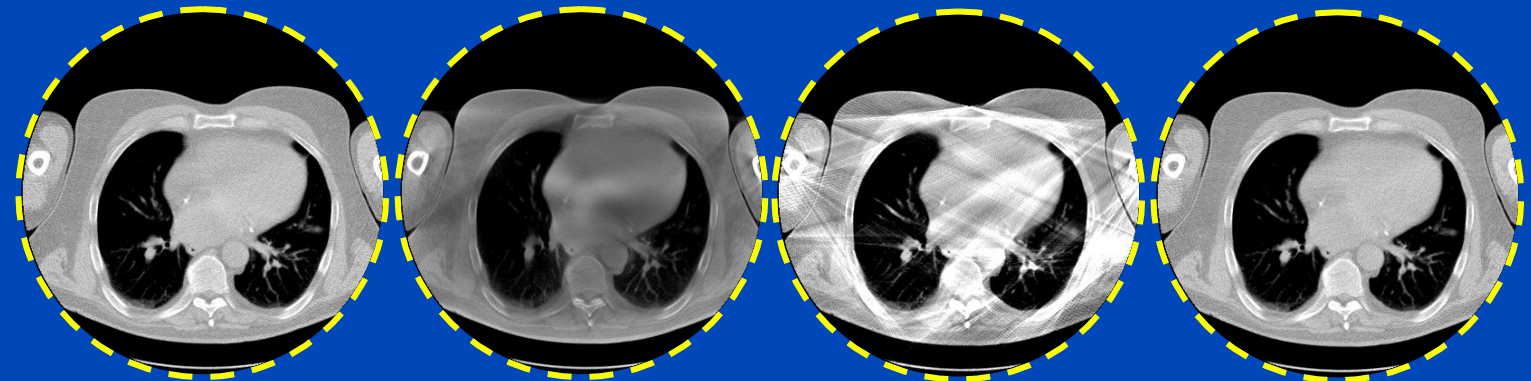
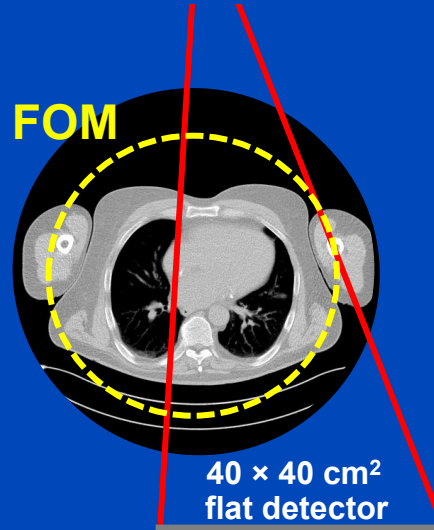


Ground truth

Uncorrected

MC-corrected

DSE



To learn why MC fails at truncated data and what significant efforts are necessary to cope with that situation see [Kachelrieß et al. Effect of detruncation on the accuracy of MC-based scatter estimation in truncated CBCT. Med. Phys. 45(8):3574-3590, August 2018].

# Does DSE Generalize to Different Anatomical Regions?

- **DSE:**

<b>DSE</b>	Head	Thorax	Abdomen
Head	1.2	21.1	32.7
Thorax	8.8	1.5	9.1
Abdomen	11.9	10.9	1.3
All data	1.8	1.4	1.4

Values shown are the mean absolute percentage errors (MAPEs) of the testing data.  
Note that thorax and head suffer from truncation due to the small size of the 40×30 cm flat detector.

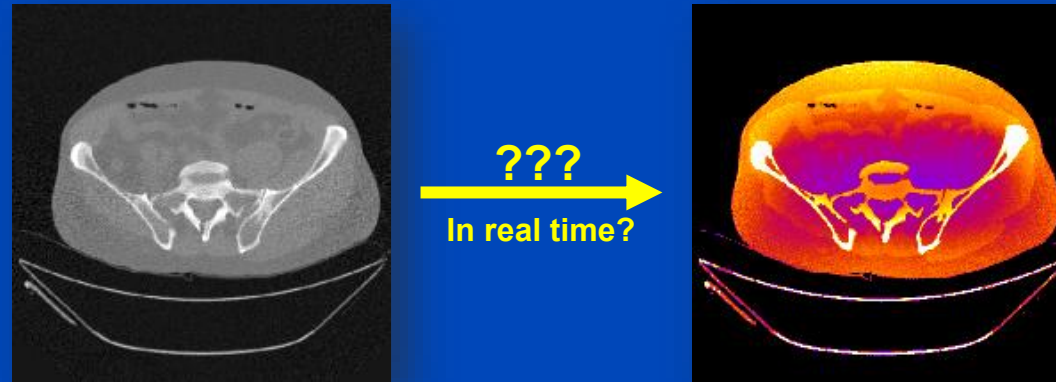
- **KSE** (“trained” using the same data):

<b>KSE</b>	Head	Thorax	Abdomen
Head	14.5	26.8	32.5
Thorax	16.2	18.5	19.4
Abdomen	16.8	22.1	17.8
All data	14.9	20.5	19.3

# Conclusions on DSE

- DSE needs about 3 ms per CT and 10 ms per CBCT projection (as of 2020).
- DSE is a fast and accurate alternative to MC simulations.
- DSE outperforms kernel-based approaches in terms of accuracy and speed.
- Facts:
  - DSE can estimate scatter from a single (!) x-ray image.
  - DSE can accurately estimate scatter from a primary+scatter image.
  - DSE generalizes to all anatomical regions.
  - DSE works for geometries and beam qualities differing from training.
  - DSE may outperform MC even though DSE is trained with MC.
- DSE is not restricted to reproducing MC scatter estimates.
- DSE can rather be trained with any other scatter estimate, including those based on measurements.

# Deep Dose Estimation



**RESEARCH ARTICLE****MEDICAL PHYSICS**

# Real-time estimation of patient-specific dose distributions for medical CT using the deep dose estimation

Joscha Maier<sup>1</sup> | Laura Klein<sup>1,2</sup> | Elias Eulig<sup>1,2</sup> | Stefan Sawall<sup>1,2</sup> |  
Marc Kachelrieß<sup>1,2</sup>

<sup>1</sup> German Cancer Research Center (DKFZ), Heidelberg, Germany

<sup>2</sup> Ruprecht-Karls-University, Heidelberg, Germany

**Correspondence**

Joscha Maier, German Cancer Research Center (DKFZ), Heidelberg, Germany.  
Email: [joscha.maier@dkfz.de](mailto:joscha.maier@dkfz.de)

**Funding information**

Deutsche Forschungsgemeinschaft,  
Grant/Award Number: KA 1678/24

**Abstract**

**Purpose:** With the rising number of computed tomography (CT) examinations and the trend toward personalized medicine, patient-specific dose estimates are becoming more and more important in CT imaging. However, current approaches are often too slow or too inaccurate to be applied routinely. Therefore, we propose the so-called deep dose estimation (DDE) to provide highly accurate patient dose distributions in real time

**Methods:** To combine accuracy and computational performance, the DDE algorithm uses a deep convolutional neural network to predict patient dose distributions. To do so, a U-net like architecture is trained to reproduce Monte Carlo simulations from a two-channel input consisting of a CT reconstruction and a

# Why Dose Distributions?

- **Useful to study dose reduction techniques**
  - Tube current modulation
  - Prefiltration and shaped filtration
  - Tube voltage settings
  - ...
- **Useful to estimate patient dose**
  - Risk assessment requires segmentation of the organs
  - Often semiantropomorphic patient models take over
  - The infamous k-factors that convert DLP into  $D_{\text{eff}}$  are derived this way, e.g.  $k_{\text{chest}} = 0.014 \text{ mSv/mGy/cm}$
  - ...
- **Useful for patient-specific CT scan protocol optimization**
- **However: Dose estimation is often said not to work in real time.**

# Classical Patient-Specific Dose Estimation

- **Accurate solutions:**
  - Monte Carlo (MC) simulation<sup>1</sup>, **gold standard**, stochastic LBTE solver
  - Analytic linear Boltzmann transport equation (LBTE) solver<sup>2</sup>
    - **Accurate but computationally expensive**
- **Fast alternatives:**
  - Application of patient-specific conversion factors to the DLP<sup>3</sup>.
  - Application of look-up tables using MC simulations of phantoms<sup>4</sup>.
  - Analytic approximation of CT dose deposition<sup>5</sup>.
    - **Fast but less accurate**

<sup>1</sup>G. Jarry et al., “A Monte Carlo-based method to estimate radiation dose from spiral CT”, Phys. Med. Biol. 48, 2003.

<sup>2</sup>A. Wang et al., “A fast, linear Boltzmann transport equation solver for computed tomography dose calculation (Acuros CTD)”. Med. Phys. 46(2), 2019.

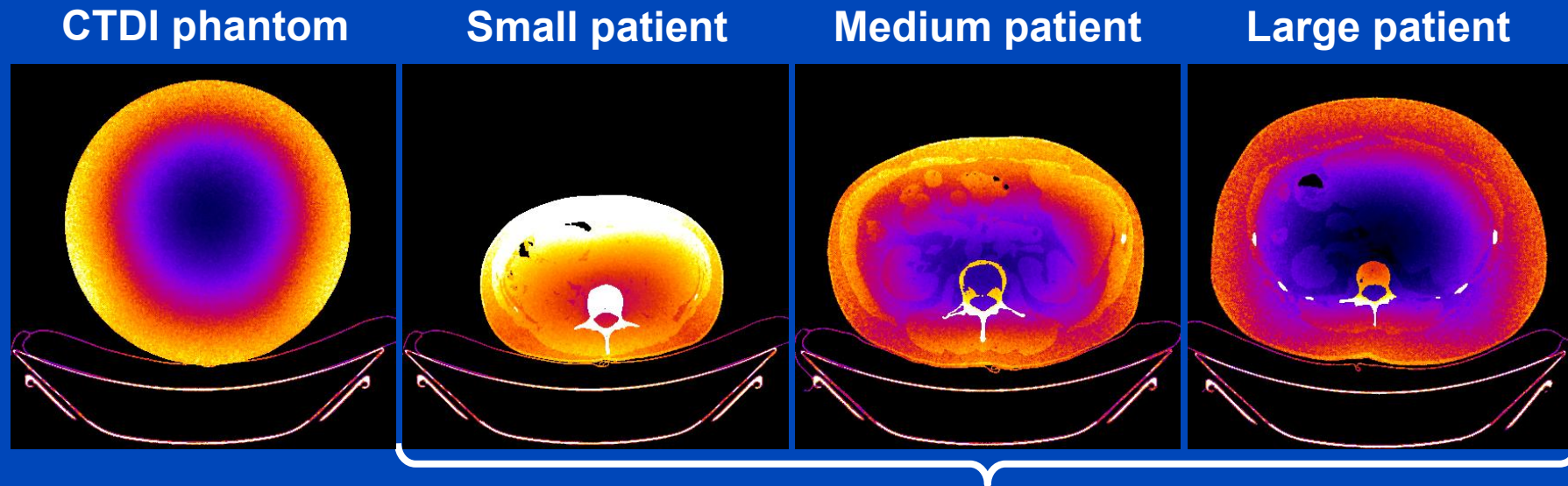
<sup>3</sup>B. Moore et al., “Size-specific dose estimate (SSDE) provides a simple method to calculate organ dose for pediatric CT examinations”, Med. Phys. 41, 2014.

<sup>4</sup>A. Ding et al., “VirtualDose: a software for reporting organ doses from CT for adult and pediatric patients”, Phys. Med. Biol. 60, 2015.

<sup>5</sup>B. De Man, “Dose reconstruction for real-time patient-specific dose estimation in CT”, Med. Phys. 42, 2015.

# Motivation

- The potential risk of ionizing radiation makes dose assessment an important issue in CT imaging.
- Limitation of common metrics (e.g.  $CTDI_w$ ,  $CTDI_{vol}$ , DLP, k-factor, SSDE, ...) to provide information on organ or patient dose.

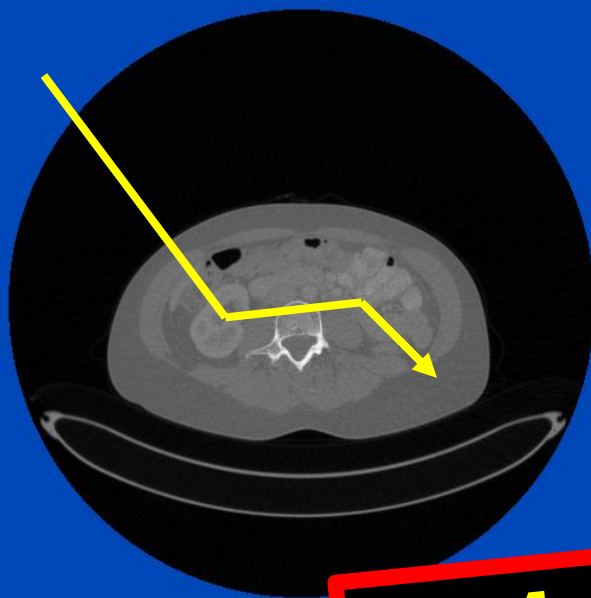


Same CTDI, but different dose distribution

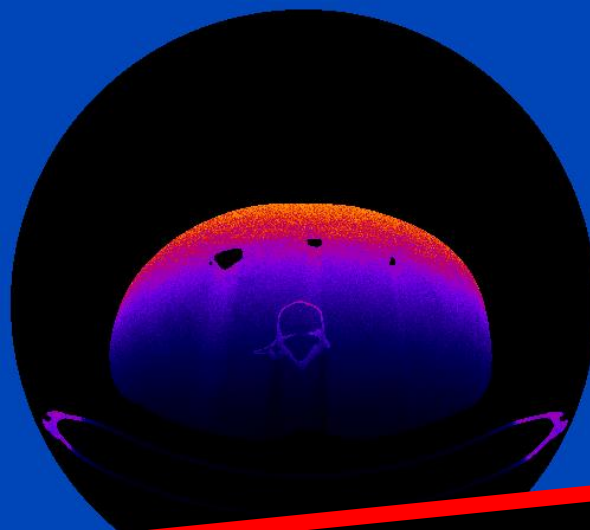
Dose values in air voxels are set to zero (black) in this presentation.

# MC Dose Simulation for a 360° Scan

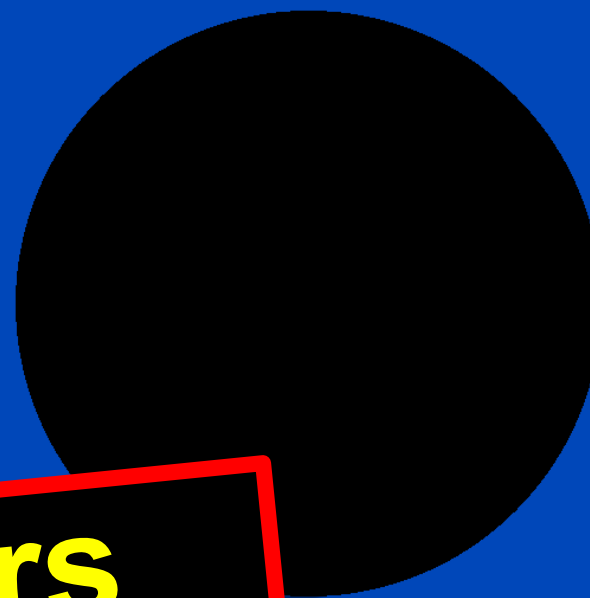
Patient



Dose per Projection



Cumulative Dose

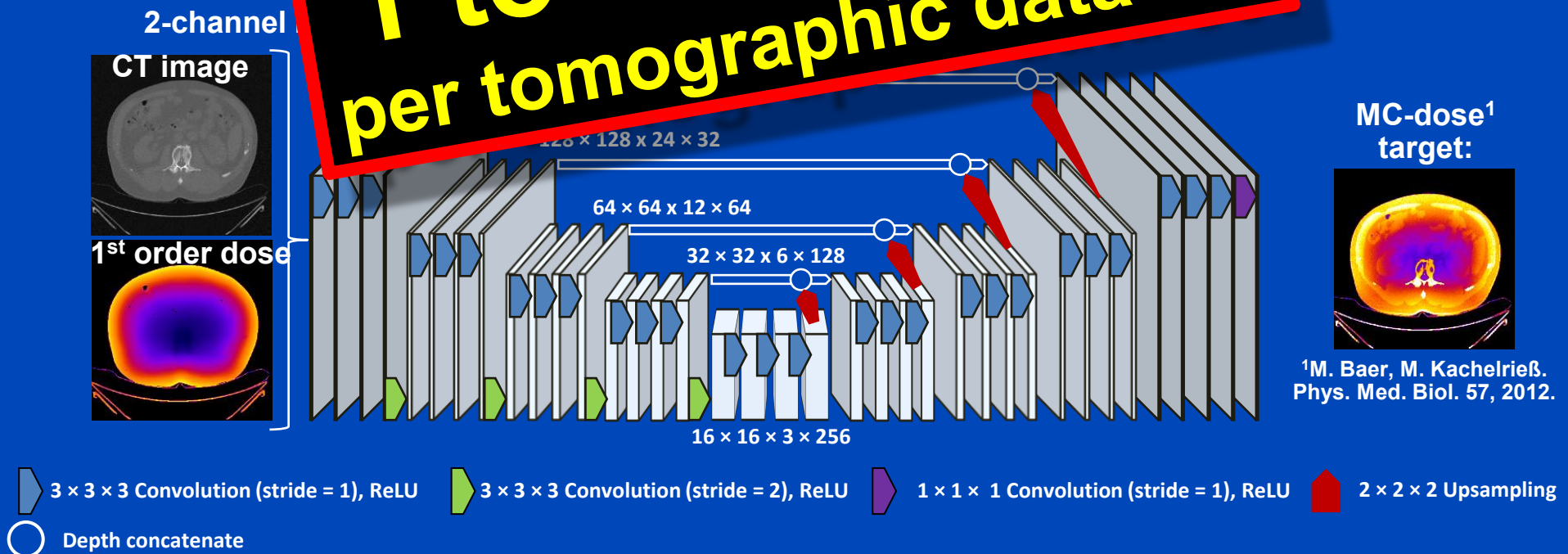


**1 to 10 hours  
per tomographic data set**

# Deep Dose Estimation (DDE)

- Combine fast and accurate CT dose estimation using a deep convolutional neural network.
- Train the network to reproduce MC-dose given the CT image and a first-order dose.

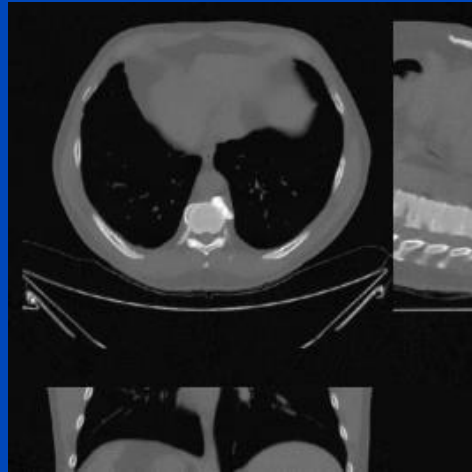
**1 to 10 seconds per tomographic data set**



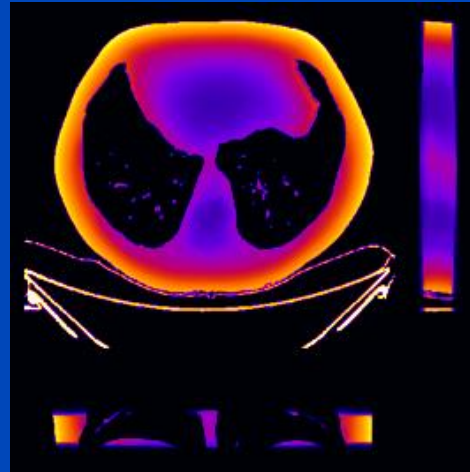
# Results

Thorax, tube A, 120 kV, no bowtie

CT image



First order dose

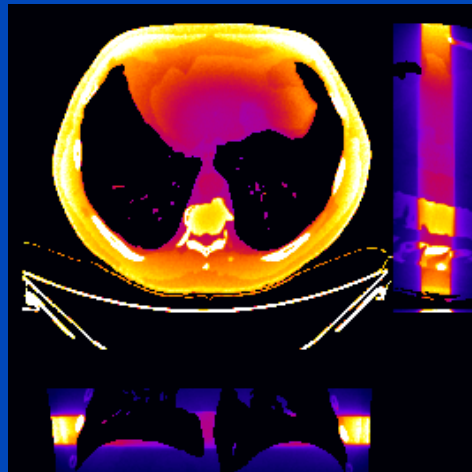


	MC	DDE
48 slices	1 h	0.25 s
whole body	20 h	5 s

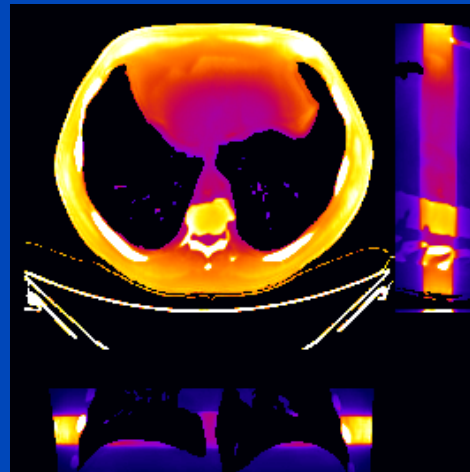
MC uses 16 CPU kernels  
DDE uses one Nvidia Quadro P600 GPU

DDE training took 74 h for 300 epochs,  
1440 samples, 48 slices per sample

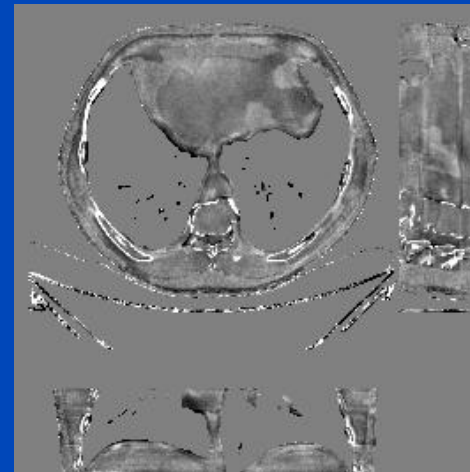
MC ground truth



DDE



Relative error

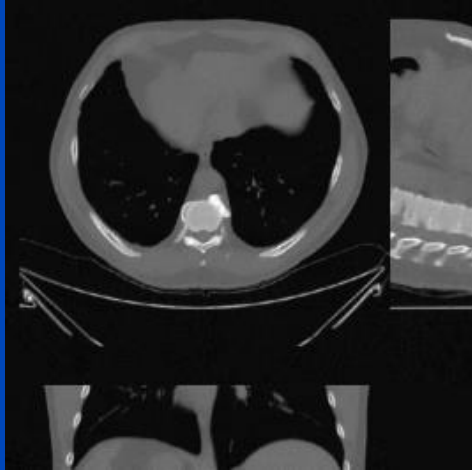


C = 0%  
W = 40%

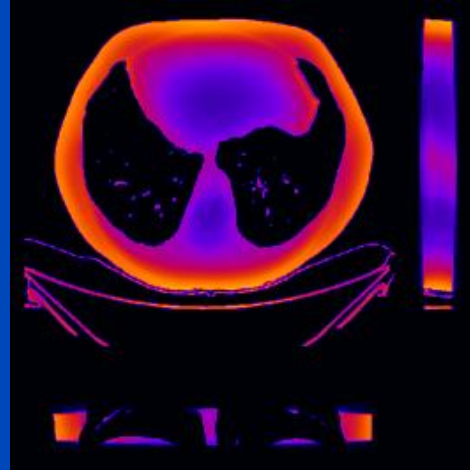
# Results

Thorax, tube B, 120 kV, no bowtie

CT image



First order dose

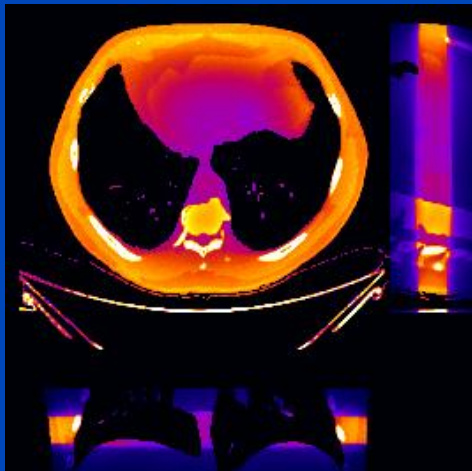


	MC	DDE
48 slices	1 h	0.25 s
whole body	20 h	5 s

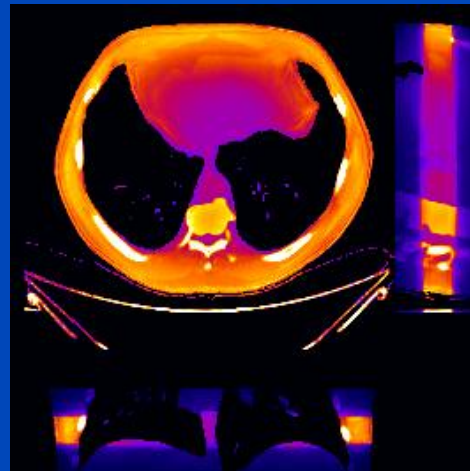
MC uses 16 CPU kernels  
DDE uses one Nvidia Quadro P600 GPU

DDE training took 74 h for 300 epochs,  
1440 samples, 48 slices per sample

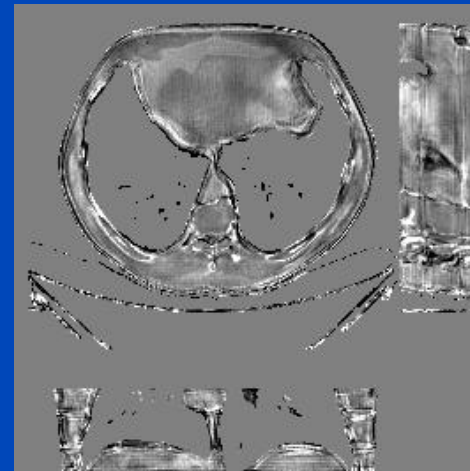
MC ground truth



DDE



Relative error



C = 0%  
W = 40%

# Comments for Practical Use

- **DDE needs to use the actual**
  - x-ray spectrum (not available in DICOM)
  - scan trajectory (not available in DICOM)
- **The patient volume**
  - must laterally show the full patient cross-section
  - should longitudinally show the scanned range plus, say, 10 cm at each end.

Monte Carlo (180 min)

Compute times as of 2021

Deep Dose Estimation (2 s)

Percentage Error

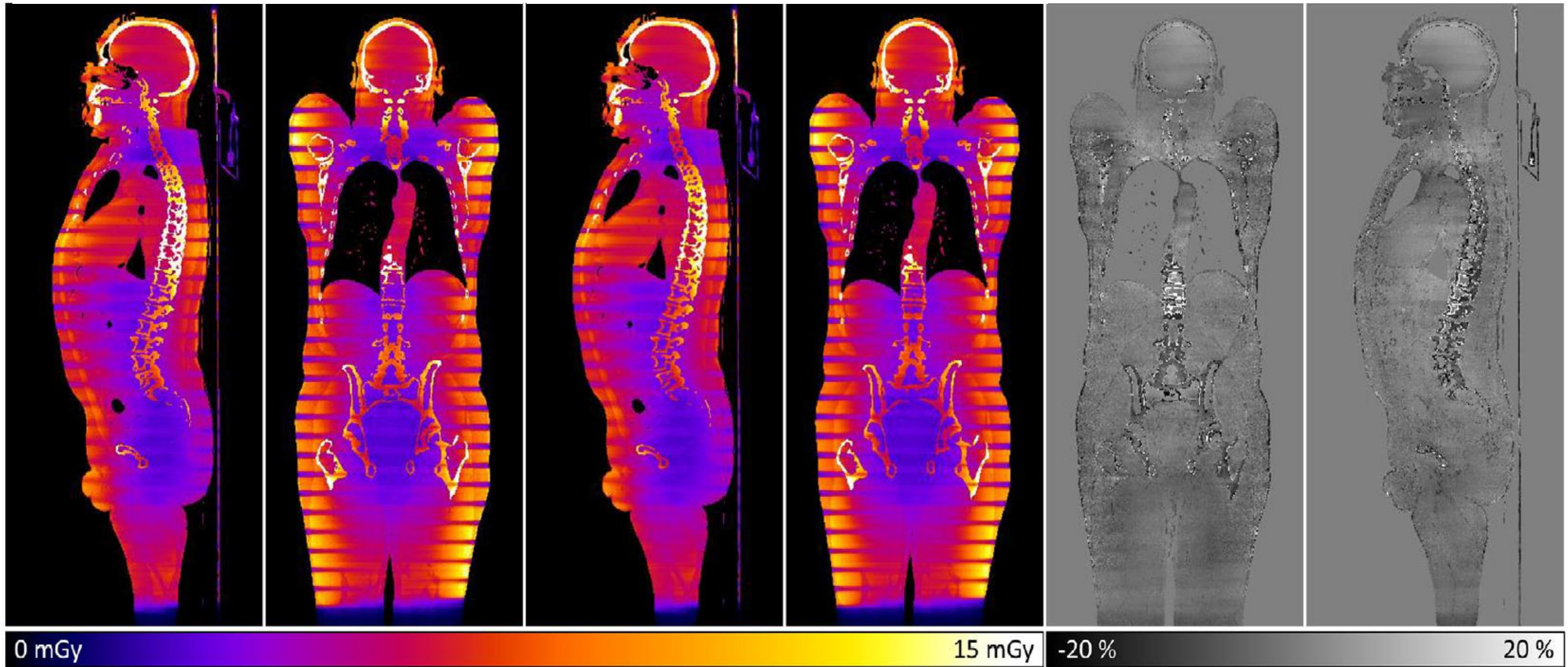


**FIGURE 5** Sagittal and coronal view of the dose distribution of a 100 kV whole-body spiral computed tomography (CT) scan including a bowtie filter and an angular tube current modulation. Here, the two left columns show the ground truth, the middle columns show the deep dose estimation (DDE) prediction and the two right columns the corresponding percentage error. Note that dose to air is neglected for computational reasons, and therefore, displayed as zero

# Conclusions on DDE

- **DDE provides accurate dose predictions**
  - for circle scans
  - for sequence scans
  - for partial scans (less than 360°)
  - for limited angle scans (less than 180°)
  - for spiral scans
  - for different tube voltages
  - for scans with and without bowtie filtration
  - for scans with tube current modulation
  - for DSCT scanners, i.e. with large (A) and small (B) detector
- **In practice it may therefore be not necessary to perform separate training runs for these cases.**
- **Thus, accurate real-time patient dose estimation may become feasible with DDE.**

# OTHER APPLICATIONS

# Patient Risk-Minimizing Tube Current Modulation (riskTCM)

## 1. Coarse reconstruction from two scout views

- E.g. X. Ying, et al. X2CT-GAN: Reconstructing CT from biplanar x-rays with generative adversarial networks. CVPR 2019.

## 2. Segmentation of radiation-sensitive organs

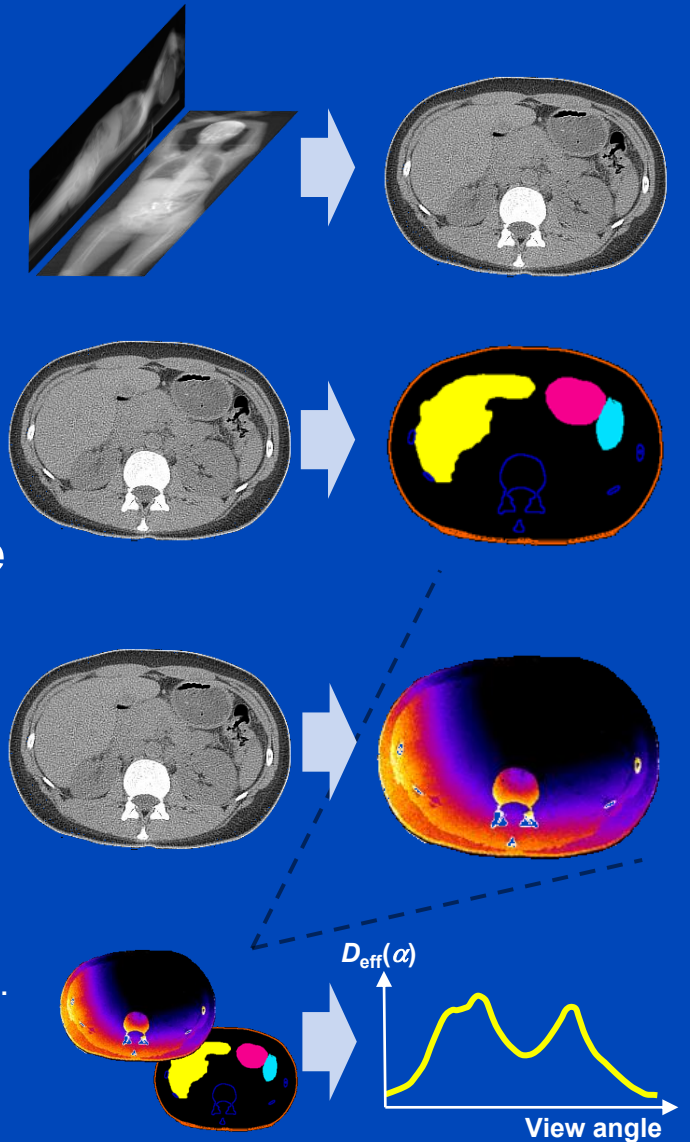
- E.g. S. Chen, M. Kachelrieß et al., Automatic multi-organ segmentation in dual-energy CT (DECT) with dedicated 3D fully convolutional DECT networks. Med. Phys. 2019.

## 3. Calculation of the effective dose per view using the deep dose estimation (DDE)

- J. Maier, E. Eulig, S. Dorn, S. Sawall and M. Kachelrieß. Real-time patient-specific CT dose estimation using a deep convolutional neural network. IEEE Medical Imaging Conference Record, M-03-178: 3 pages, Nov. 2018.

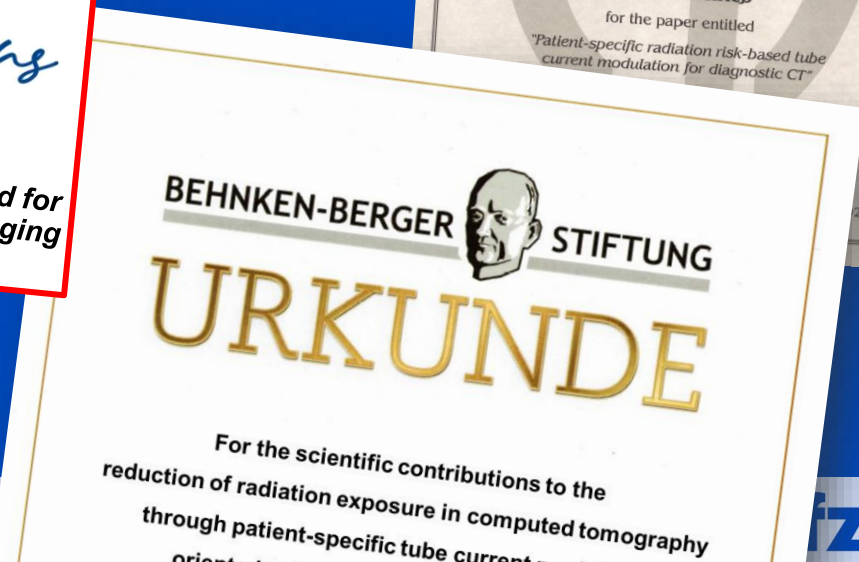
## 4. Determination of the tube current modulation curve that minimizes the radiation risk

- L. Klein, C. Liu, J. Steidel, L. Enzmann, M. Knaup, S. Sawall, A. Maier, M. Lell, J. Maier, and M. Kachelrieß. Patient-specific radiation risk-based tube current modulation for diagnostic CT. Med. Phys. 49(7):4391-4403, July 2022.



# riskTCM Recognition

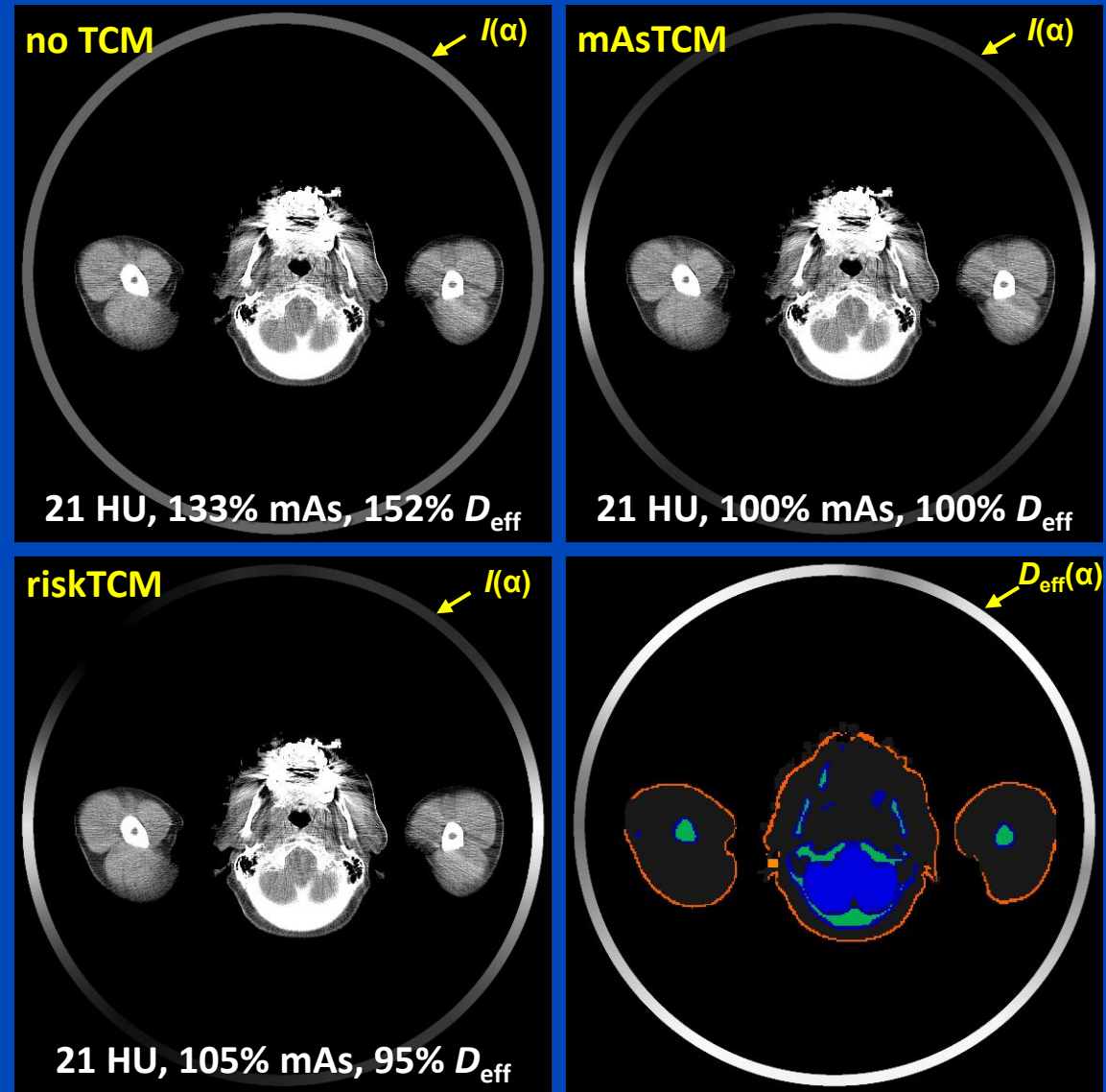
- Editor's Choice in Medical Physics 2022
- Best Research Presentation Award within Physics in Medical Imaging at the European Congress of Radiology (ECR) 2022
- Moses&Sylvia Greenfield Award 2023 for the best scientific paper on imaging in Medical Physics in 2022 (AAPM)
- Behnken-Berger-Award 2023 of the Behnken-Berger Society
- Dr. Franz Holeczke Award 2023 of the Association for Medical Radiation Protection in Austria (VMSÖ)



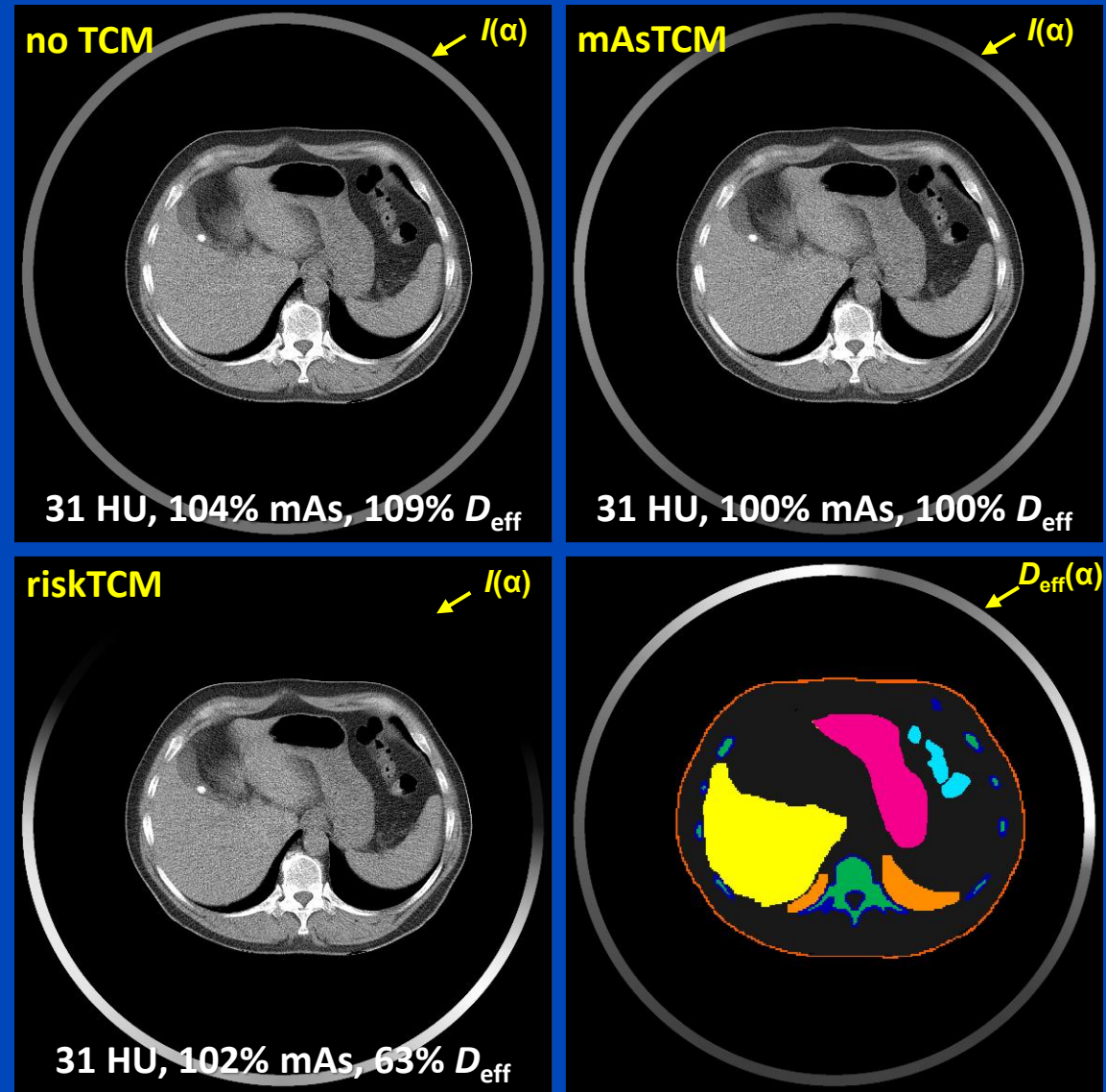
RESEARCH  
Patient-specific radiation risk-based tube current modulation for diagnostic CT  
Laura Klein, Chang Liu, Jörg Steidel, Lucia Enzmann, Michael Knaup, Stefan Sawall, Andreas Maier, Michael Lell, Joscha Maier, Marc Kachelrieß  
First published: 14 April 2022 | <https://doi.org/10.1002/mp.15673> | Citations: 1



Volume 49, Issue 7  
July 2022  
Pages 4391-4403  
This article also appears in:  
Editor's Choice



C = 25 HU, W = 400 HU



C = 25 HU, W = 400 HU

# Effective Dose Values Relative to mAsTCM

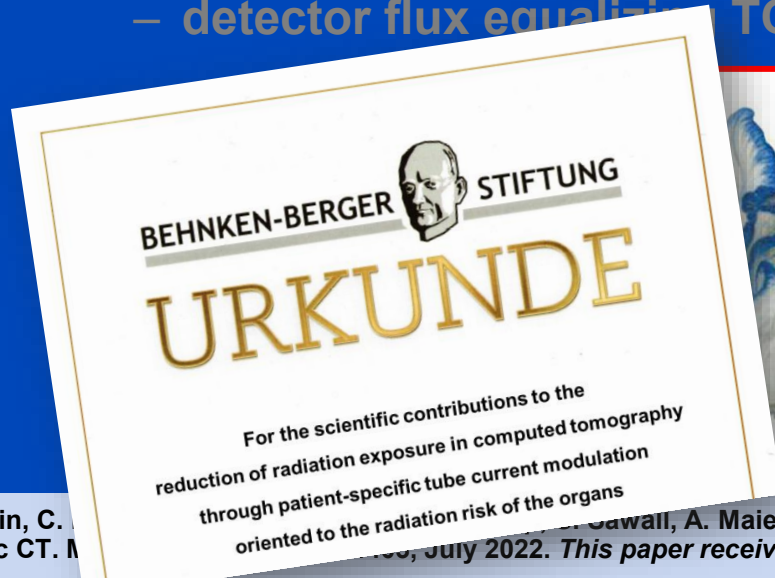
Average over all patients and across all tube voltages (70 to 150 kV)

	noTCM	mAsTCM	riskTCM
Head	110%	100%	92%
Head+Arms	162%	100%	88%
Neck	223%	100%	76%
Thorax	113%	100%	81%
Abdomen	114%	100%	71%
Pelvis	152%	100%	79%

# Conclusions on riskTCM

- Risk-specific TCM minimizes the patient risk.
- With  $D_{\text{eff}}$  as a risk model riskTCM can reduce risk to 30%, compared with the gold standard.
- Other risk models, e.g. organ-specific, weight- and sex-specific models, can be used with riskTCM as well.
- Note:
  - mAsTCM = good for the x-ray tube
  - **riskTCM = good for the patient**
  - detector flux equalizing TCM = good for the detector

**It is up to the vendors to take action!**



## ECR 2022 – Best Research Presentation Abstract

within the topic Physics in Medical Imaging  
with the presentation:

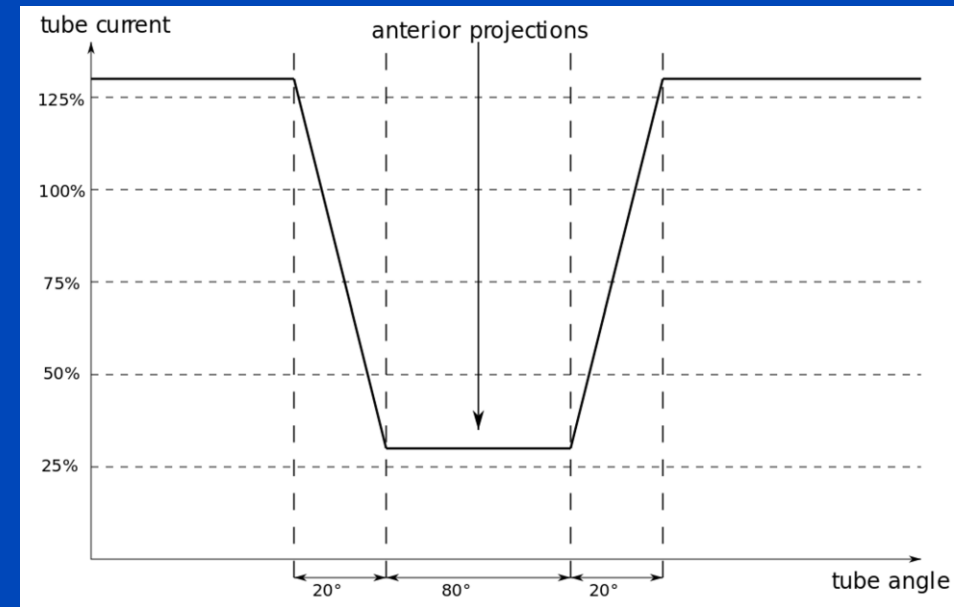
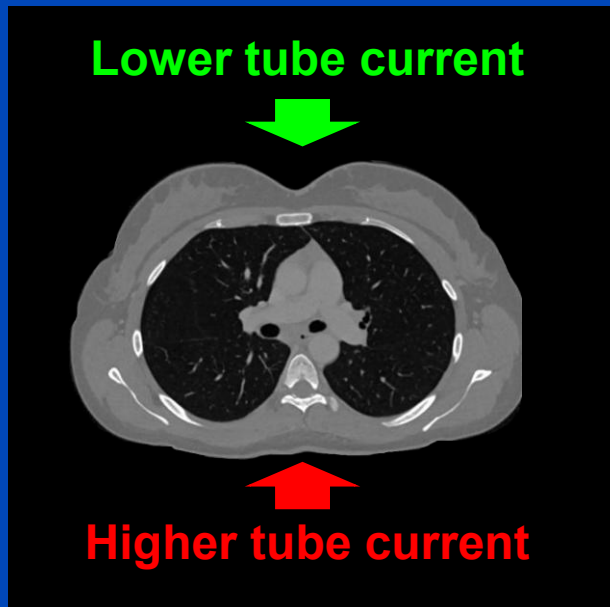
Risk-minimising tube current modulation (riskTCM)  
for CT – potential dose reduction across different  
tube voltages (16765)

L. Klein<sup>1</sup>, C. Liu<sup>2</sup>, J. Steidel<sup>1</sup>, L. Enzmann<sup>1</sup>, S. Sawall<sup>1</sup>, J. Maier<sup>1</sup>,  
A. Maier<sup>2</sup>, M. Lell<sup>3</sup>, M. Kachelrieß<sup>1</sup>; <sup>1</sup>Heidelberg/DE,  
<sup>2</sup>Erlangen/DE, <sup>3</sup>Nuremberg/DE



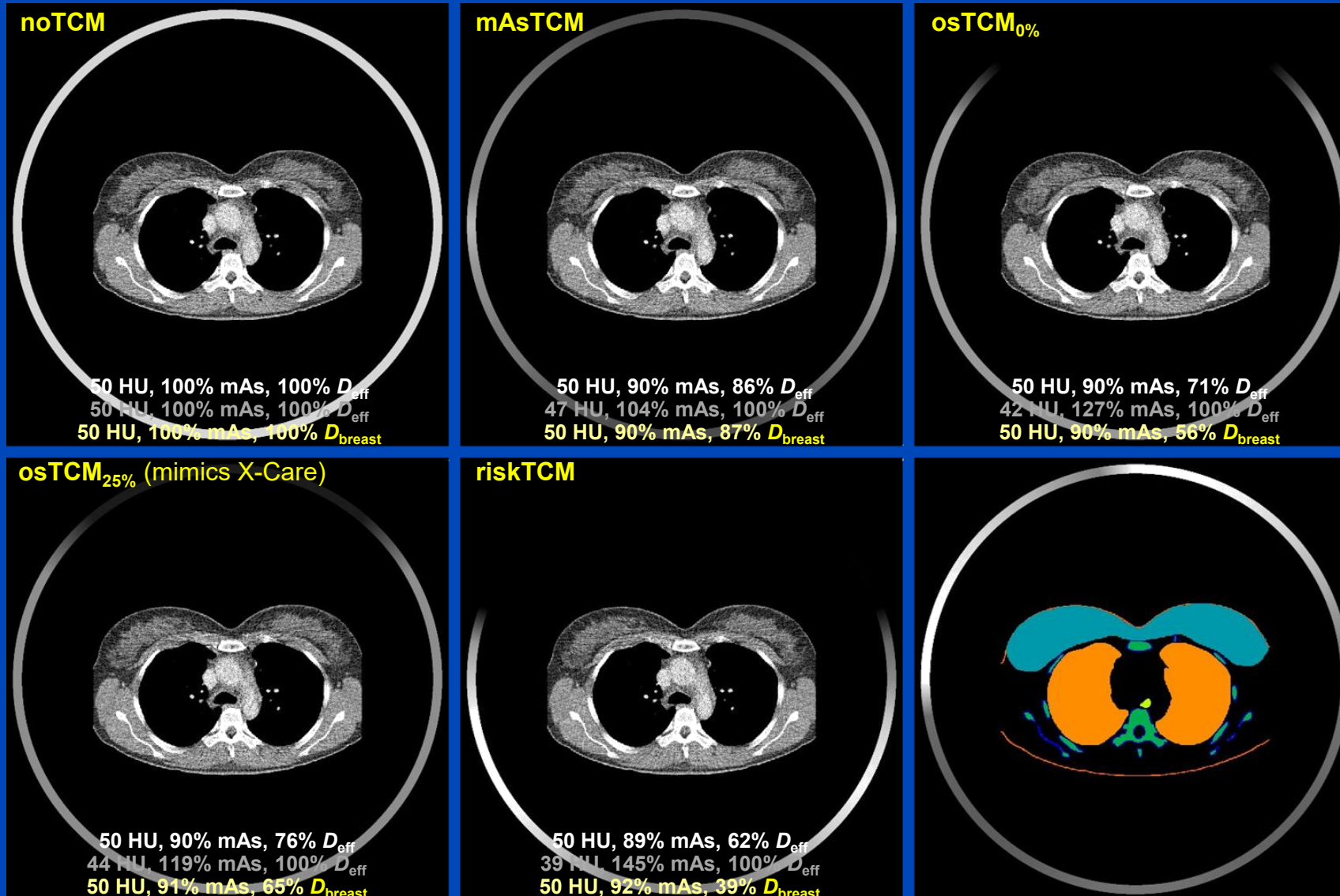
# riskTCM vs. Breast-Specific TCM

- osTCM mimics X-Care (Siemens Healthineers)
- Reduces the tube current to 25% for the anterior 120°
- Higher tube current for the remaining 240°



D. Ketelsen et al. Automated computed tomography dosesaving algorithm to protect radiosensitive tissues: estimation of radiation exposure and image quality considerations. *Invest Radiol*, 47(2):148–52, 2012

# Results



Data courtesy of Prof. Lell, Nürnberg. C = 25 HU, W = 400 HU

# Dose Values for the Thorax at Same Image Noise for 70 kV

Average over all patients

TCM Method	Effective Dose $D_{\text{eff}}$	Dose to the Breast $D_{\text{Breast}}$
noTCM	<b>116%</b> from 111% to 132%	<b>108%</b> from 102% to 125%
mAsTCM	<b>100%</b>	<b>100%</b>
osTCM <sub>25%</sub>	<b>95%</b> from 91% to 100%	<b>77%</b> from 74% to 90%
osTCM <sub>0%</sub>	<b>91%</b> from 83% to 98%	<b>70%</b> from 65% to 87%
riskTCM	<b>77%</b> from 67% to 81%	<b>49%</b> from 40% to 66%

# REGISTRATION AND MOCO

# Deep Cosmetic Motion Artifact Reduction

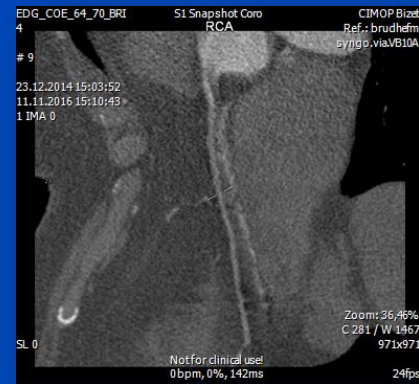
- Image-based correction  
= cosmetic correction  
= similar to pic beauty and others
- May not be the most effective



**Don't do that!  
It's not physical!**

**Stick to estimating  
motion vector  
fields!**

# Deep Cardiac CT MoCo



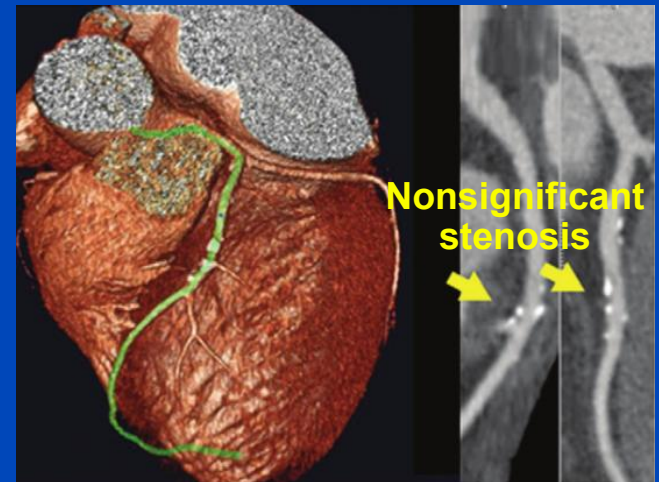
# Motivation

- Cardiac CT imaging is routinely used for the diagnosis of cardiovascular diseases, especially those related to coronary arteries.
- Imaging of coronary arteries places high demands on the spatial and temporal resolution of the CT reconstruction.
- Motion artifacts and image noise may impair the diagnostic value of the CT examination.

CTCA image of the right coronary artery<sup>1</sup>



CTCA image of the left coronary artery<sup>2</sup>



<sup>1</sup>W. B. Meijboom et al., "64-Slice Computed Tomography Coronary Angiography in Patients With High, Intermediate, or Low Pretest Probability of Significant Coronary Artery Disease", *J. Am. Coll. Cardiol.* 50 (15): 1469–1475 (2007).

<sup>2</sup>R. Leta et al., "Ruling Out Coronary Artery Disease with Noninvasive Coronary Multidetector CT Angiography before Noncoronary Cardiovascular Surgery", *Heart* 258 (2) (2011).

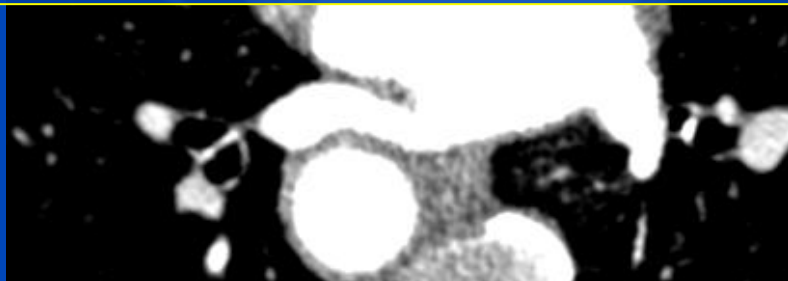
# Motivation



Motion artifacts

High noise

→ Deep learning-based motion compensation to remove motion artifacts.  
→ Iterative reconstruction (Siemens ADMIRE) to reduce noise.



C = 0 HU, W = 1200 HU

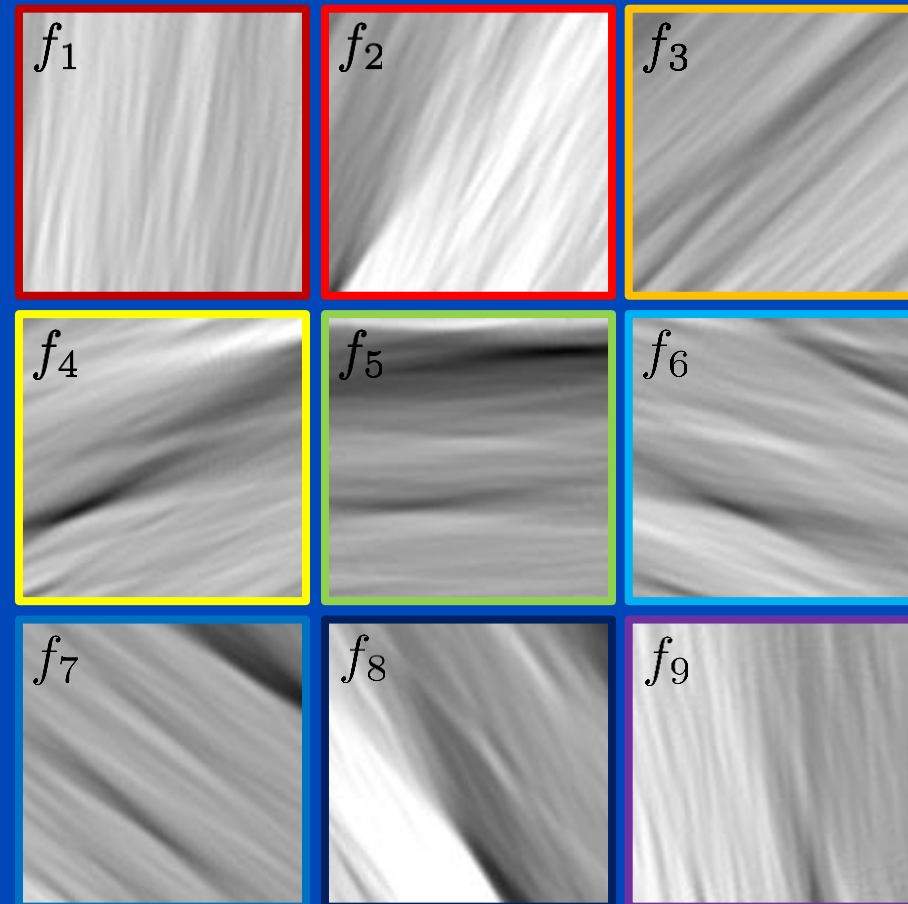
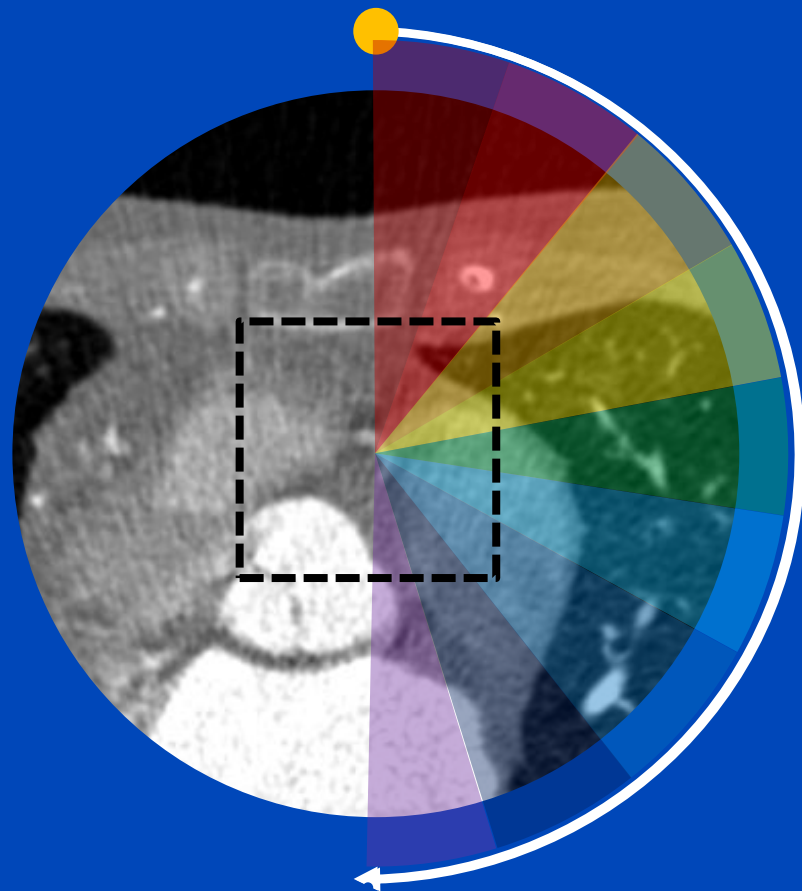
Table 3: Reason for FFR<sub>CT</sub> Rejection in the ADVANCE Registry and Clinical Cohort

	FFR <sub>CT</sub> Rejected*	ADVANCE Clinical Cohort
Inadequate image quality		(n = 892)
Blooming	4 (5.0)	29 (3.0)
Clipped structure	4 (5.0)	39 (4.3)
Motion artifacts	63 (78.0)	729 (81.4)
Image noise	2 (2.5)	198 (22.1)
Inappropriate submission		
Stent or previous coronary artery bypass graft present	5 (6.2)	116 (13.0)
Cardiac hardware present	2 (2.5)	29 (3.2)



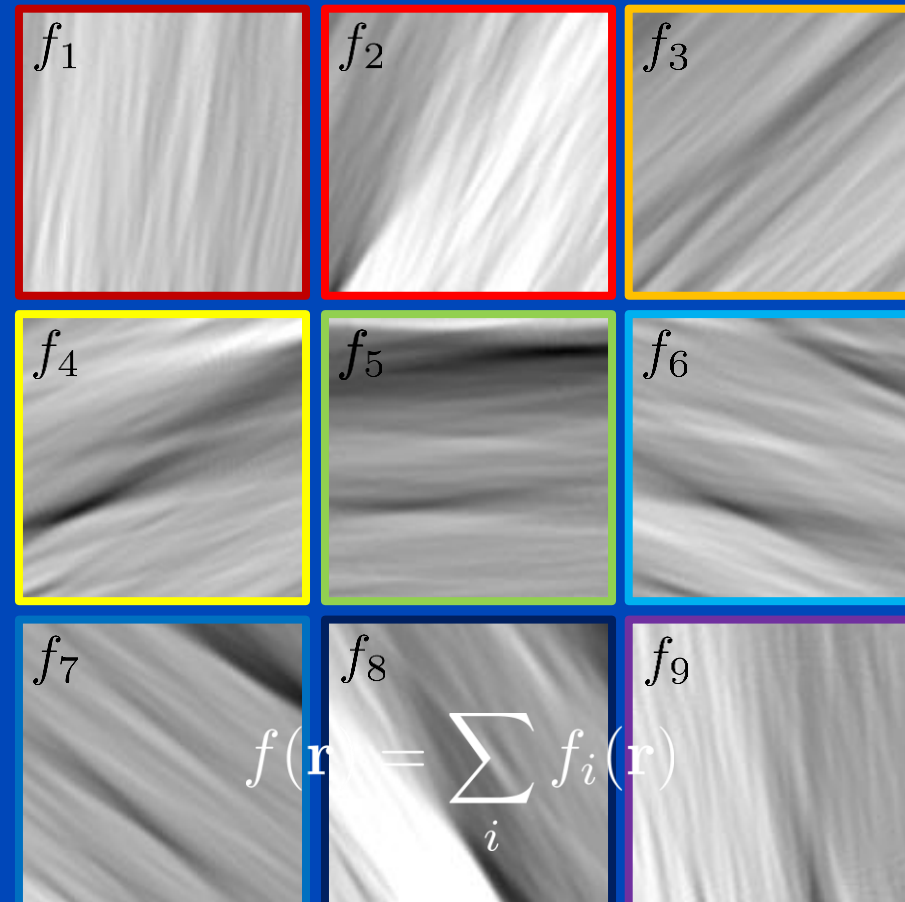
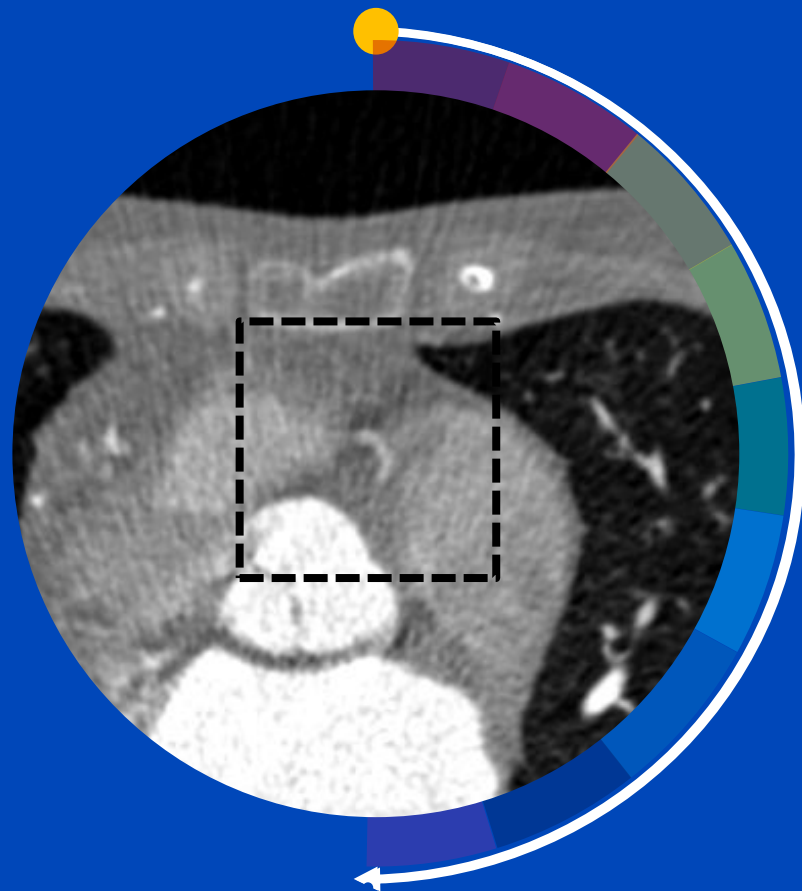
The rejection rate was 892 of 10 416 cases submitted

# Partial Angle-Based Motion Compensation (PAMoCo)

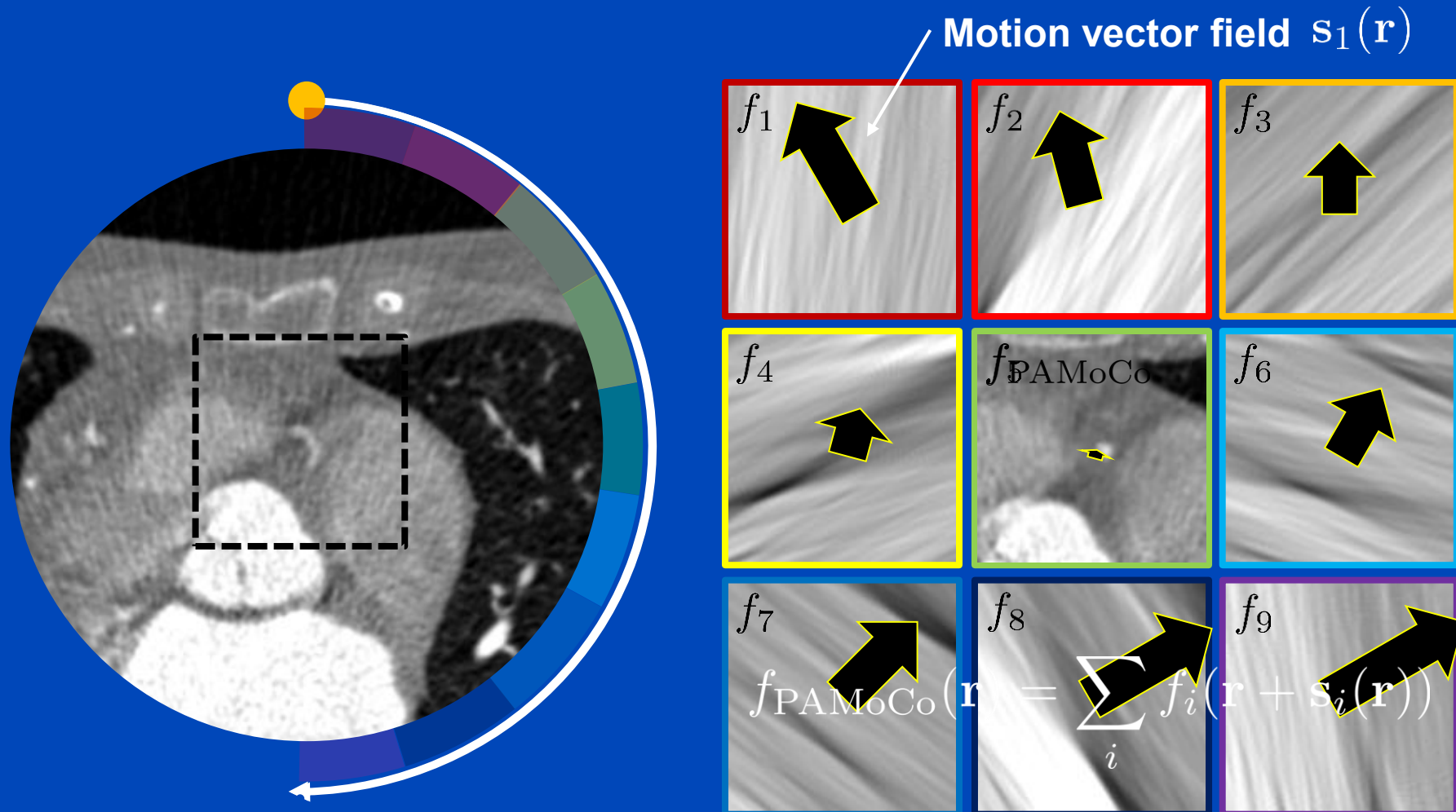


Animated rotation time =  $100 \times$  real rotation time

# Partial Angle-Based Motion Compensation (PAMoCo)

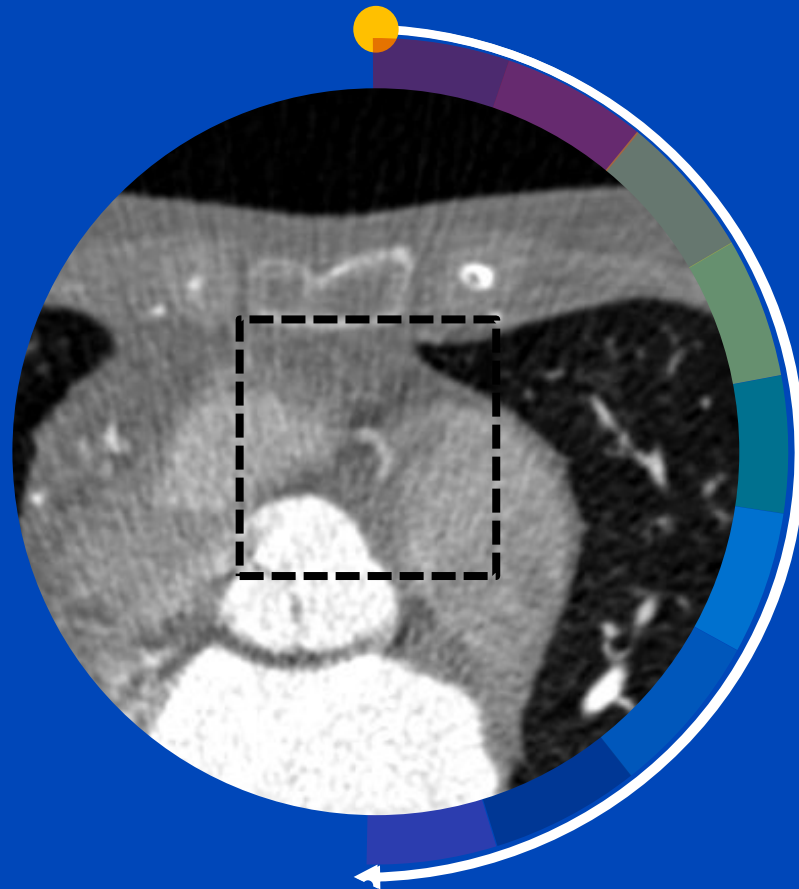


# Partial Angle-Based Motion Compensation (PAMoCo)



Apply motion vector fields (MVFs) to partial angle reconstructions

# Partial Angle-Based Motion Compensation (PAMoCo)



## Prior work:

[1] S. Kim et al., “Cardiac motion correction based on partial angle reconstructed images in x-ray CT”, Med. Phys. 42 (5): 2560–2571 (2015).

[2] J. Hahn, M. Kachelrieß et al., “Motion compensation in the region of the coronary arteries based on partial angle reconstructions from short-scan CT data”, Med. Phys. 44 (11): 5795–5813 (2017).

[3] S. Kim et al., “Cardiac motion correction for helical CT scan with an ordinary pitch”, IEEE TMI 37 (7): 1587–1596 (2018).

→ **Limitation: Challenging / time-consuming optimization**

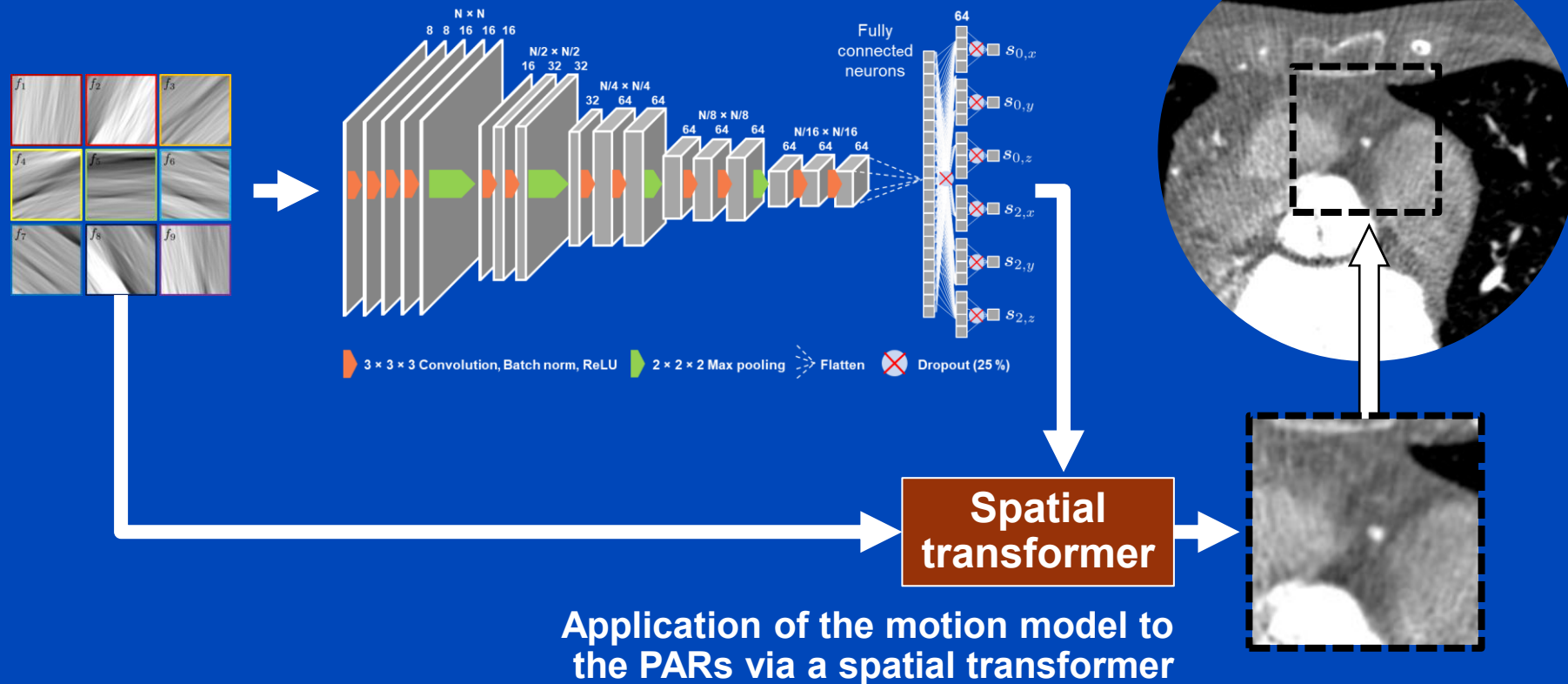
# Deep PAMoCo

## with fully connected final layers

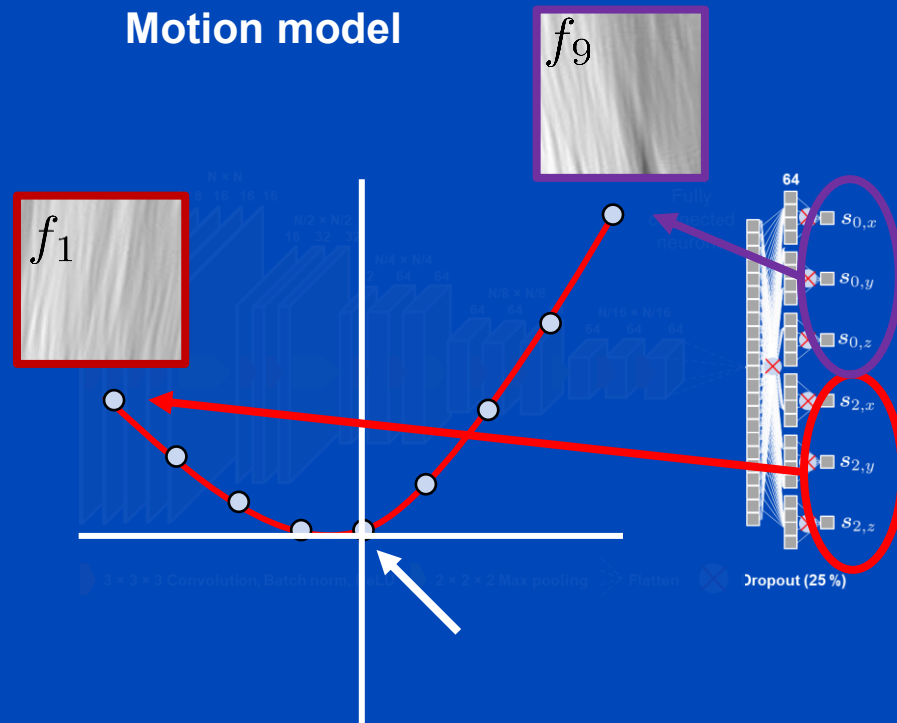
PARs centered around coronary artery

Neural network to predict parameters of a motion model

Reinsertion of patch into initial reconstruction



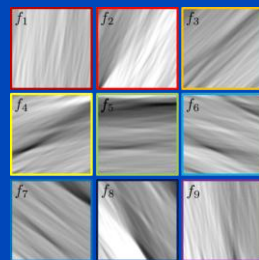
# Deep Partial Angle-Based Motion Compensation (Deep PAMoCo)



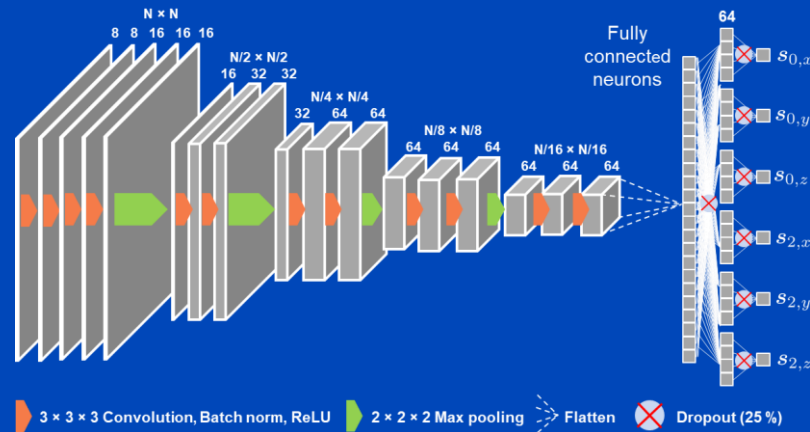
# Deep PAMoCo

## with fully connected final layers

PARs centered around coronary artery



Neural network to predict parameters of a motion model

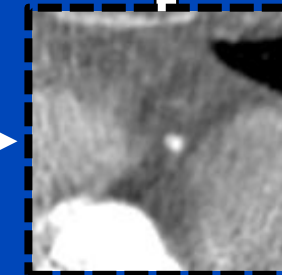


Reinsertion of patch into initial reconstruction



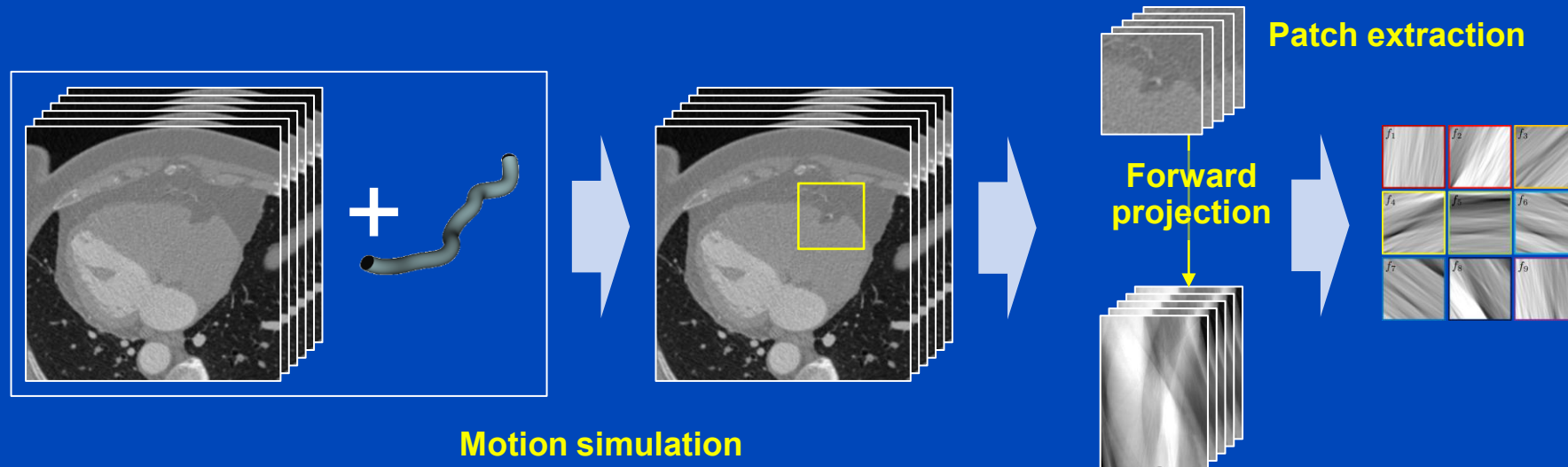
Spatial transformer

Application of the motion model to the PARs via a spatial transformer



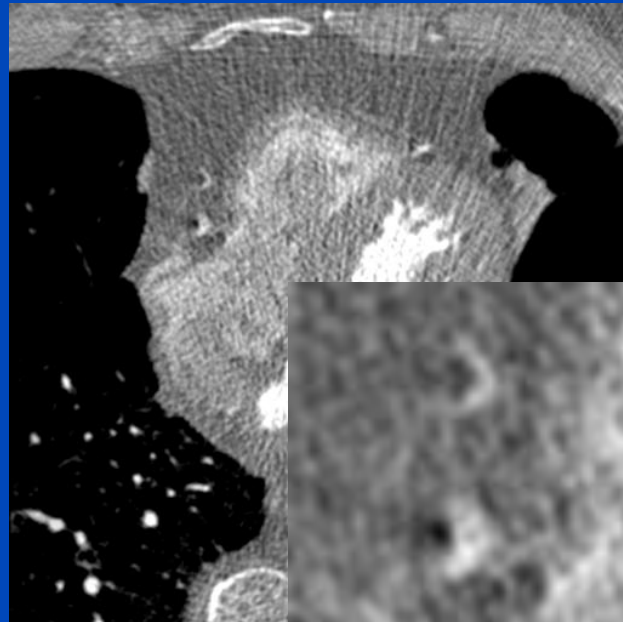
# Training Data Generation

- Removal of coronary arteries from real CT reconstructions.
- Insertion of artificial coronary arteries with different shape, size, and contrast.
- Simulation of CT scans with coronary artery motion.

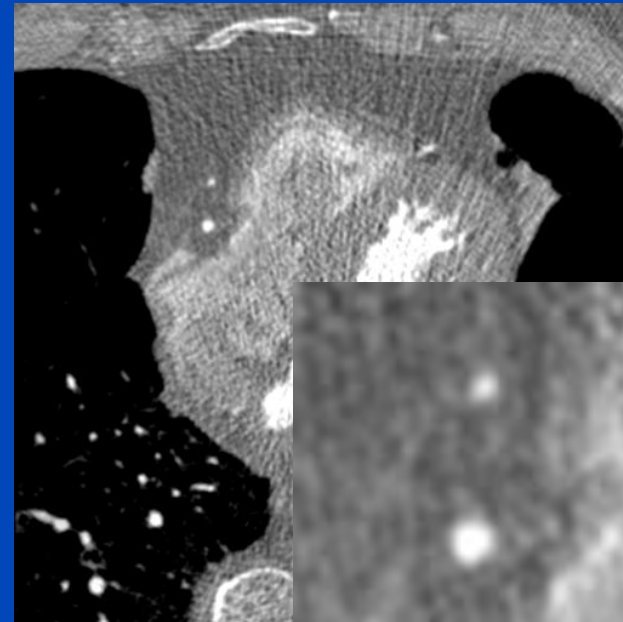


# Patient 6

Original



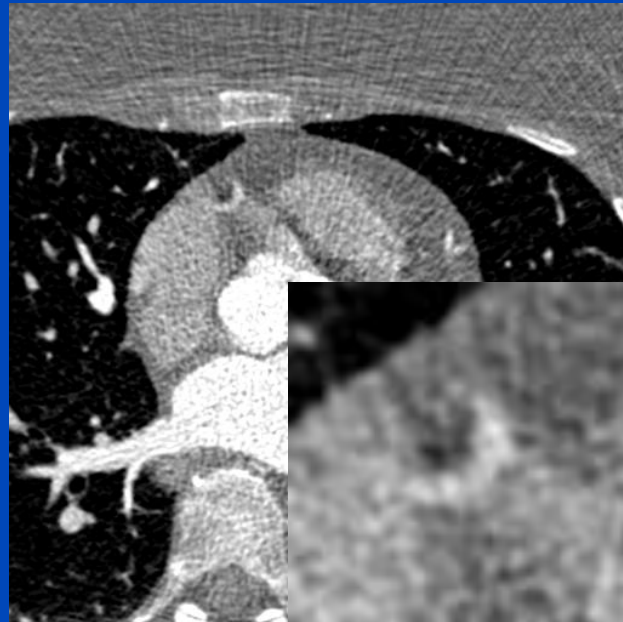
Deep PAMoCo



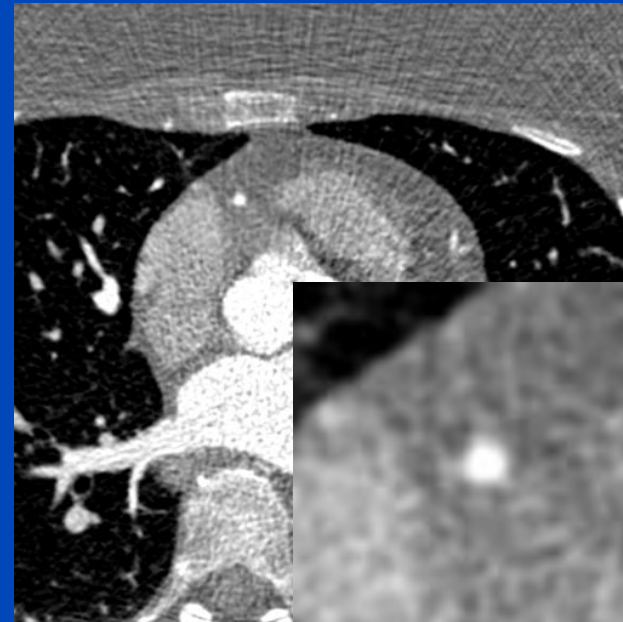
$C = 0 \text{ HU}$ ,  $W = 1400 \text{ HU}$

# Patient 7

Original



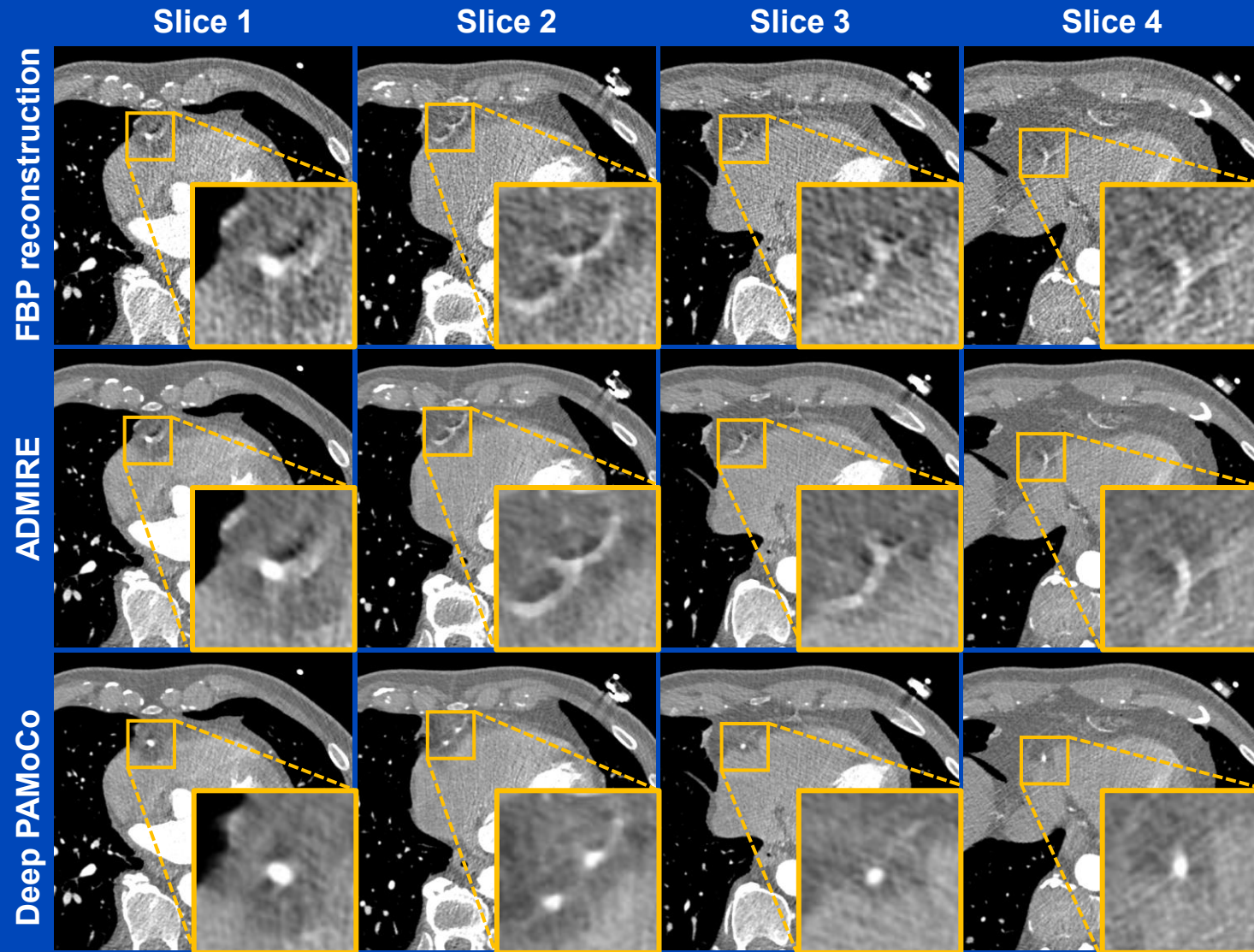
Deep PAMoCo



$C = 0 \text{ HU}$ ,  $W = 1600 \text{ HU}$

# Results

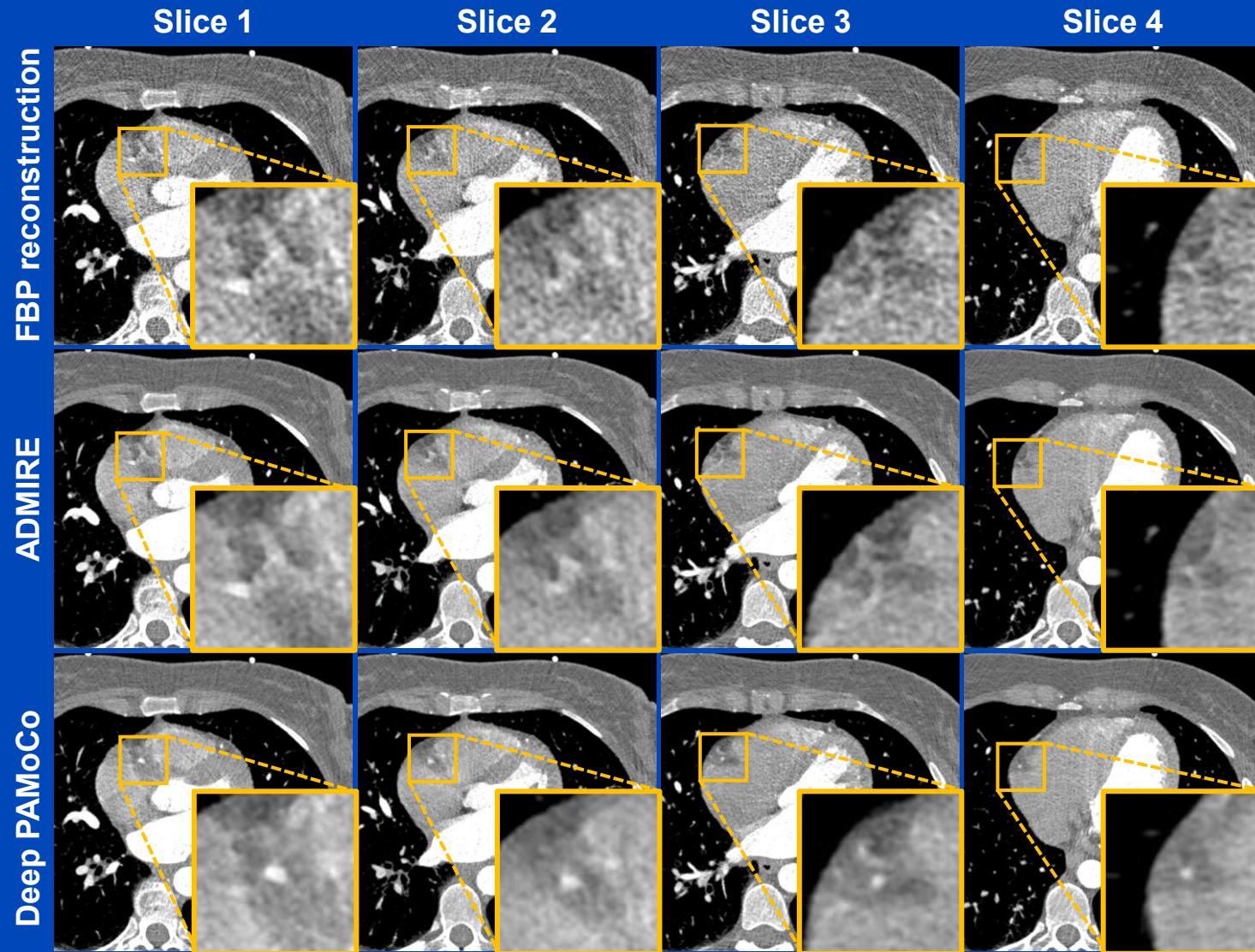
## Measurements at a Siemens Somatom AS, patient 1



$C = 0$  HU,  $W = 1200$  HU

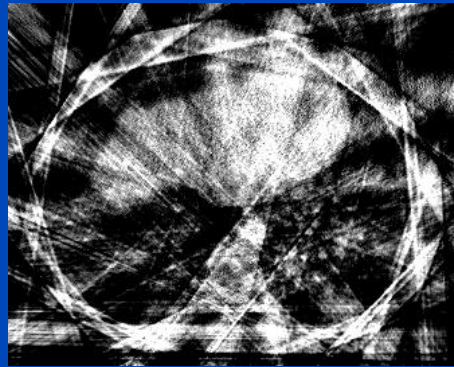
# Results

## Measurements at a Siemens Somatom AS, patient 2



$C = 0$  HU,  $W = 1200$  HU

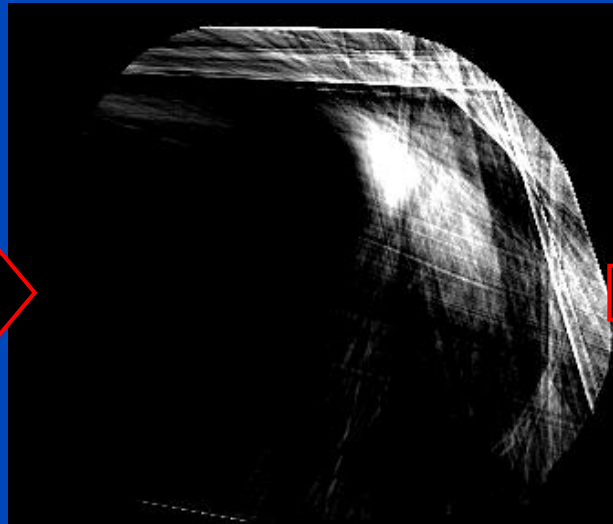
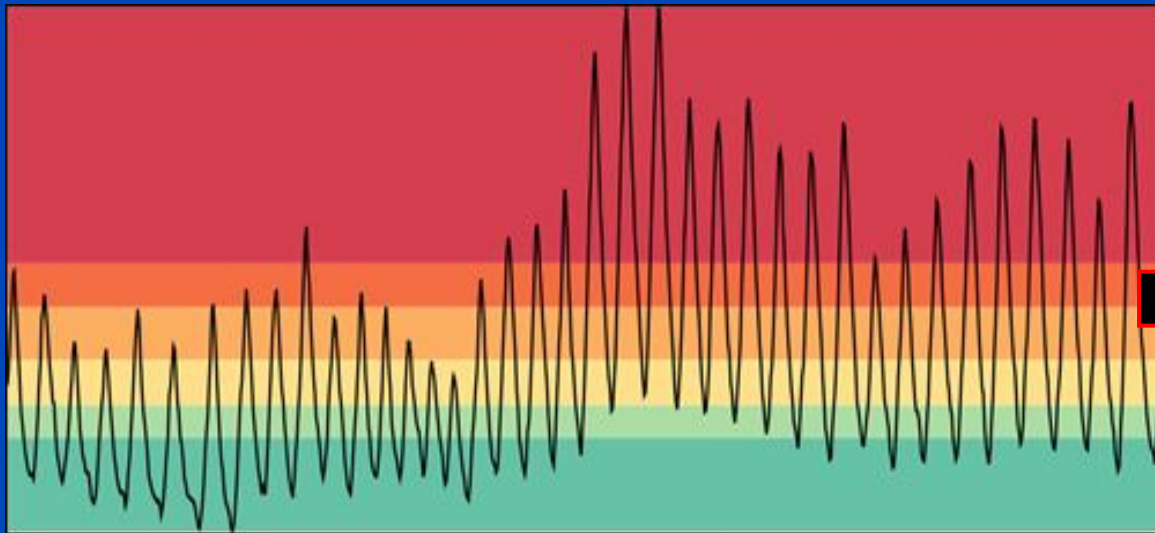
# Deep Respiratory CBCT MoCo



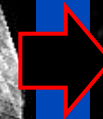
# Yet Unsolved Problems

## Gating and gating-based motion compensation (MoCo)

- require gating signal,
- assume periodic motion,
- have low temporal resolution,
- fail on irregular breathing:



Gating = bad



Gating + MoCo = still bad

# PAMoCo Adaptions for CBCT

- **Consideration of the entire FOM**
  - Estimation of a dense vector field for every voxel within the FOM.
- **Slow rotation speed**
  - Projections can only be grouped into tiny groups (here, no grouping is performed at all)
  - Partial angle reconstruction (PAR)
- **4D output**
  - Estimation of MVF from two arbitrary PARs
  - Similar to Voxelmorph but with PARs
- **Modification of PARs to add morphological context.**

# Deep learning-based cone-beam CT motion compensation with single-view temporal resolution

Joscha Maier<sup>1</sup> | Stefan Sawall<sup>1,2</sup> | Marcel Arheit<sup>3</sup> | Pascal Paysan<sup>3</sup> |  
Marc Kachelrieß<sup>1,2</sup>

<sup>1</sup>Division of X-Ray Imaging and Computed Tomography, German Cancer Research Center (DKFZ), Heidelberg, Germany

<sup>2</sup>Medical Faculty Heidelberg, Heidelberg University, Heidelberg, Germany

<sup>3</sup>Varian Medical Systems Imaging Laboratory, GmbH, Baden-Daettwil, Switzerland

## Correspondence

Marc Kachelrieß, Division of X-Ray Imaging and Computed Tomography, German Cancer Research Center (DKFZ), Heidelberg, Germany.

Email: marc.kachelriess@dkfz.de

## Abstract

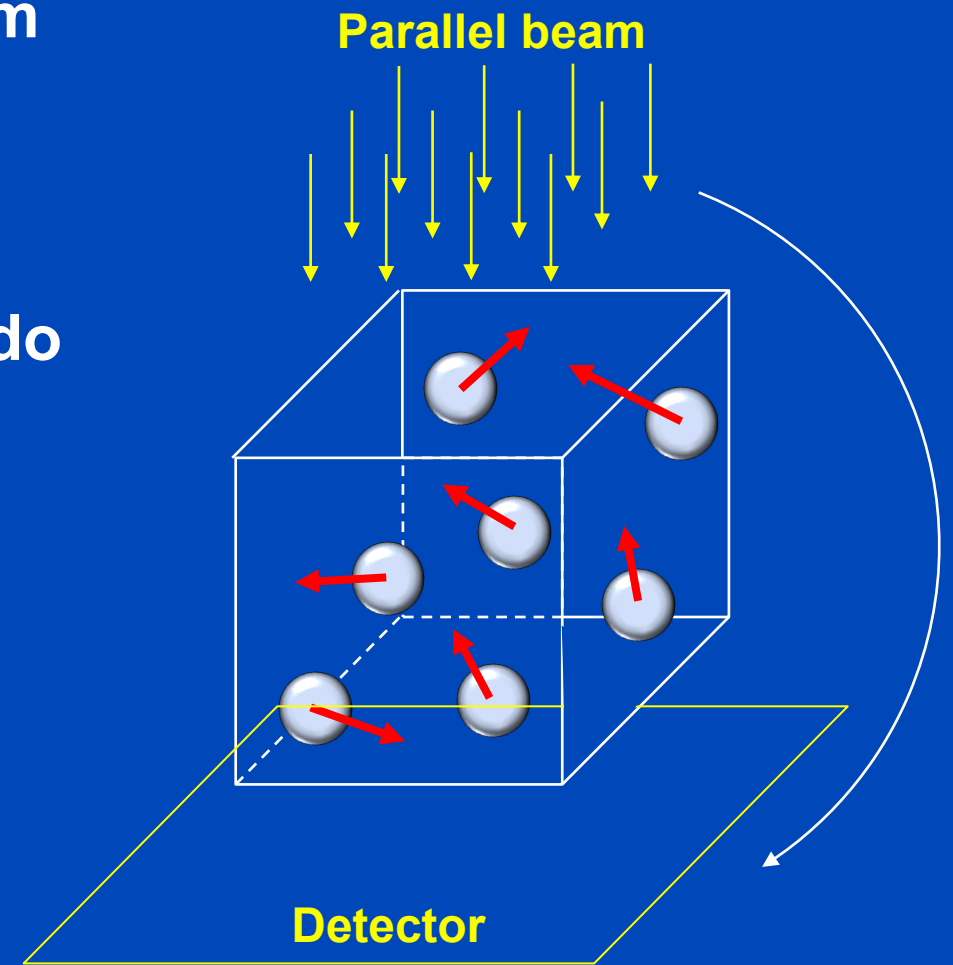
**Background:** Cone-beam CT (CBCT) scans that are affected by motion often require motion compensation to reduce artifacts or to reconstruct 4D (3D+time) representations of the patient. To do so, most existing strategies rely on some sort of gating strategy that sorts the acquired projections into motion bins. Subsequently, these bins can be reconstructed individually before further post-processing may be applied to improve image quality. While this concept is useful for periodic motion patterns, it fails in case of non-periodic motion as observed, for example, in irregularly breathing patients.

**Purpose:** To address this issue and to increase temporal resolution, we propose the deep single angle-based motion compensation (SAMoCo).

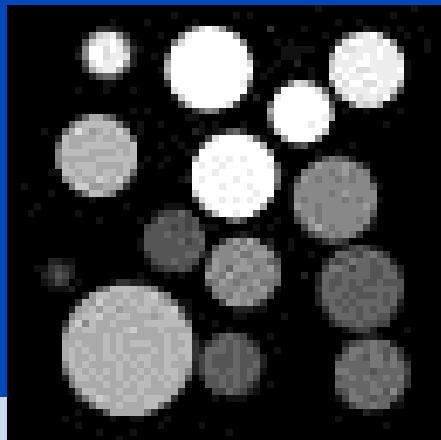
**Methods:** To avoid gating, and therefore its downsides, the deep SAMoCo trains

# Bouncing Spheres

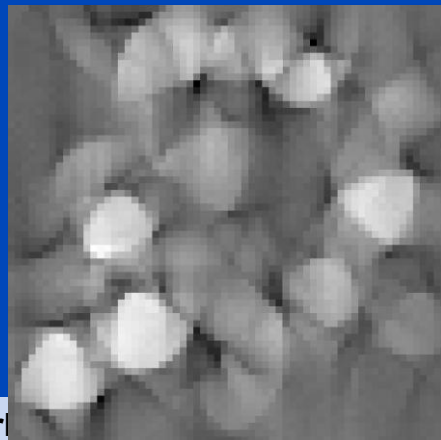
- Spheres with random velocity and random density in a box.
- Elastic collisions with other spheres and walls are elastic.
- 180° scan (180 projections) using a pseudo parallel-beam geometry.
- FDK reconstruction (64×64×32) of single views → 180 PARs.



Slice of prior volume



3D reconstruction



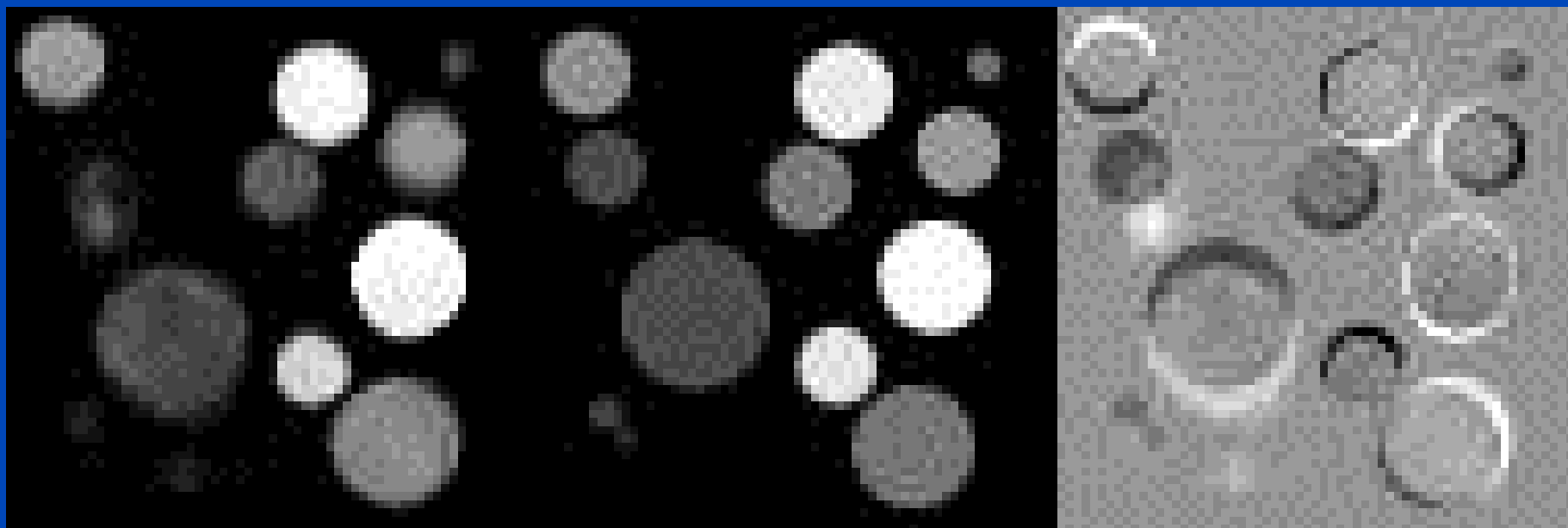
# Results

## Spheres

Prediction

Ground truth

Difference



# Single Angle Reconstructions (SARs)

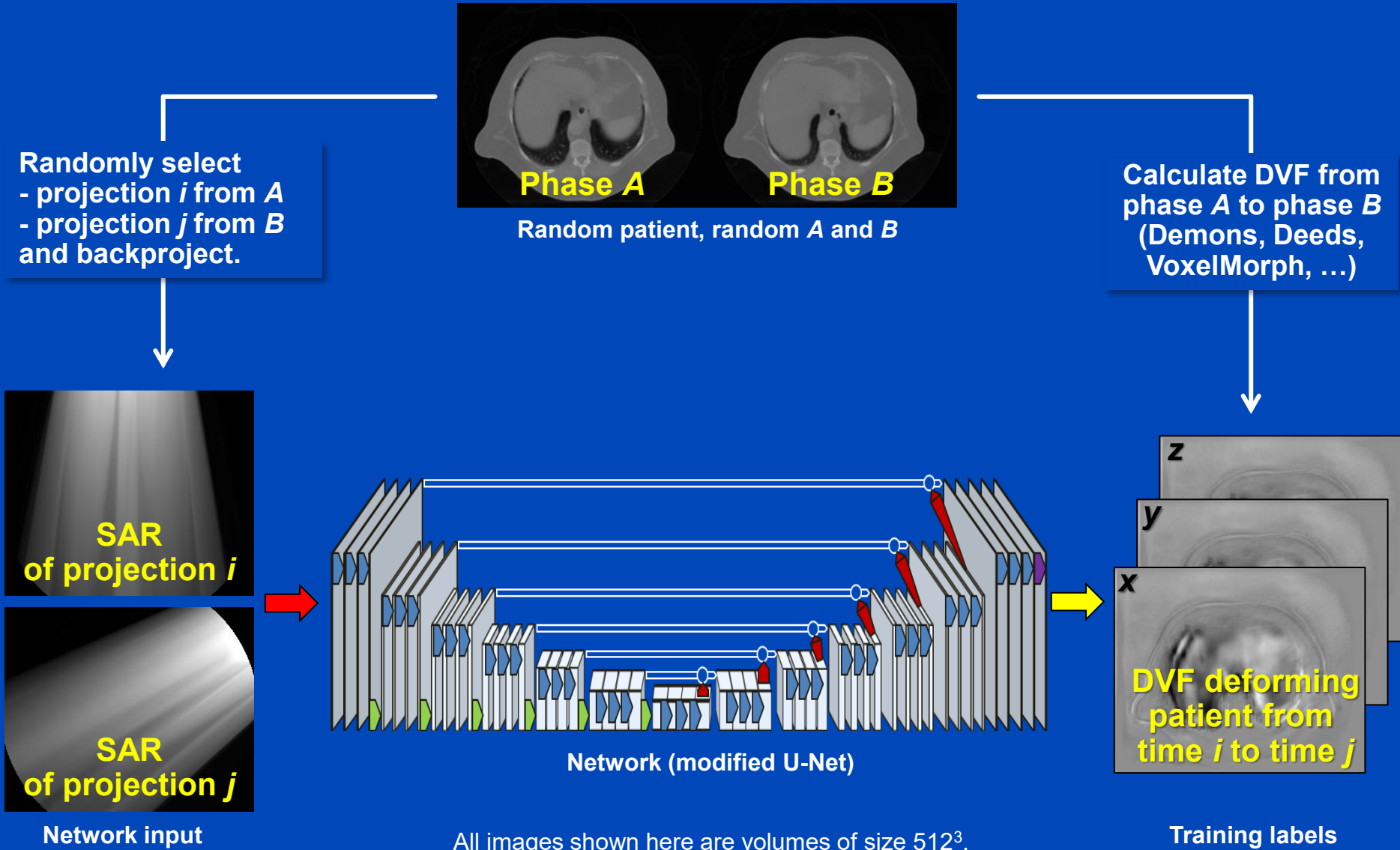


**84 4D CT scans (no artifacts, high temporal resolution)**

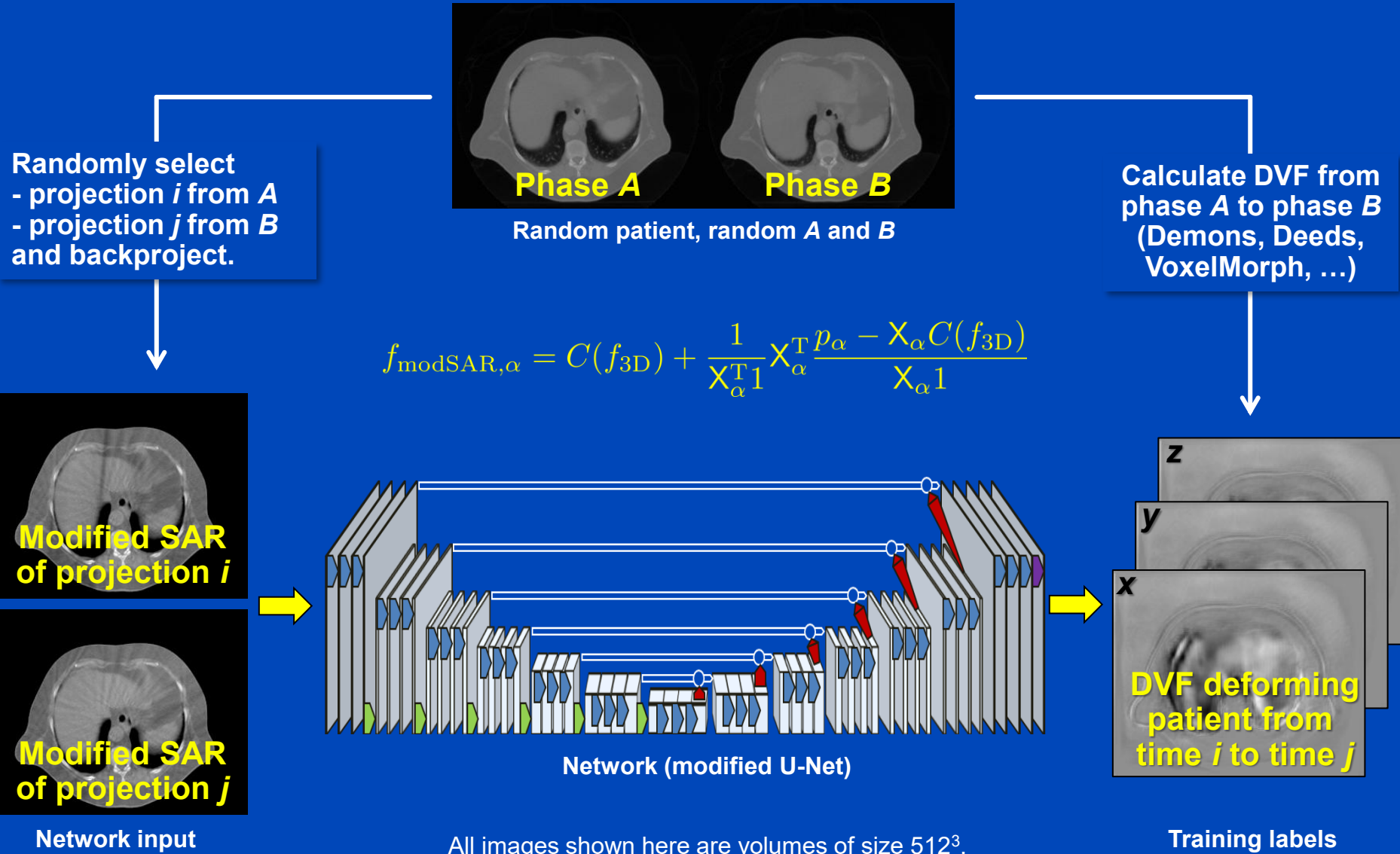
- 10 respiratory phases each (WashU/Colorado dataset)
- 10·10 combinations of phase *A* and *B* possible (including  $A=B$ )
- 84·10·10 displacement vector fields (DVF) known
- 720 CBCT projections<sup>1</sup> simulated for each CT scan (each phase)
- 84·10·720·10·720 projection pairs with known DVF

<sup>1</sup>The actual projection numbers are between 420 and 900 and depend on the scan mode.

# Training Workflow of Deep SAMoCo



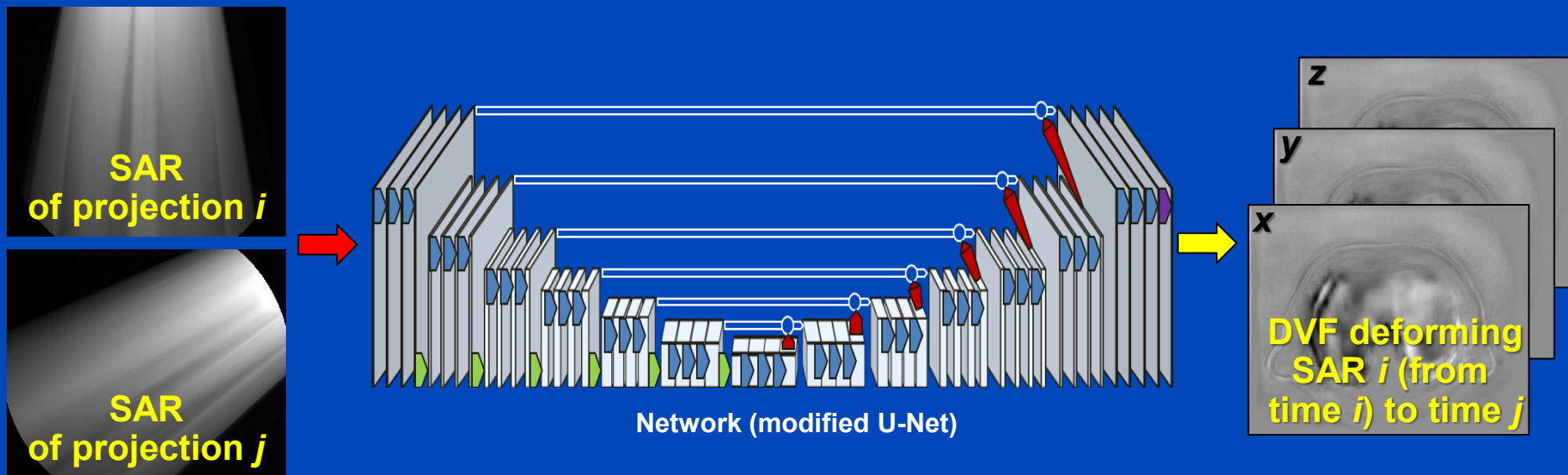
# Training Workflow of Deep SAMoCo



# Inference Workflow of Deep SAMoCo

- For a new patient
  - decide for the desired time point  $j$ , e.g. the one from 1 millisecond ago
  - for all  $i \neq j$  get the DVFs pointing from  $i$  to  $j$  from the neural network
  - deform SARs for all  $i \neq j$  into time point  $j$
  - add all the volumes

For all  $i \neq j$  do



Network input

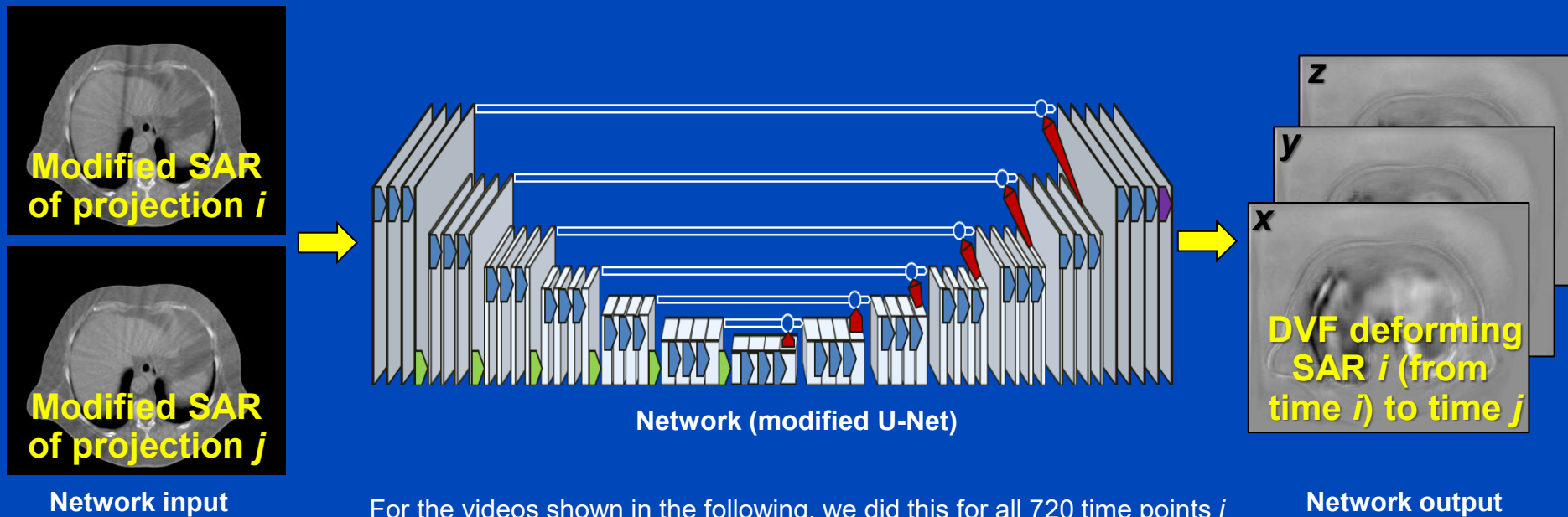
For the videos shown in the following, we did this for all 720 time points  $j$

Network output

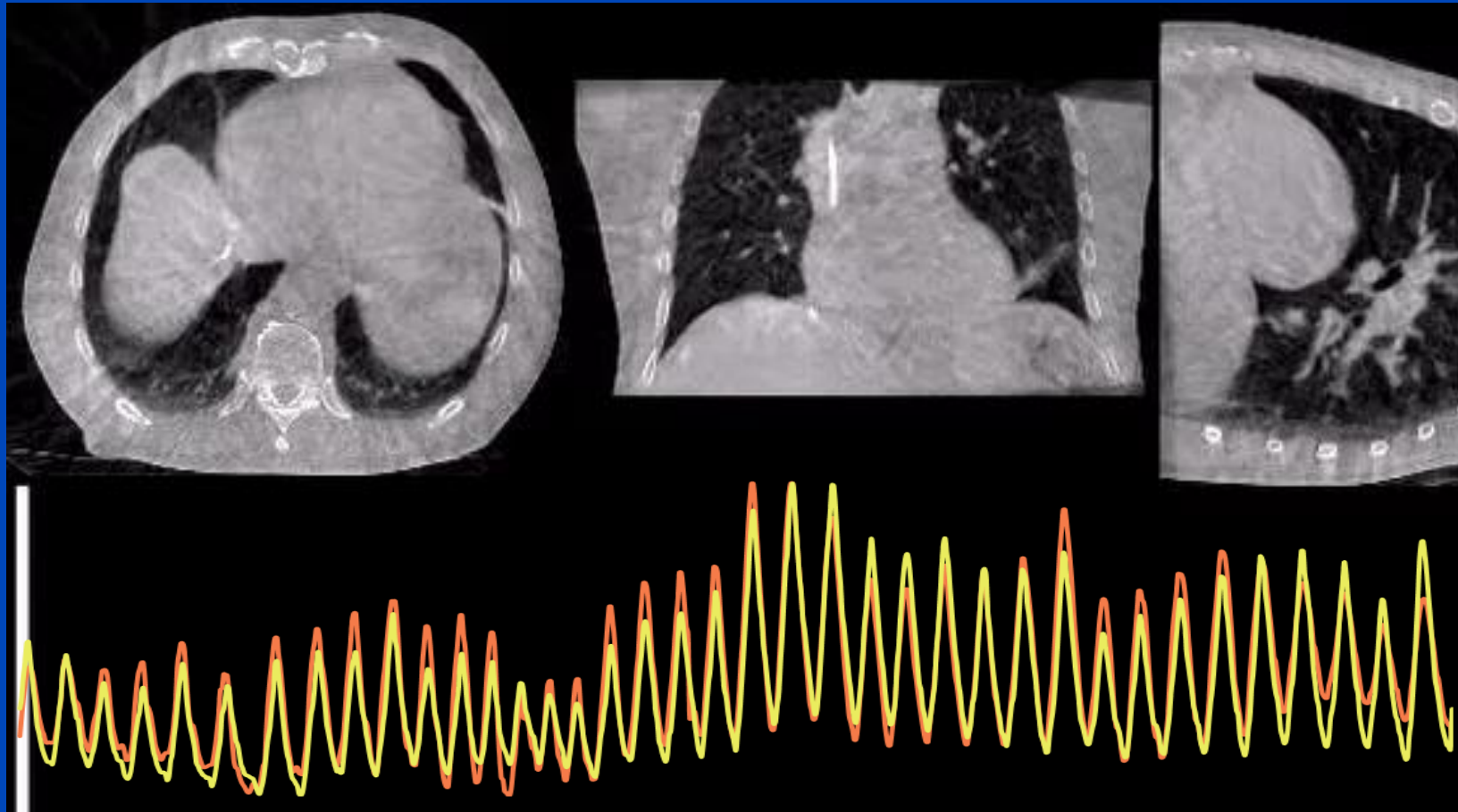
# Inference Workflow of Deep SAMoCo

- For a new patient
  - decide for the desired time point  $j$ , e.g. the one from 1 millisecond ago
  - for all  $i \neq j$  get the DVFs pointing from  $i$  to  $j$  from the neural network
  - deform SARs for all  $i \neq j$  into time point  $j$
  - add all the volumes

For all  $i \neq j$  do

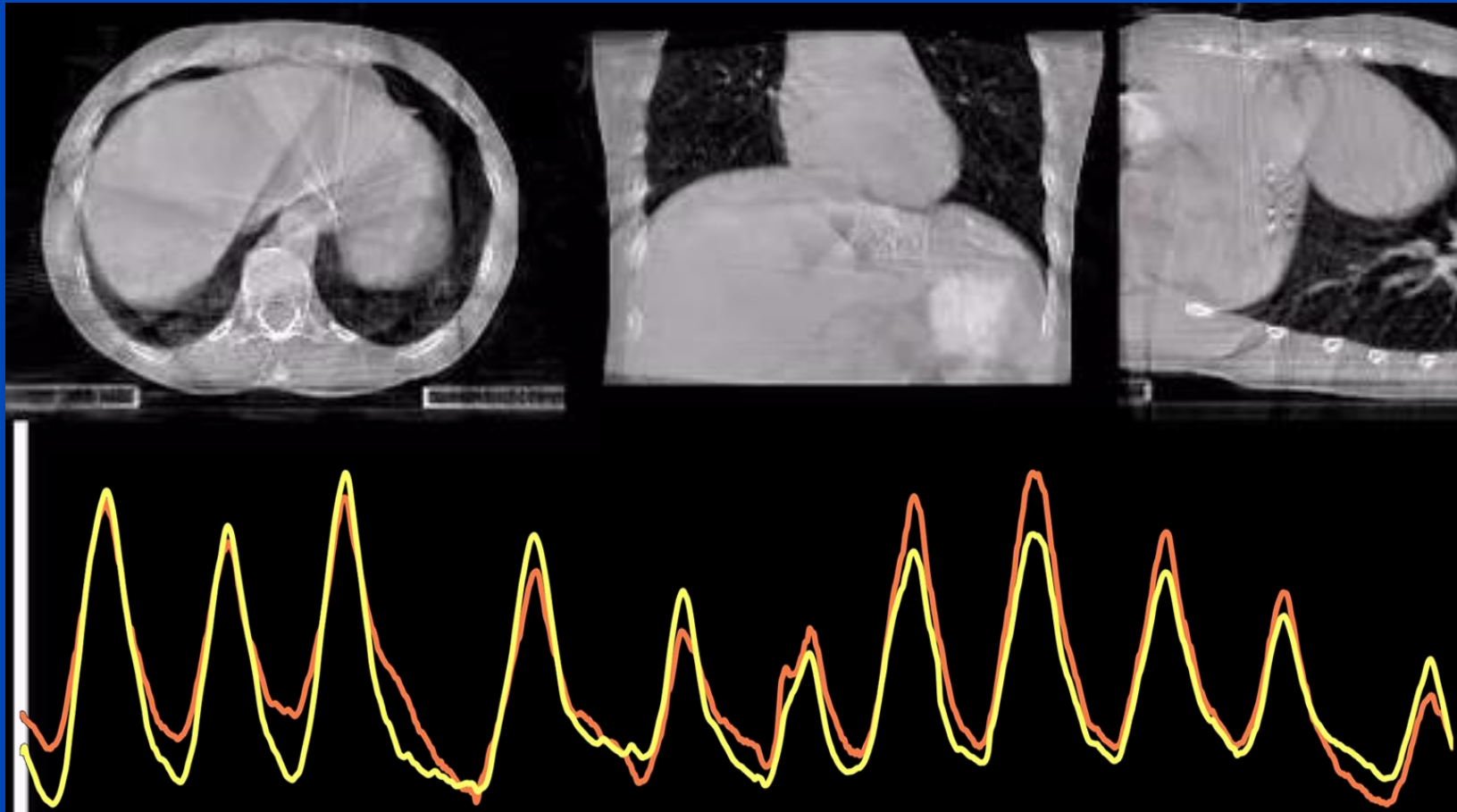


# VUMC\_4DThorax



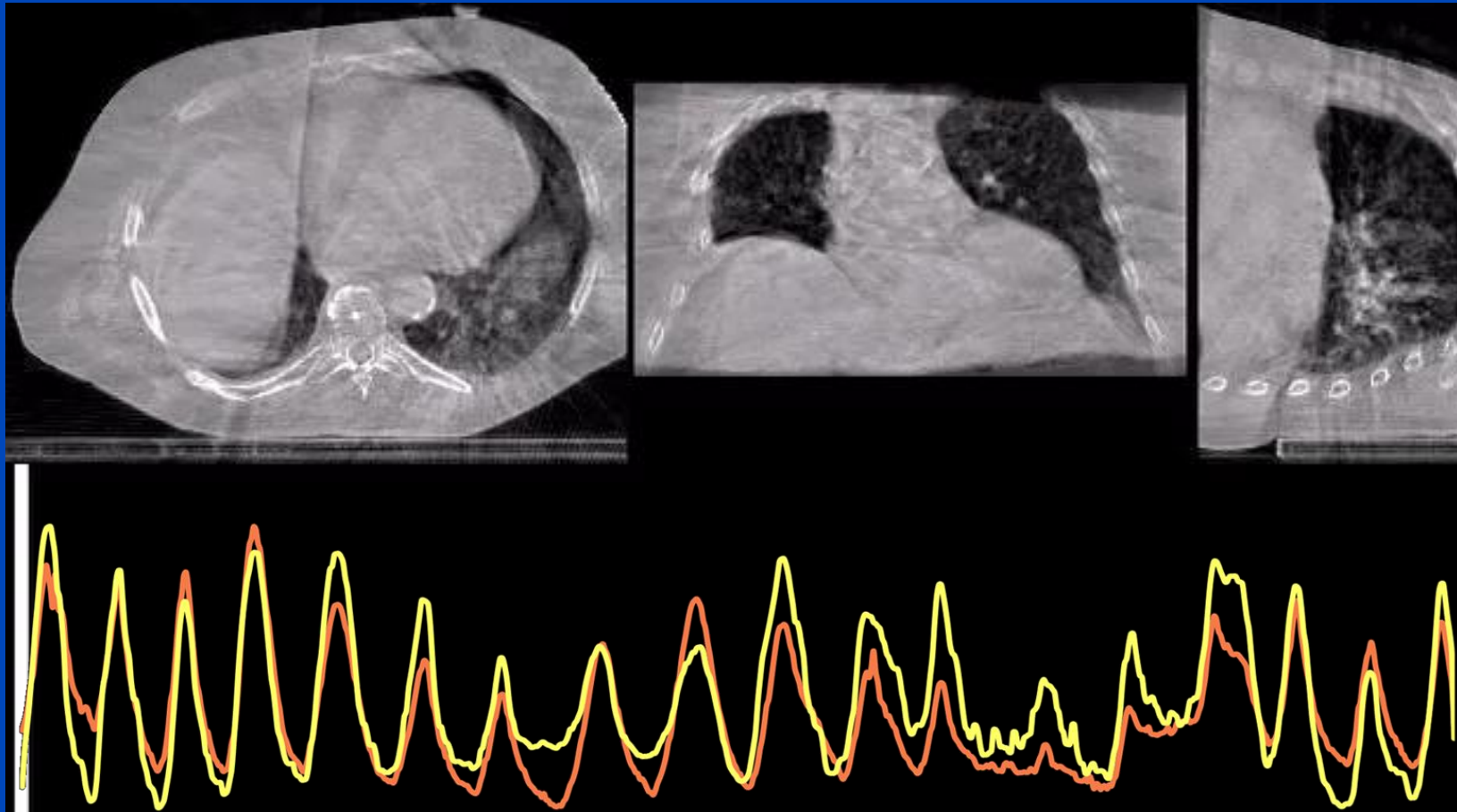
Red: RPM signal (external signal – not used for recon)  
Yellow: Diaphragm motion (intrinsic signal – from PAMoCo recon)

# MSK 7

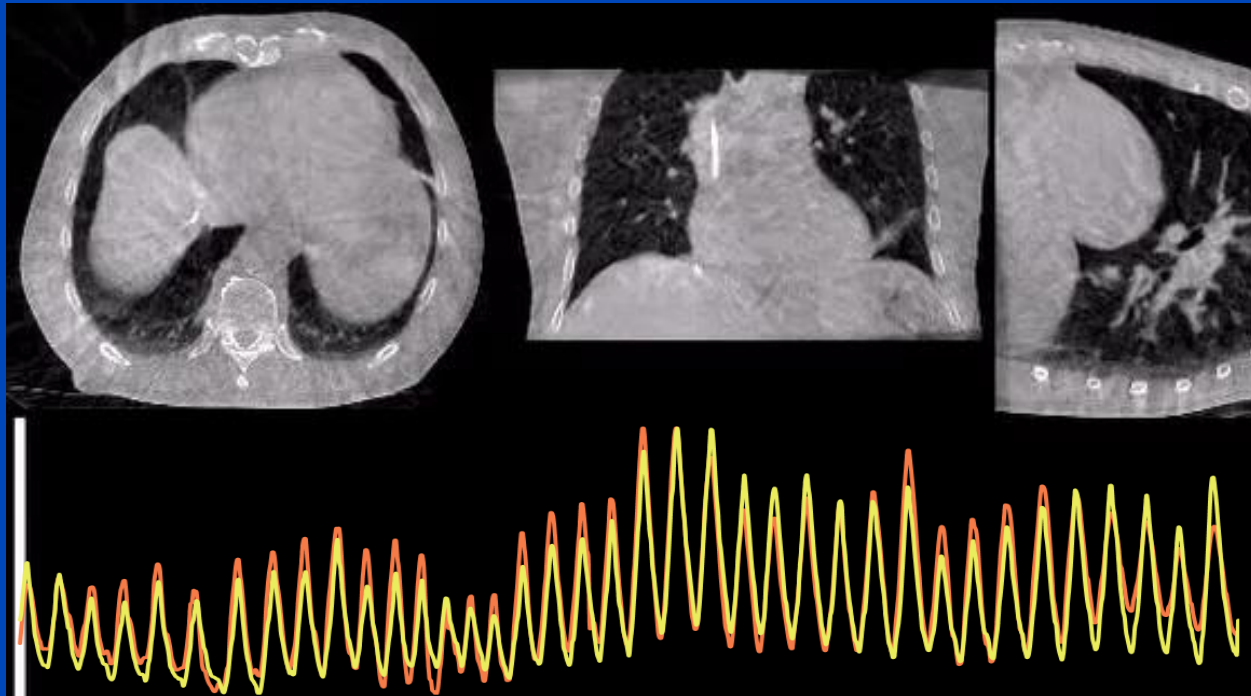


Red: RPM signal (external signal – not used for recon)  
Yellow: Diaphragm motion (intrinsic signal – from PAMoCo recon)

# MSK 1



Red: RPM signal (external signal – not used for recon)  
Yellow: Diaphragm motion (intrinsic signal – from PAMoCo recon)



**Upcoming in  
2026**  
(yet to be developed)

A dark, vertical, tapered shape, possibly representing a beam or a specific component, is shown below the text.



# Hypersight Patient Example

60 s Scan

FDK recon (3D)



SAMoCo recon (true 4D)

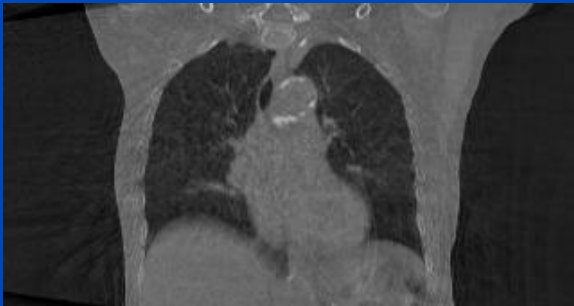


6 s Scan

FDK recon (3D)



SAMoCo recon (true 4D)

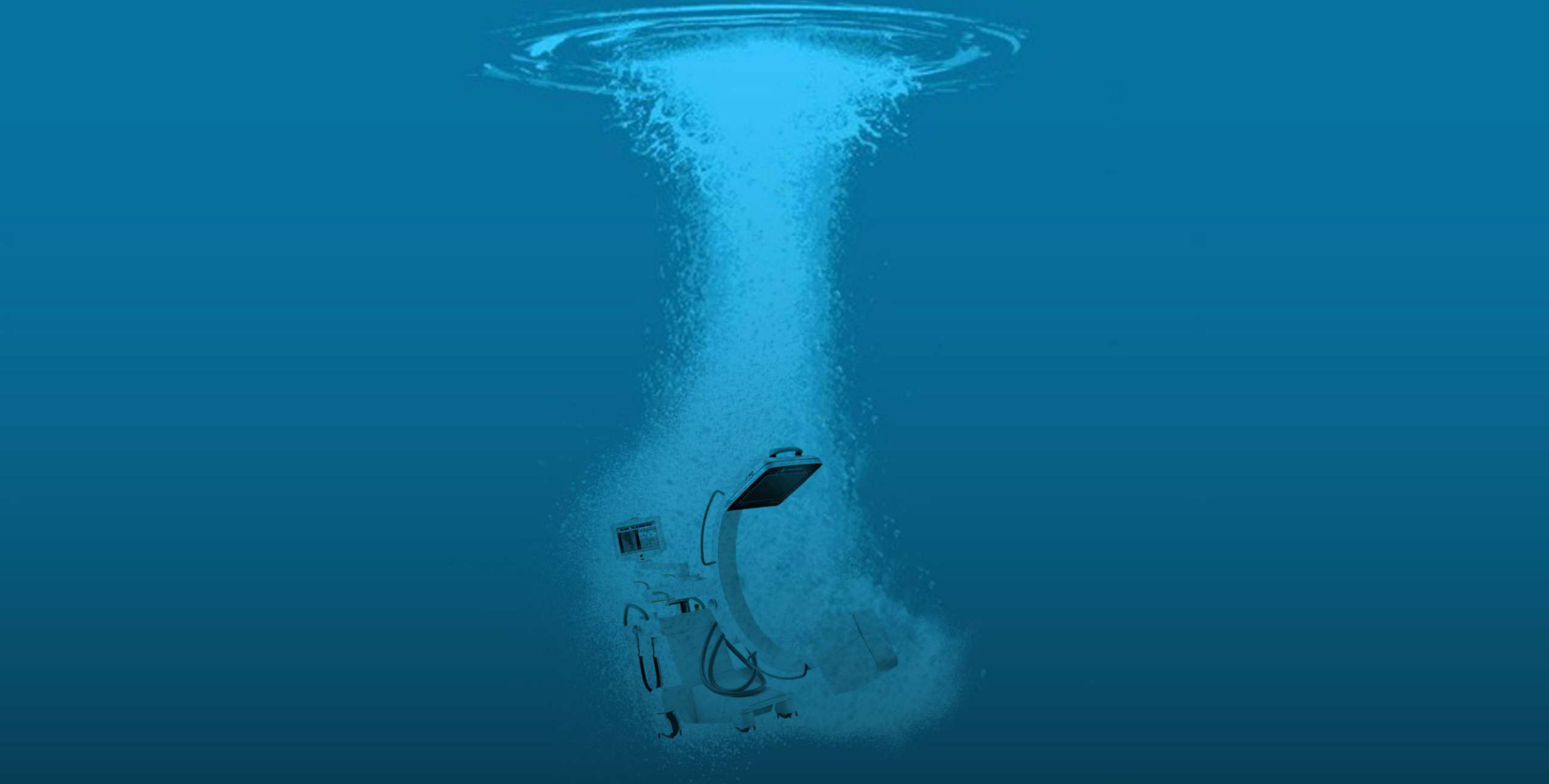


60 s, 200° short scan, 867 projections, MA\_53\_Lung\_60s.  
Displayed are 434 time points with 0.14 s increment at 10 fps.

6 s, 200° short scan, 406 projections, MA\_53\_Lung\_BH\_6s  
Displayed are 41 time points with 0.14 s increment at 10 fps.

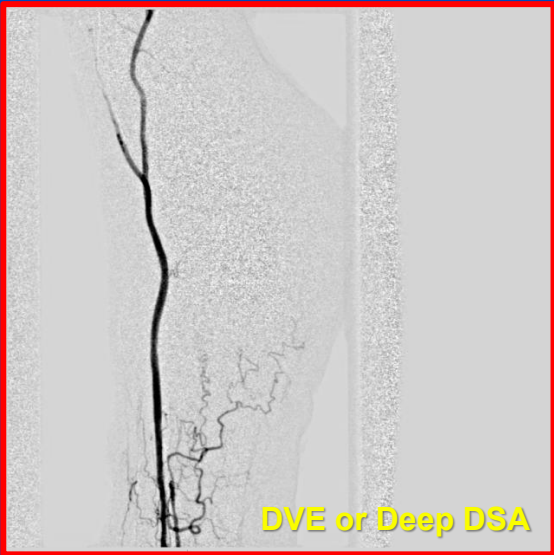
Numbers show frame numbers and not projection numbers

# INTERVENTIONAL IMAGING

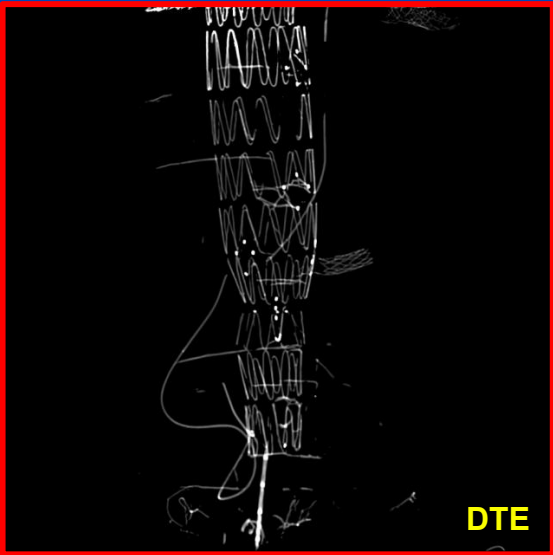
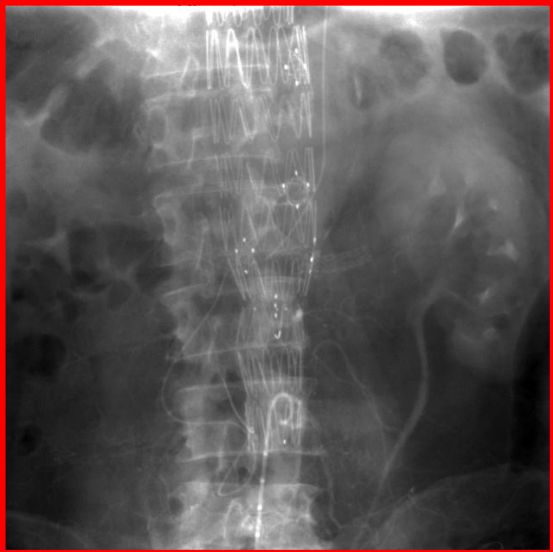
A medical C-arm X-ray machine is shown submerged underwater. A bright light source from above creates a large, shimmering column of light that illuminates the machine and the surrounding water. The machine is positioned in the lower half of the frame, with its curved arm and various components visible. The water is a deep blue color, and the overall scene is dramatic and surreal.

**Intervention goes Deep!**

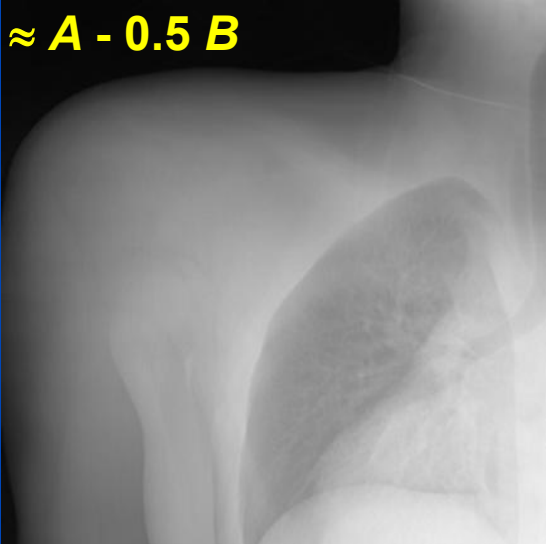
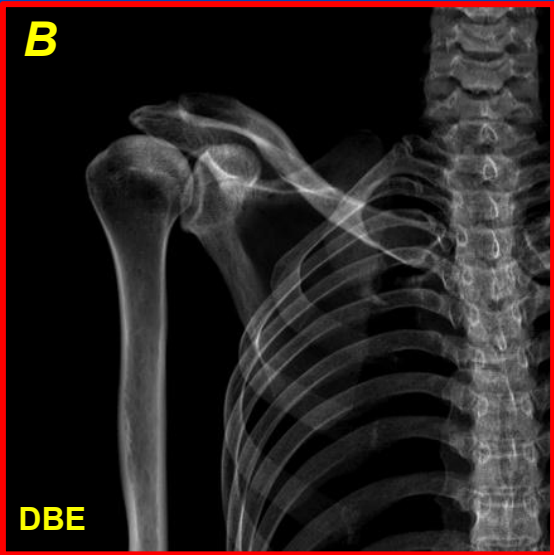
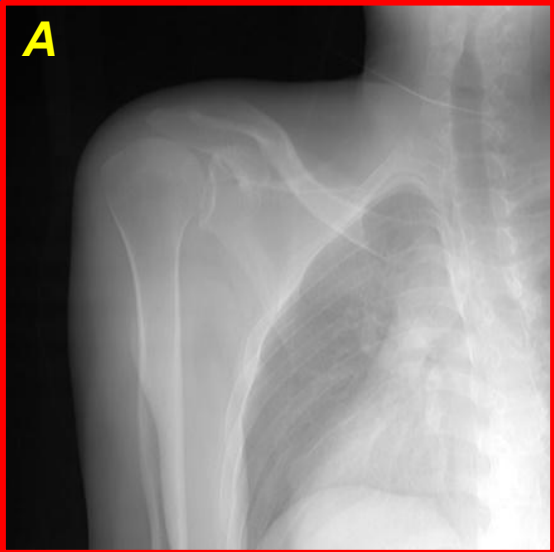
# Deep Vessel Extraction



# Deep Tool Extraction



# Deep Bone Extraction



# Deep DSA



WILEY

**CONGRATULATIONS!**  
YOUR WORK HAS RECEIVED OVER  
**1,000**  
VIEWS

Dear Marc Kachelrieß,  
Your work, [Training of a deep learning based digital subtraction angiography method using synthetic data](#), has received over 1,000 views\*. Now that's something to celebrate!

Received: 20 June 2023 | Revised: 30 November 2023 | Accepted: 4 January 2024  
DOI: 10.1002/mp.16973

RESEARCH ARTICLE MEDICAL PHYSICS

## Training of a deep learning based digital subtraction angiography method using synthetic data

Lizhen Duan<sup>1,2,3</sup> | Elias Eulig<sup>1,4</sup> | Michael Knaup<sup>1</sup> | Ralf Adamus<sup>5</sup> | Michael Lell<sup>5</sup> | Marc Kachelrieß<sup>1,6</sup>

In the first year since being published, your article has received:

 **2020**  
Downloads

# Digital Subtraction Angiography (DSA)

- **DSA principle:**
  - Before contrast injection acquire a mask image.
  - When injecting contrast, perform fluoroscopy.
  - Display each fluoroscopic image minus the mask image
- **For decades, DSA is used world-wide with great success in many clinical angiographic exams.**
- **Downsides:**
  - Need to start acquisition before injecting the contrast medium
  - Works for only static situations.
- **Future<sup>1,2</sup>:**
  - Use AI to compute DSA without needing the mask image.
  - Do this in real-time (e.g. 5 ms per x-ray image).

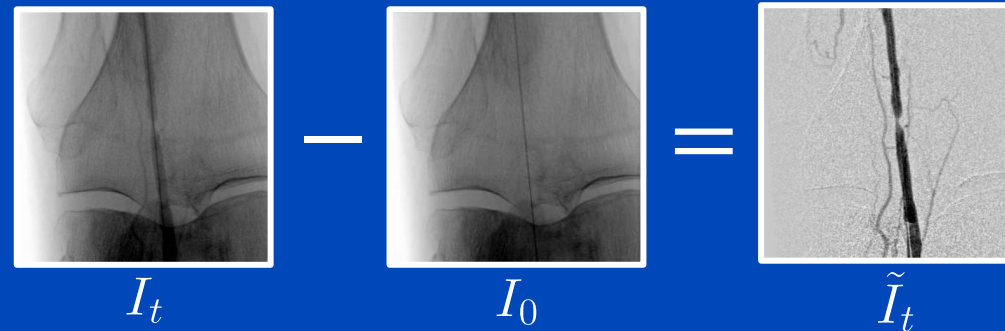


<sup>1</sup>E. Eulig, M. Kachelrieß et al. "Learned digital subtraction angiography (Deep DSA): method and application to lower extremities". Fully 3D, May 2019.

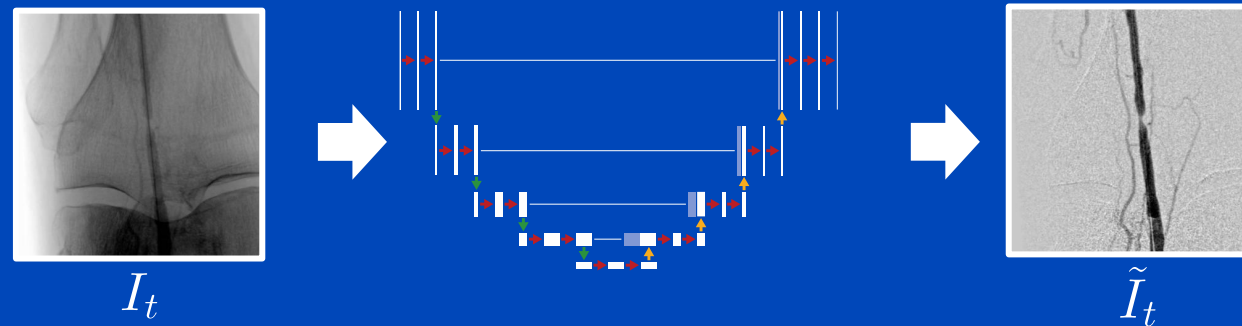
<sup>2</sup>L. Duan, M. Kachelrieß et al. "Training of a deep learning based digital subtraction angiography method using synthetic data". Med Phys. 51:4793–4810, July 2024.

# General Principle

- Conventional DSA



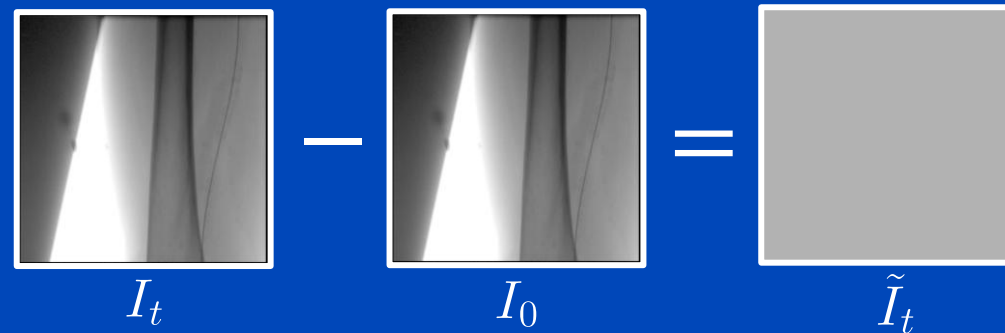
- Deep DSA



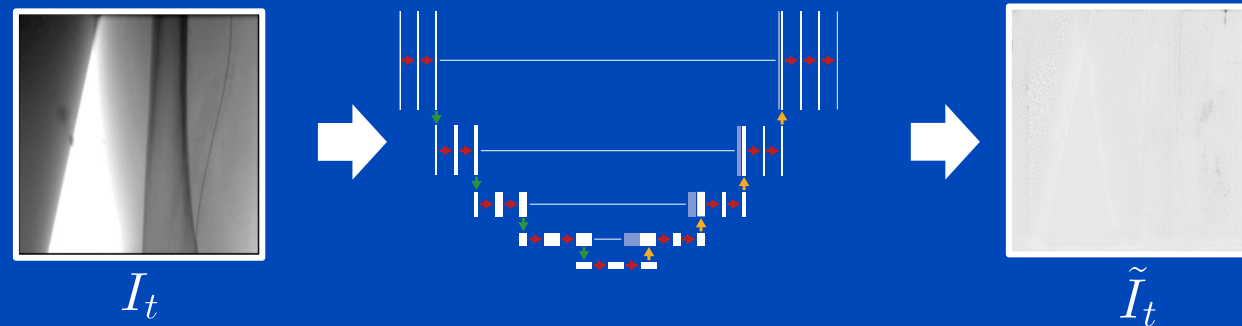
- Train on static cases where ground truth is conventional DSA
- During inference CNN can be applied to both static and dynamic cases

# General Principle

- Conventional DSA

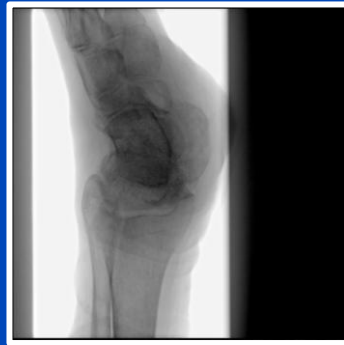


- Deep DSA

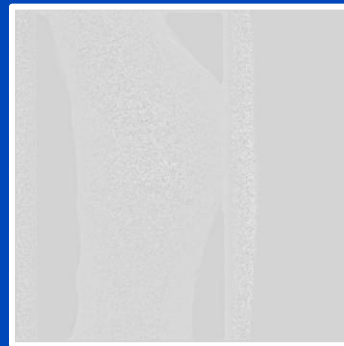


- Train on static cases where ground truth is conventional DSA
- During inference CNN can be applied to both static and dynamic cases

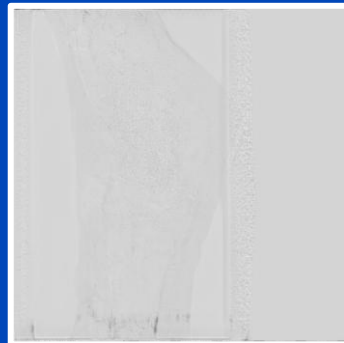
# Results



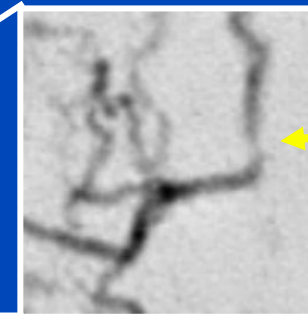
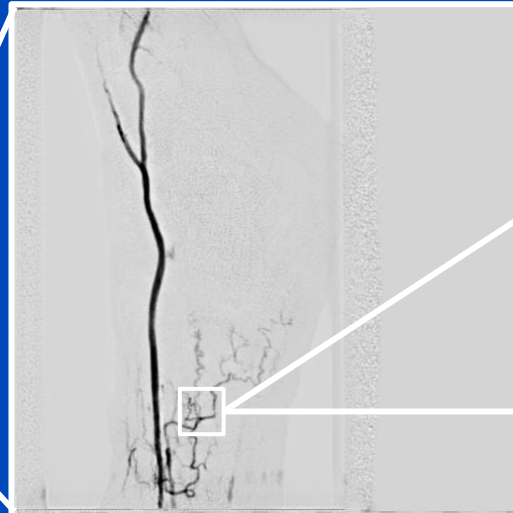
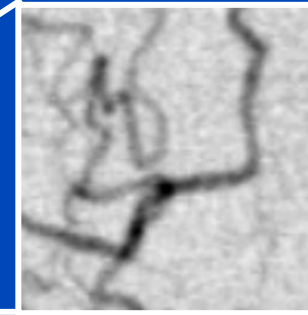
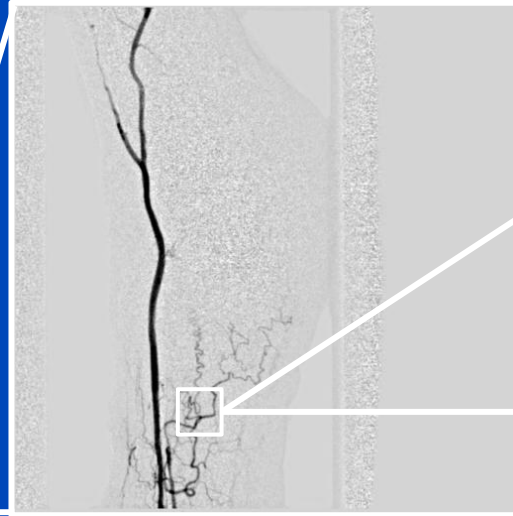
Original x-ray sequence



Ground truth DSA



CNN output

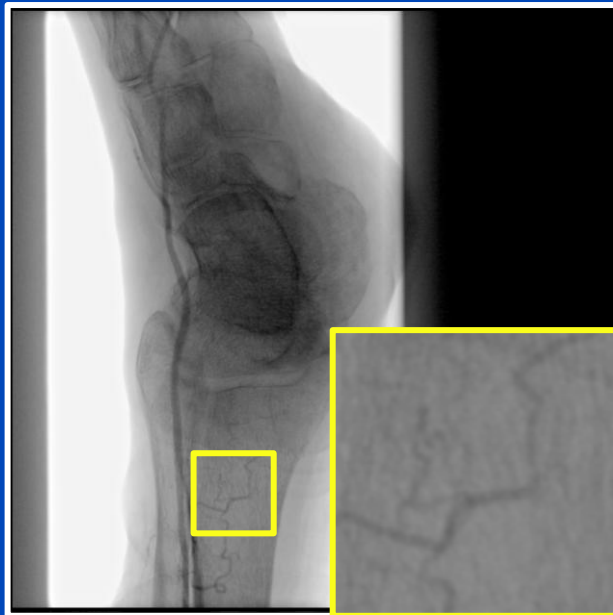


Artificially introduced stenosis?

Due to a low amount of training data and a low variability of the training data available to us the results shown on this slide are not optimal, yet.

# Deep DSA

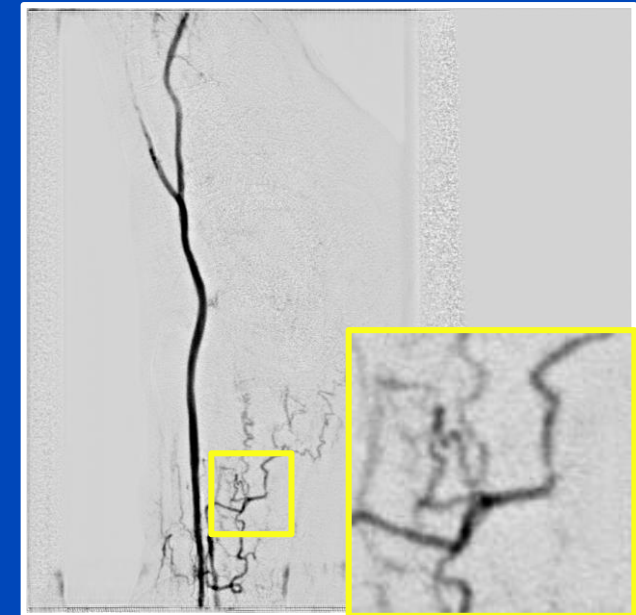
Fluoroscopy



DSA (fluoro minus mask)



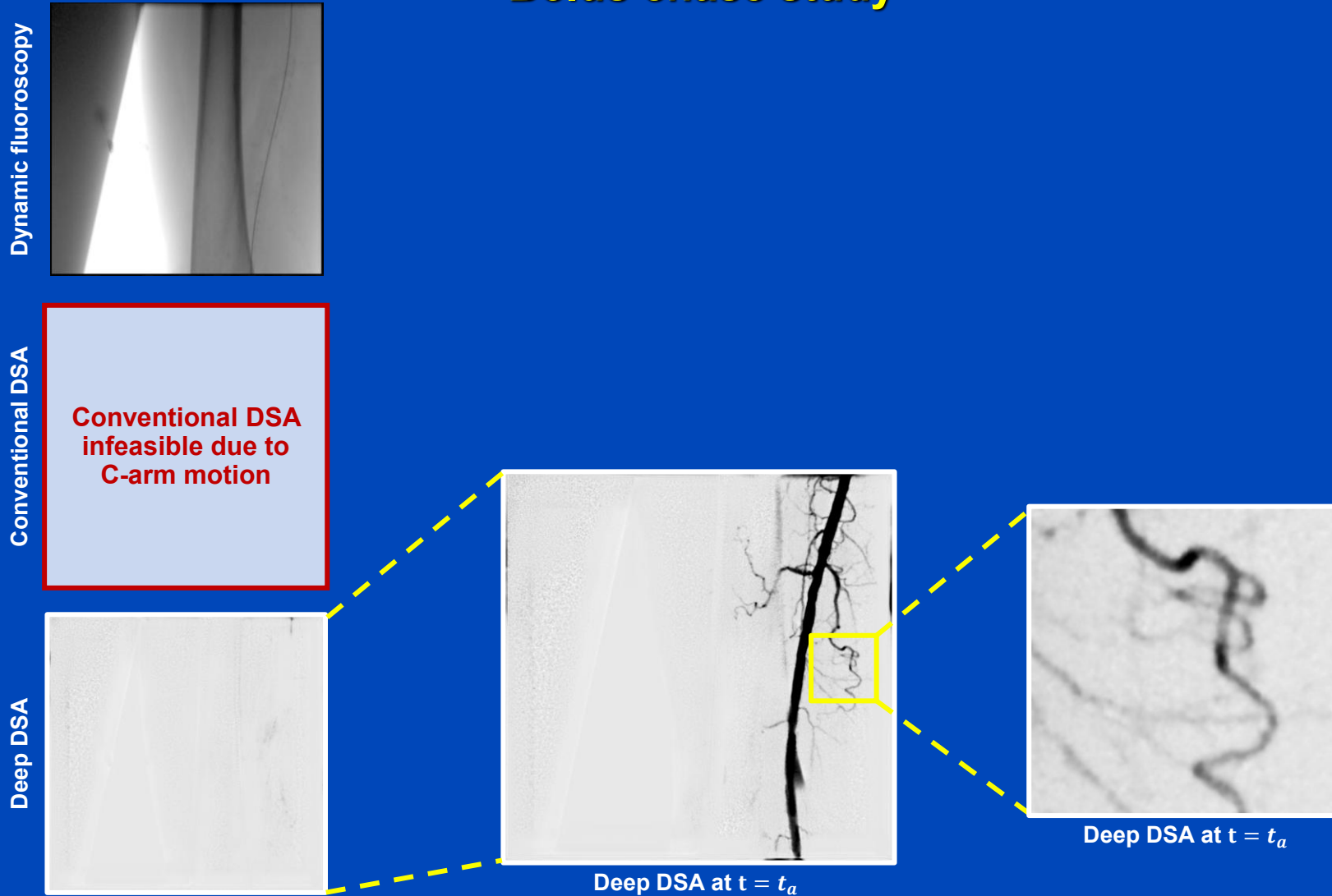
Deep DSA (from fluoro only)



Due to a low amount of training data and a low variability of the training data available to us the results shown on this slide are not optimal, yet.

# Results

## Bolus chase study



# Lessons Learned

- Background frames with vessels sneaked into our training data.



- Mismatch in simulated PSF vs. measurement PSF may cause the network to fail

**Corrupted training data**  
(here: not all background images were free of vessels)

**Forgot PSF augmentation**  
(here: random  $k \times k$  filter)

**Final good result**

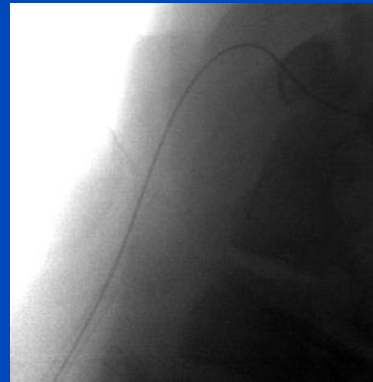
Epoch 5

Epoch 15

Epoch 30

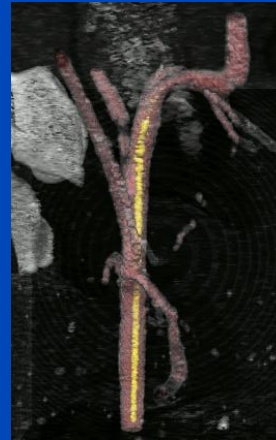


# Deep 3D+T Fluoroscopy



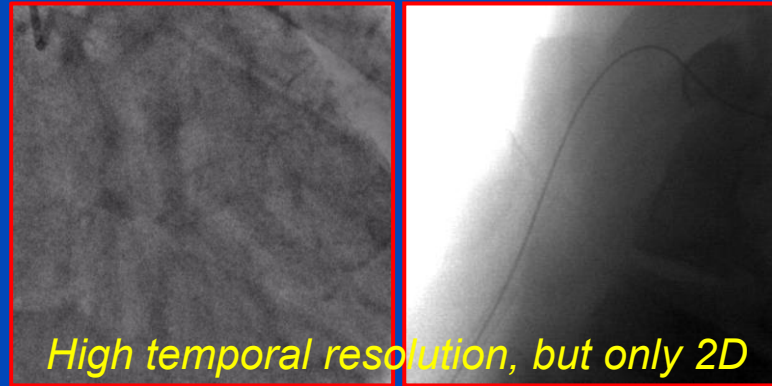
???

At 2D+T dose?

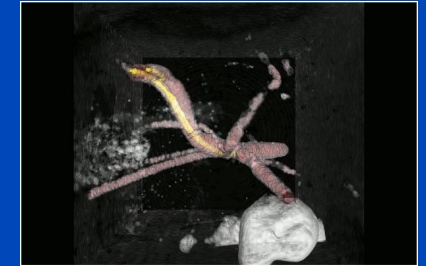
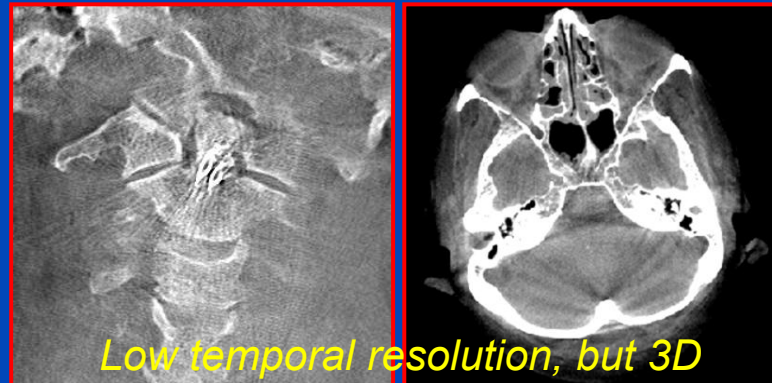


# Deep 3D+T Tomographic Fluoroscopy

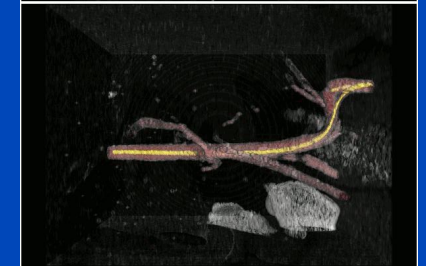
either 2D+T fluoroscopy



or 3D tomography

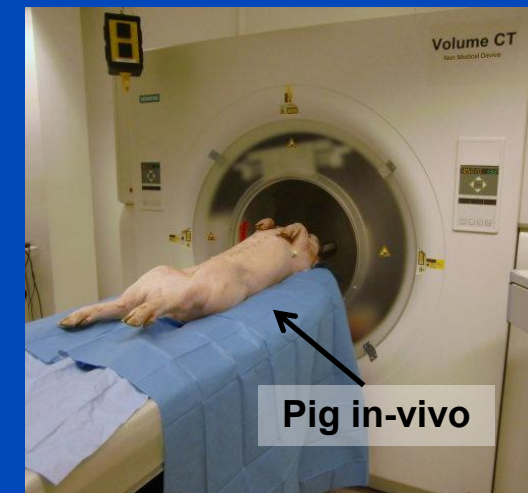
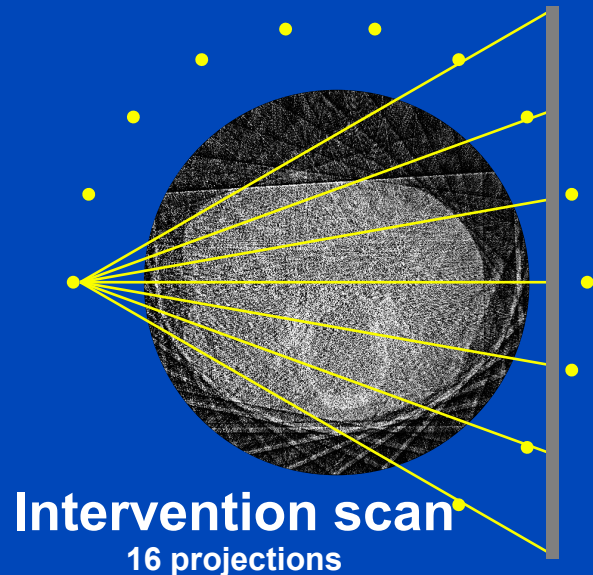
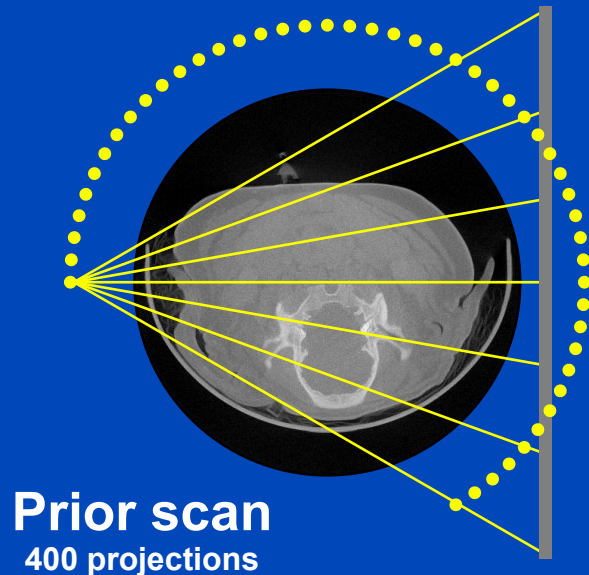


**3D+T  
tomographic  
fluoroscopy?  
At low dose?  
How???**



# How to Realize 3D+T Fluoroscopy

- Low dose by:
  - Low tube current
  - Very few projections (pulsed mode)
- Advantages of intervention guidance:
  - Repetitive scanning of the same body region: changes are **sparse**.
  - Interventional materials are fine structures (few voxels) of high contrast (metal).

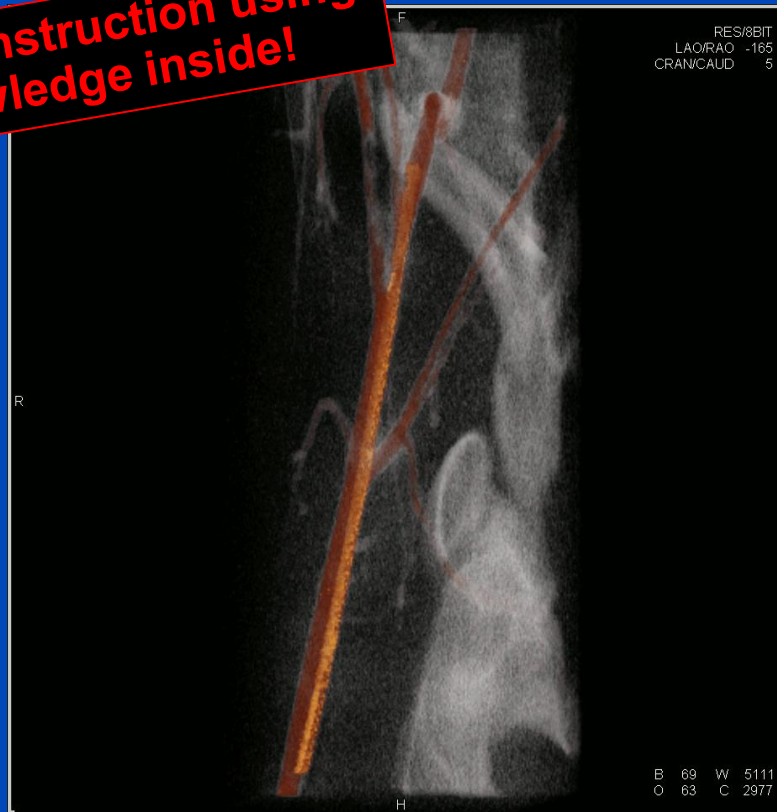


**Experimental setup**

# 3D+T Image Guidance at 2D+T Dose

## Stent Expansion in the Carotis of a Pig with Angio Roadmap Overlay

Iterative reconstruction using  
prior knowledge inside!

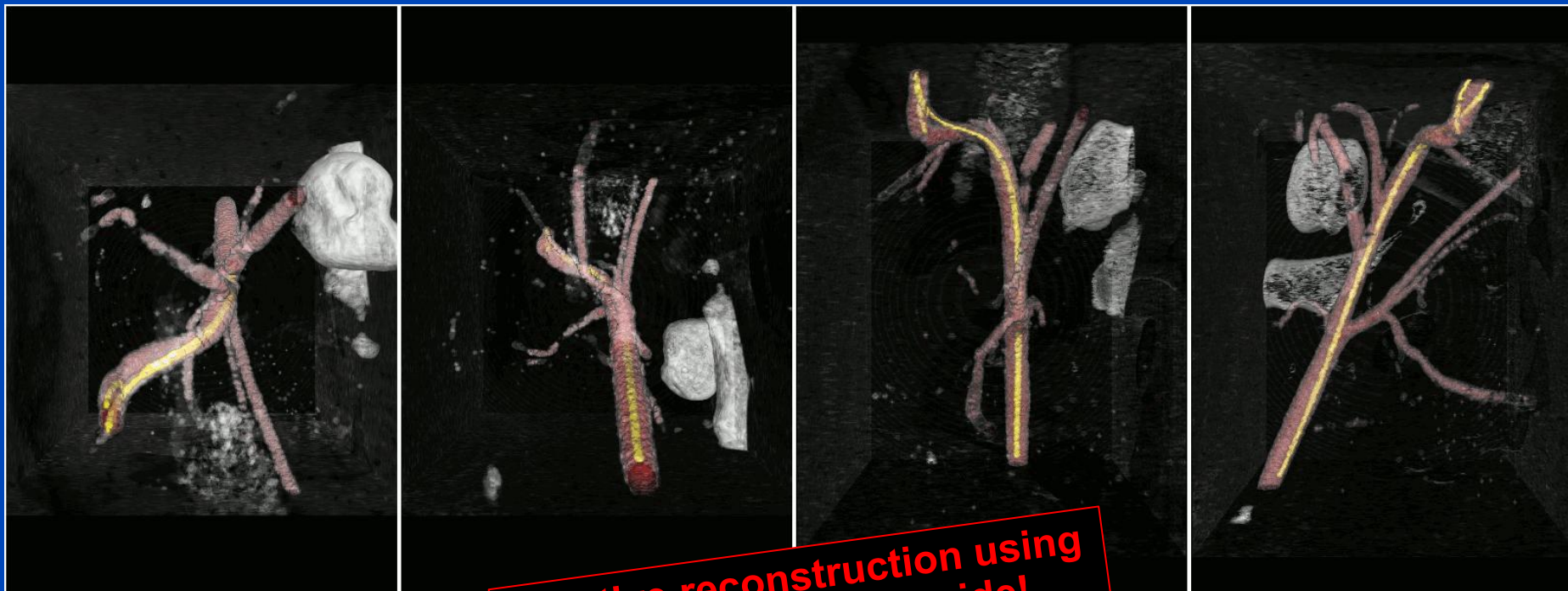


Dose of the yet unoptimized approach: 20 to 50  $\mu\text{Gy/s}$ .

This work was awarded the intervention award 2013 of the German Society of Neuroradiology (DGNR).  
This work was further selected as the Editor's Pick for the Medical Physics Scitation site.

# 3D+T Fluoroscopy at 2D+T Dose

Guide Wire in the Carotis of a Pig with Angio Roadmap Overlay



Iterative reconstruction using prior knowledge inside!

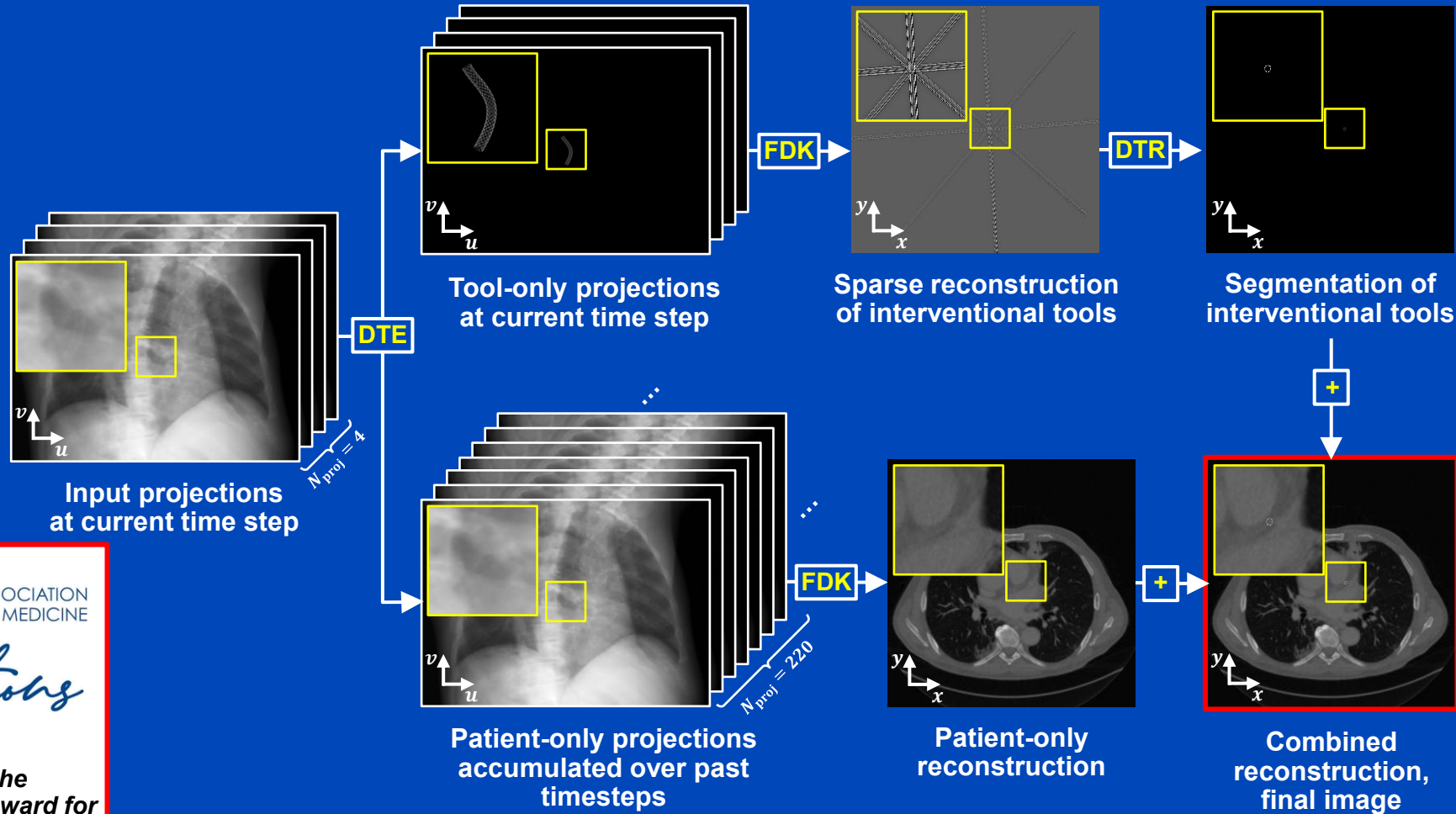
Dose of the yet unoptimized approach: 20 to 50  $\mu\text{Gy/s}$ .

Obviously, 16 projections are still too much.

Deep learning will help (5 years later)!

# Deep Learning-Based 3D+T Fluoroscopy

Deep Tool Extraction (DTE) + Feldkamp Recon (FDK) + Deep Tool Reconstruction (DTR)



 AMERICAN ASSOCIATION  
of PHYSICISTS IN MEDICINE

*Congratulations*

This paper received the  
Sylvia&Moses Greenfield Award for  
the best scientific paper on imaging  
in Medical Physics in 2021.

E. Eulig, J. Maier, M. Knaup, R. Bennett, K. Hörndler, A. Wang, and M. Kachelrieß. Deep learning-based reconstruction of interventional tools and devices from four x-ray projections for tomographic interventional guidance. *Med. Phys.* 48(10):5837-5850, October, 2021.

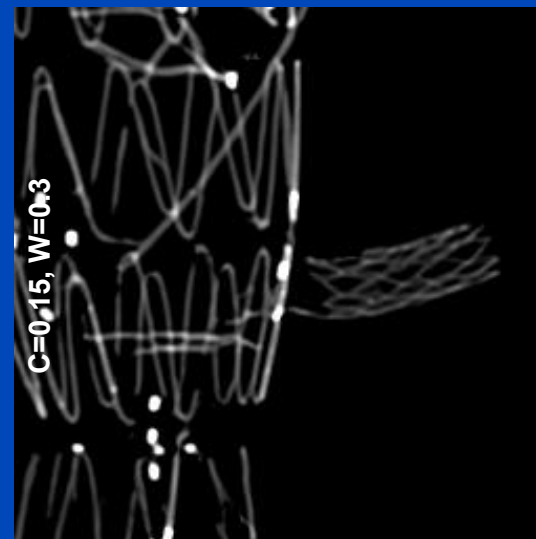
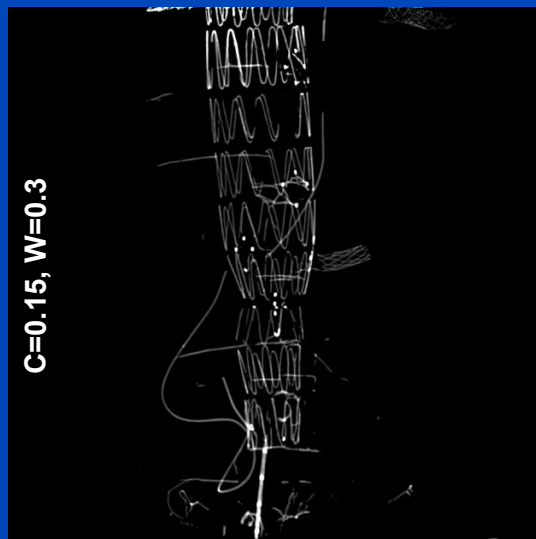
This paper received the Sylvia&Moses Greenfield Award for the best scientific paper on imaging in Medical Physics in 2021.

# DTE Example 1

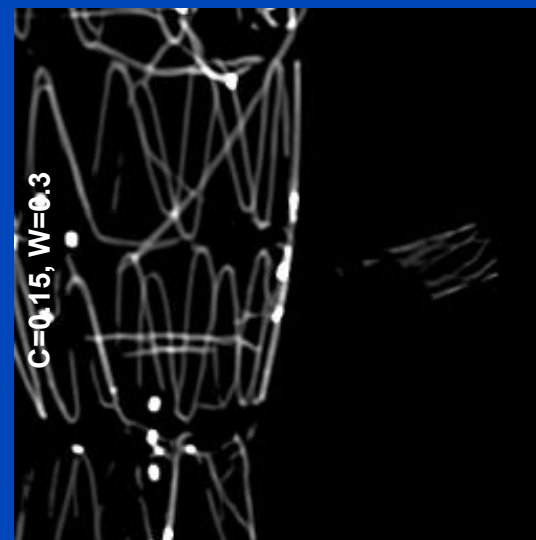
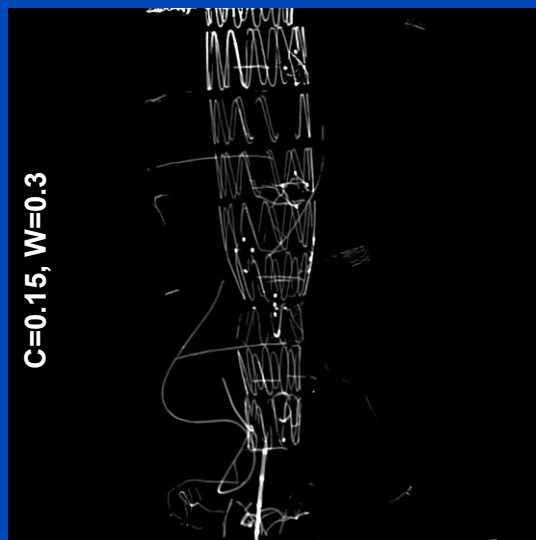


Input

Attention U-net



U-net

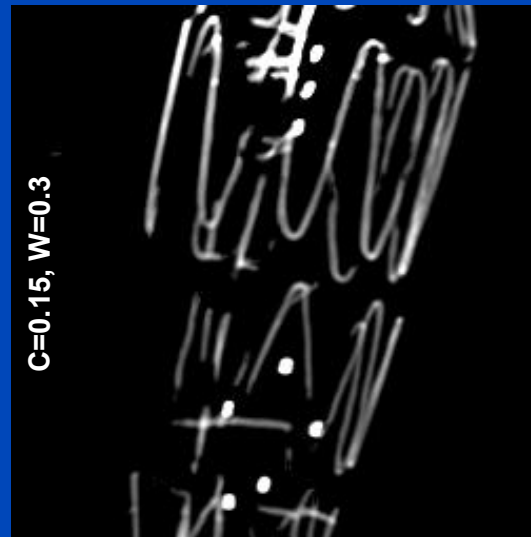


# DTE Example 2



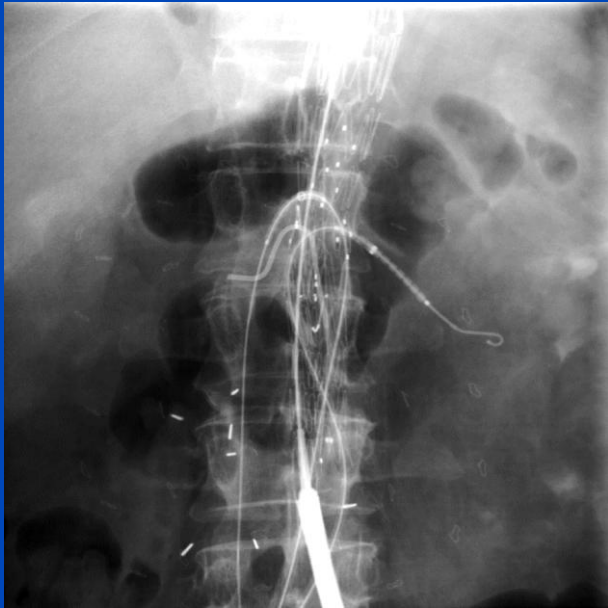
Input

Attention U-net

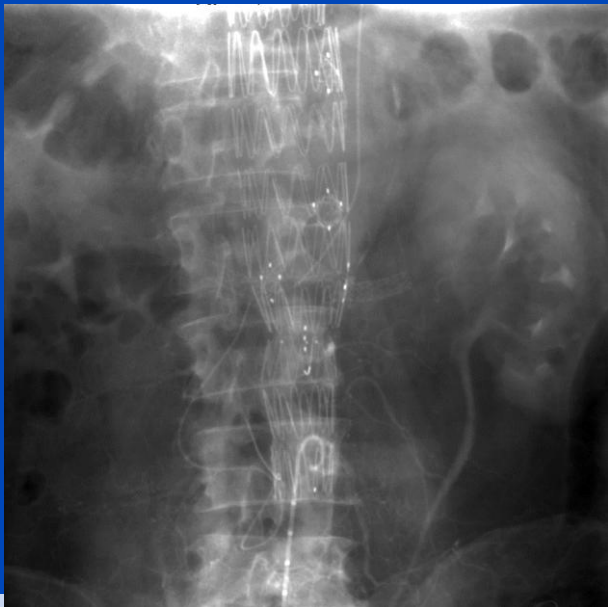


U-net

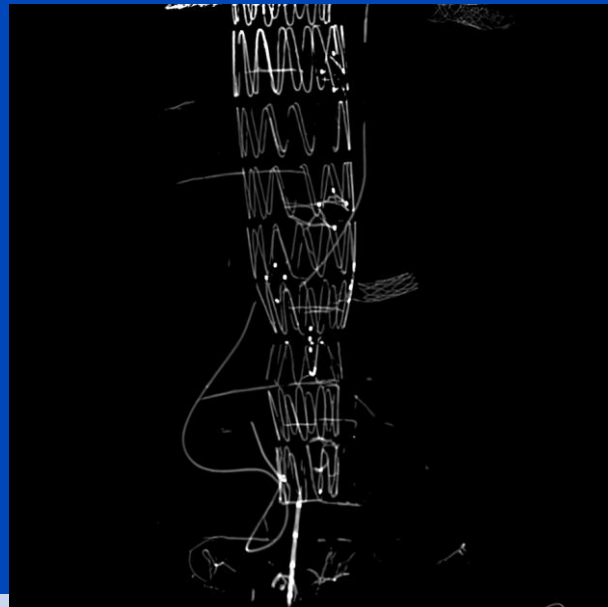




DTE



DTE

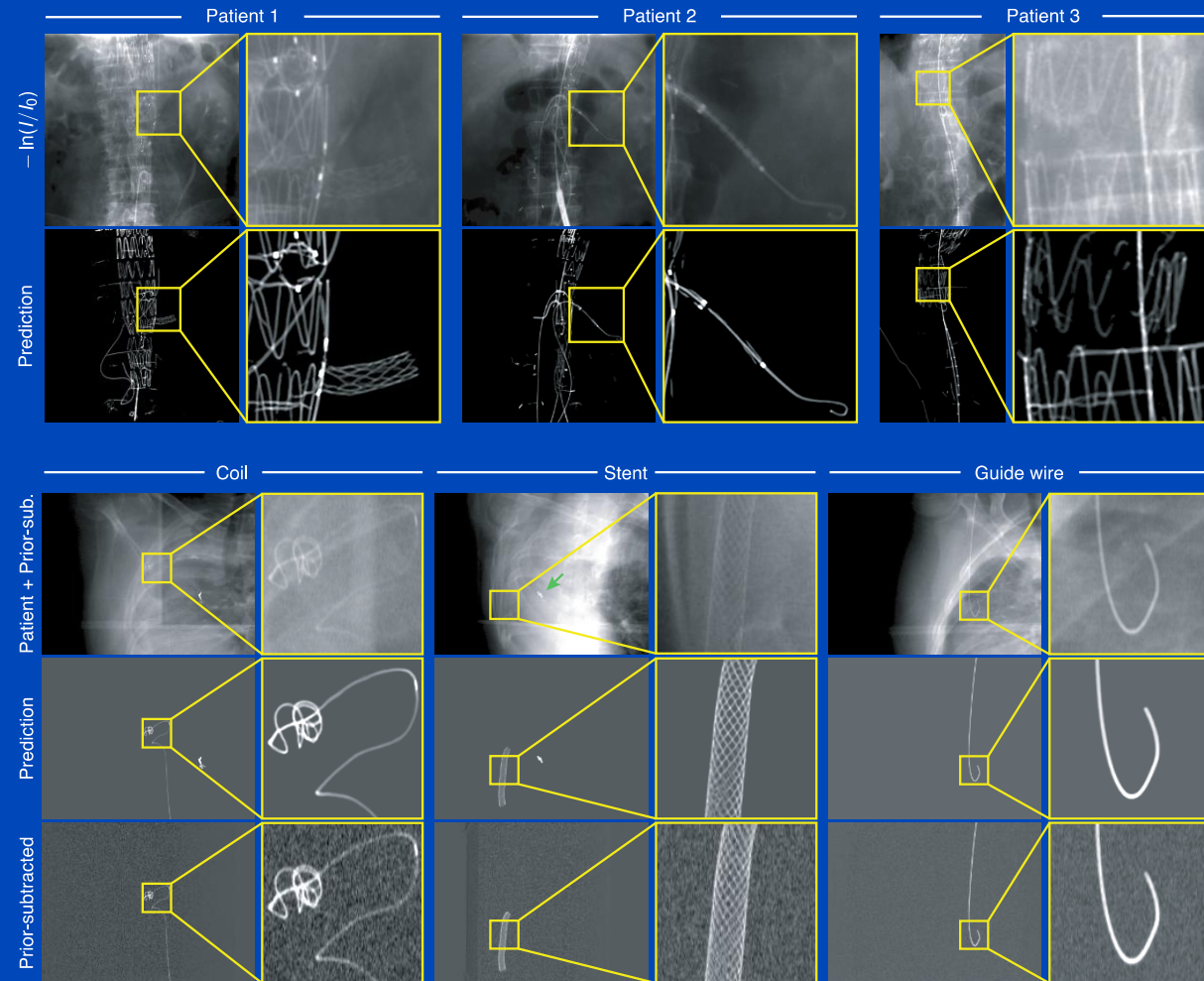


# More DTE Results

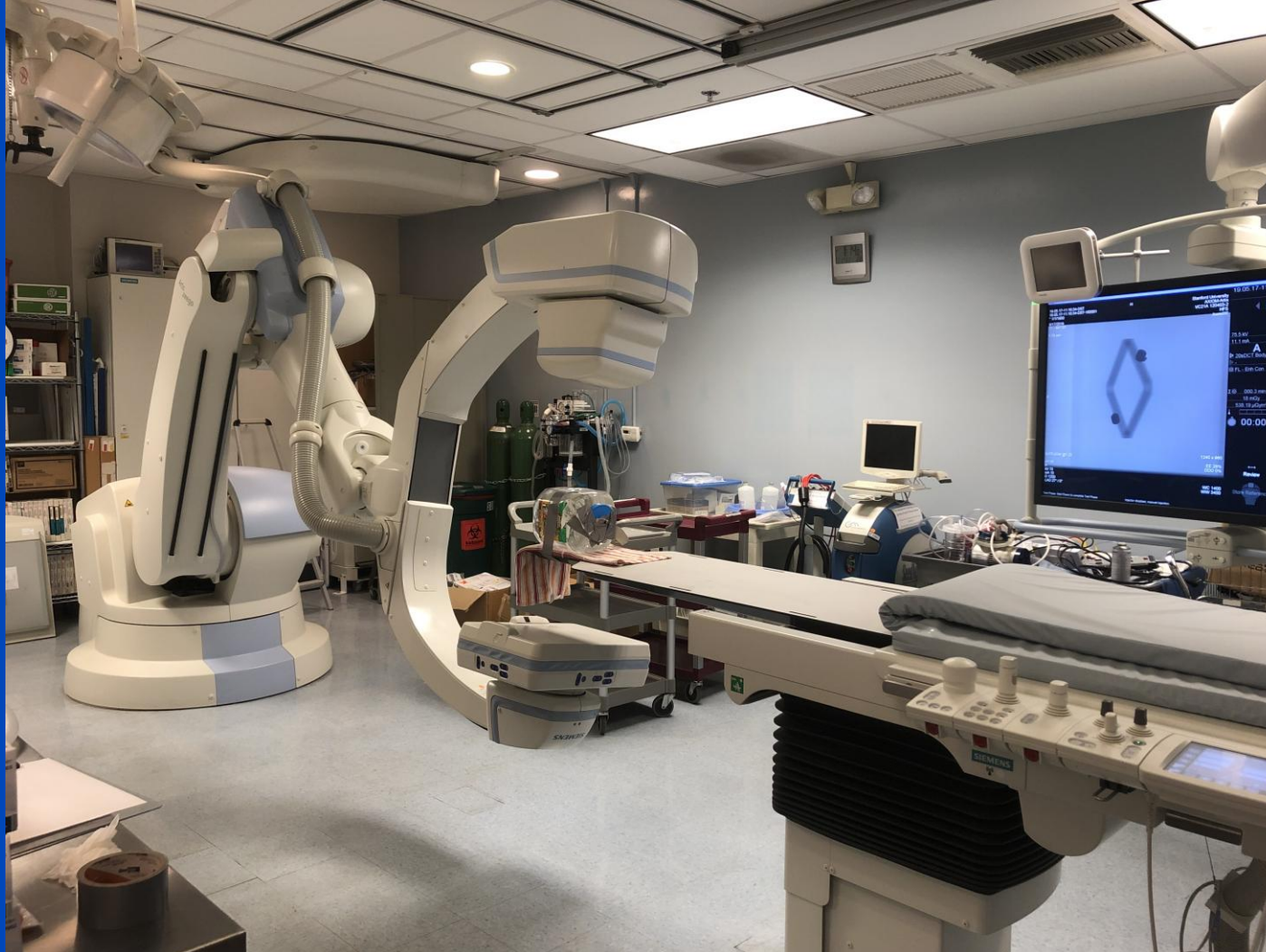
## Evaluate DTE on

- Fluoroscopy scans (top)
- Measurements of interventional tools and devices superimposed with patient CBCT (bottom)
- Good qualitative results on fluoroscopy data even though it differs from training data
- Good qualitative & quantitative results on superimposed data

Tool	MAPE [%]
Guide wires	$6.0 \pm 0.1$
Stents	$13.4 \pm 2.1$
Coils	$13.2 \pm 1.6$



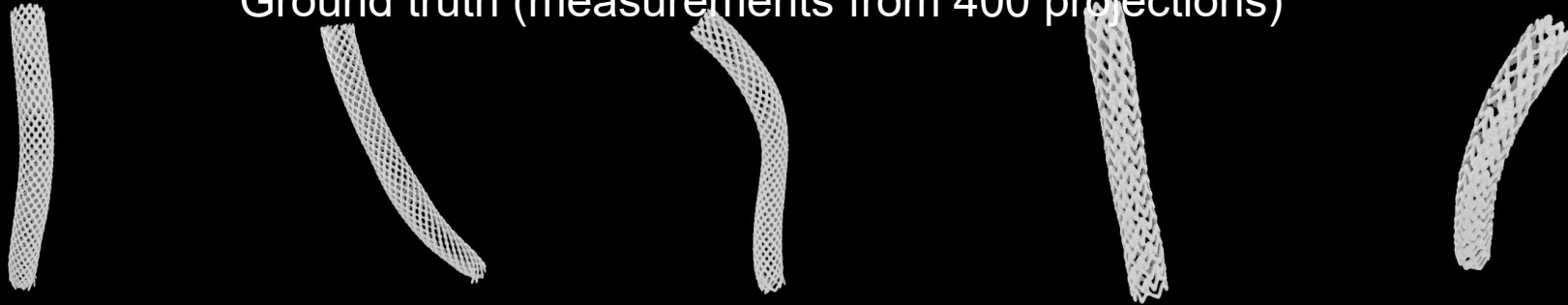
# Zeego @ Stanford University



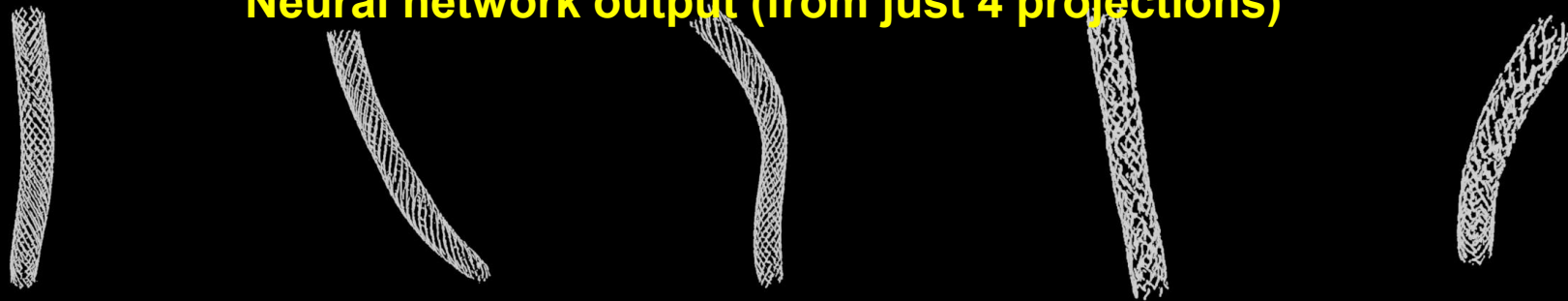
E. Eulig, J. Maier, M. Knaup, R. Bennett, K. Hörndler, A. Wang, and M. Kachelrieß. Deep learning-based reconstruction of interventional tools and devices from four x-ray projections for tomographic interventional guidance. *Med. Phys.* 48(10):5837-5850, October, 2021. *This paper received the Sylvia&Moses Greenfield Award for the best scientific paper on imaging in Medical Physics in 2021.*

# Zeego Measurements with Just 4 Projections

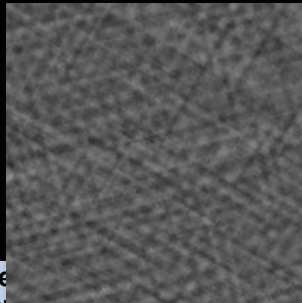
Ground truth (measurements from 400 projections)



Neural network output (from just 4 projections)

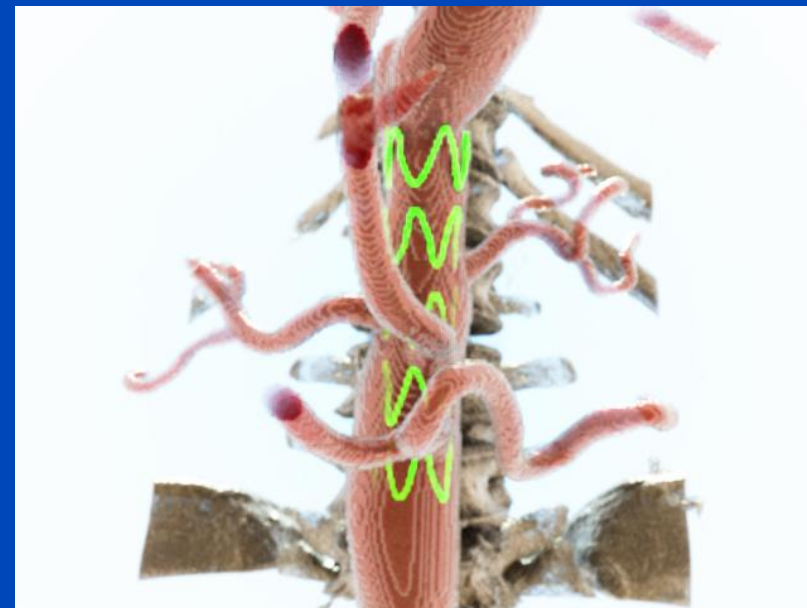
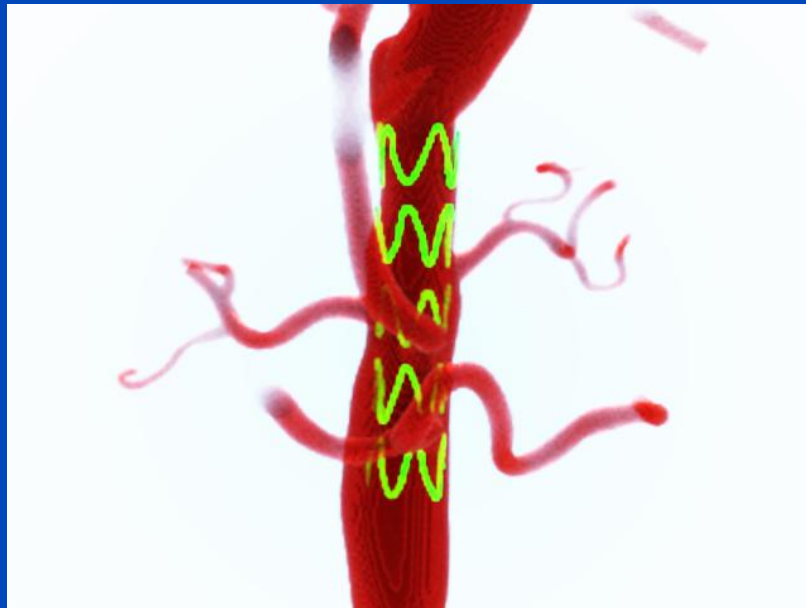


Loop through slices reconstructed from just 4 projections without AI:

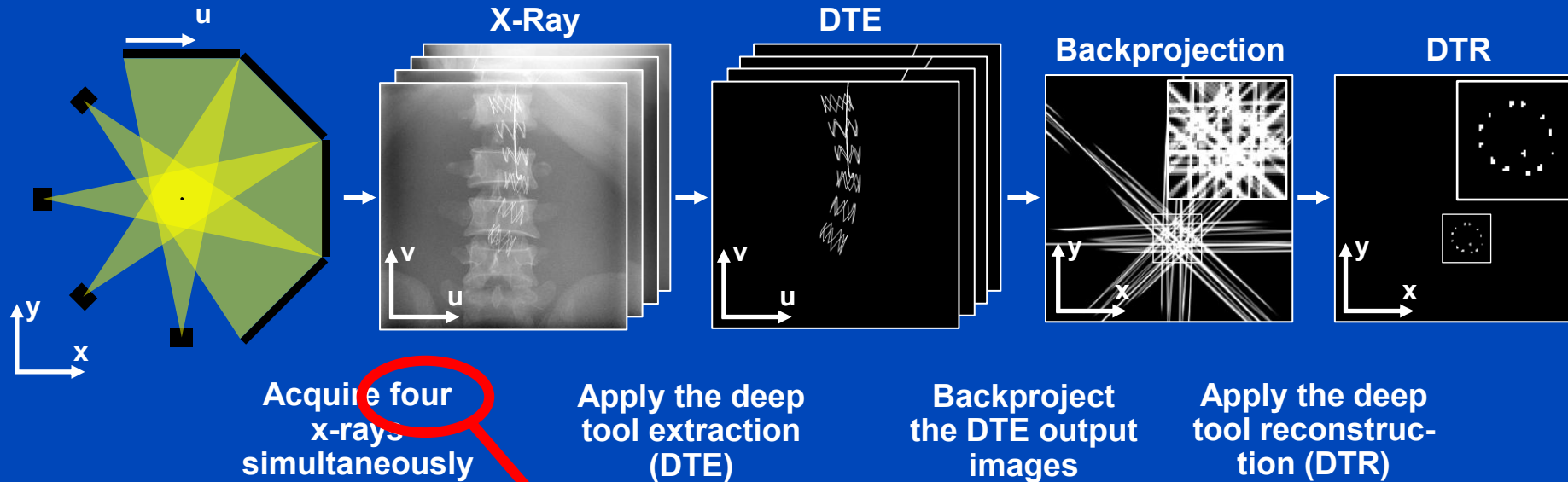


Stent examples:





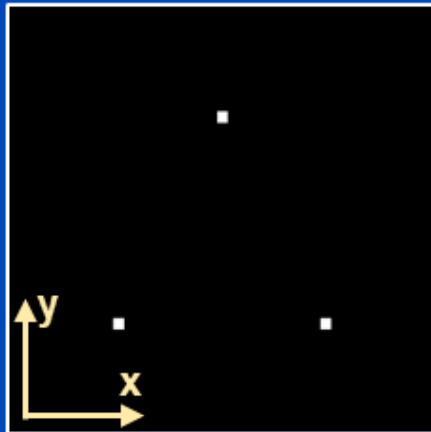
# So Far: Four-View Pipeline



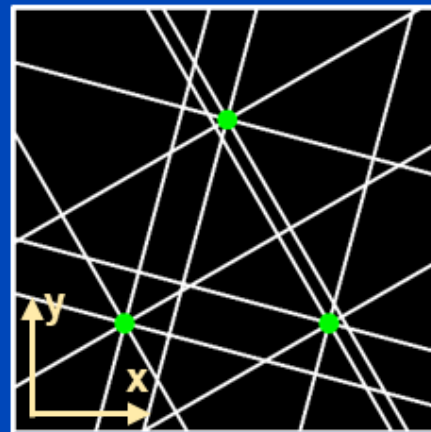
**Four is too many!  
Let's find out how to do it with two!**

# Challenge

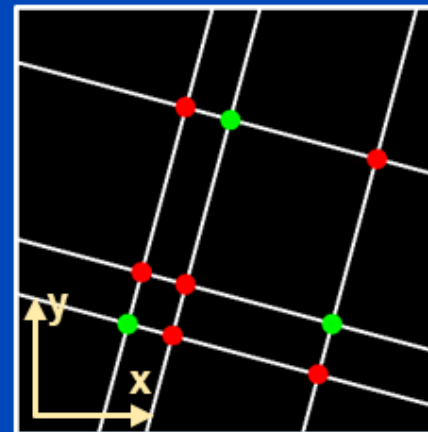
true  
object



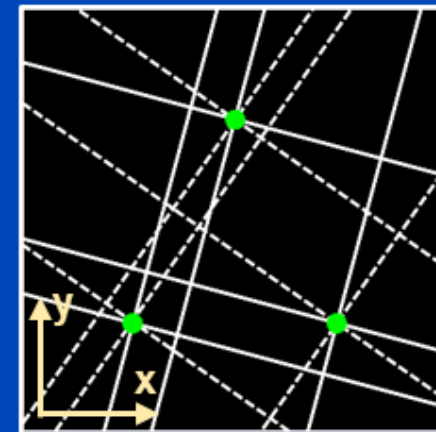
4 views  
1 time point



2 views  
1 time point

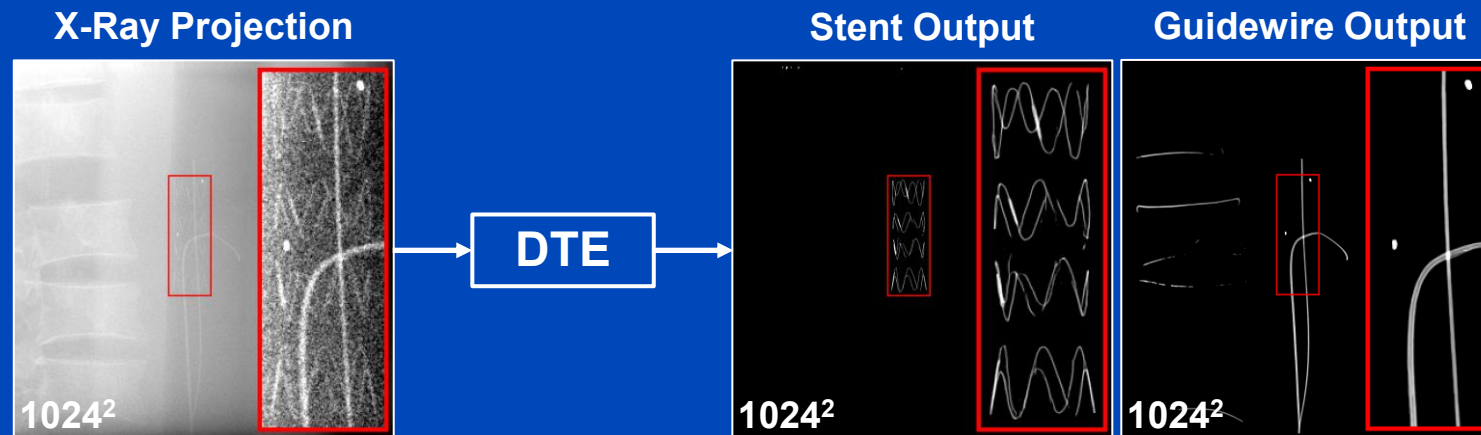


2 views  
2 time points

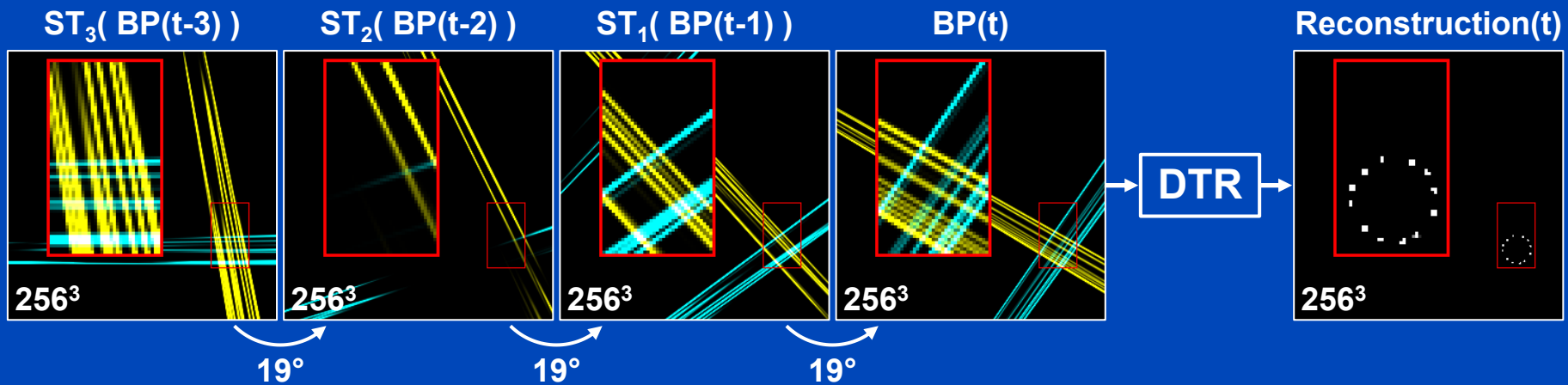
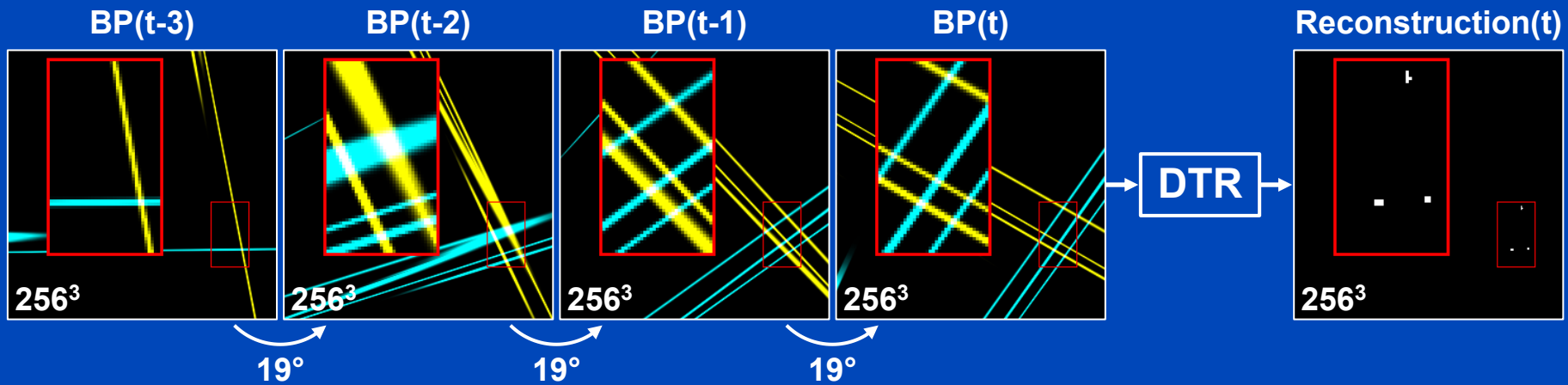




# Semantic DTE

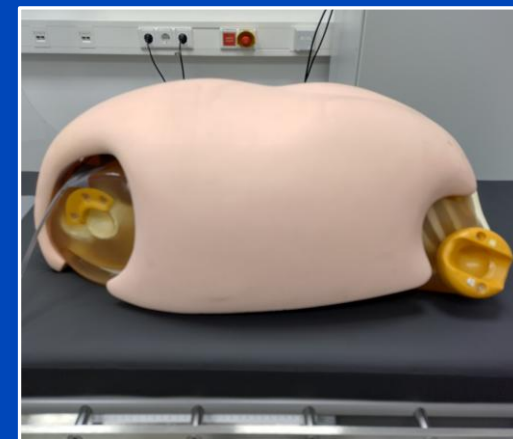


# Guidewire and Stent DTR



# Stop Motion Measurements

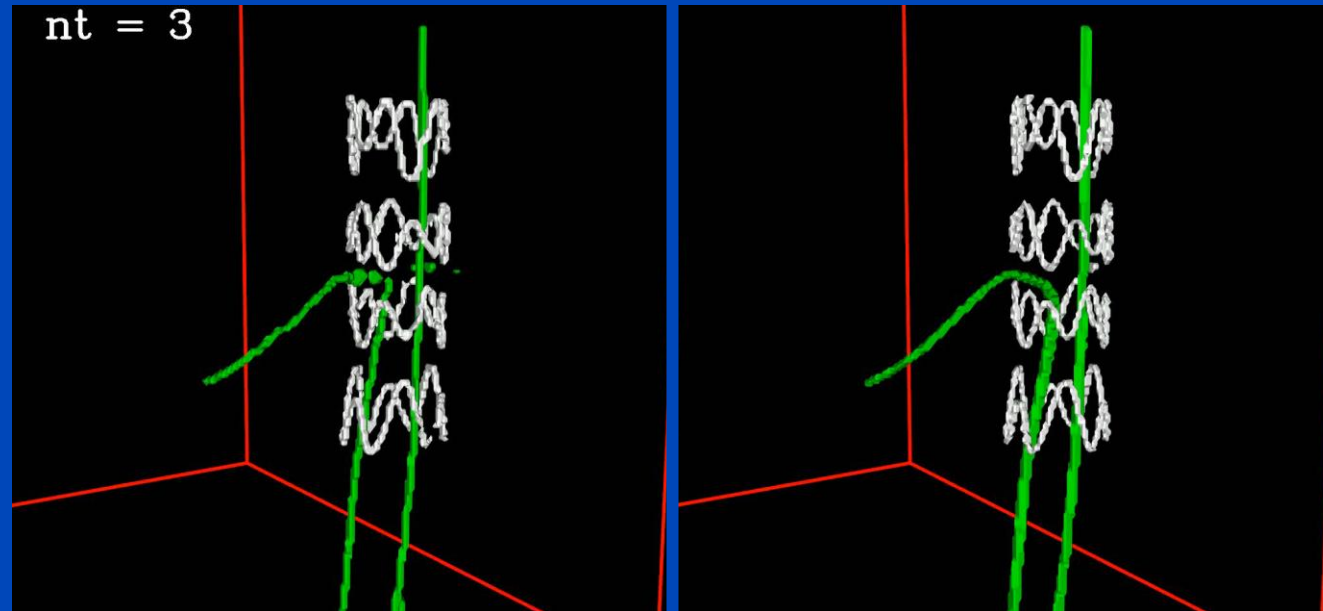
- Training: simulated data
- Results: stop motion measurements
- Flat detector
- For each time step  $t$ : 3D scan with fine angular sampling
- Choose two orthogonal projections from each 3D scan:
  - »  $t = 1$ :  $0^\circ, 90^\circ$
  - »  $t = 2$ :  $19^\circ, 109^\circ$
  - » ...
- Objects: anthropomorphic trunk phantom + extension + interventional material placed between phantom and extension
- Motion: sinusoidal motion of phantom in superior-inferior direction (mimicking respiratory motion) + pulling of guidewire
- Parameters used during stop-motion measurement:  
 $U = 100 \text{ kV}$ ,  $I = 30 \text{ mA}$ ,  $T_{\text{rot}} = 25 \text{ s}$ ,  $T_{\text{pulse}} = 20 \text{ ms}$
- Simulated parameters:  
 $U = 100 \text{ kV}$ ,  $I = 197 \text{ mA}$ ,  $T_{\text{rot}} = 3.8 \text{ s}$ ,  $T_{\text{pulse}} = 3 \text{ ms}$ ,  $\Delta t = 200 \text{ ms}$



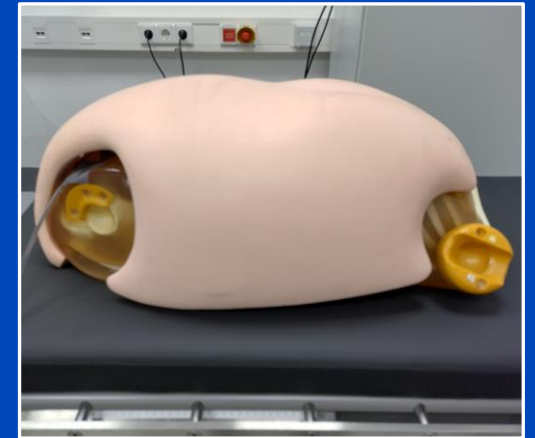
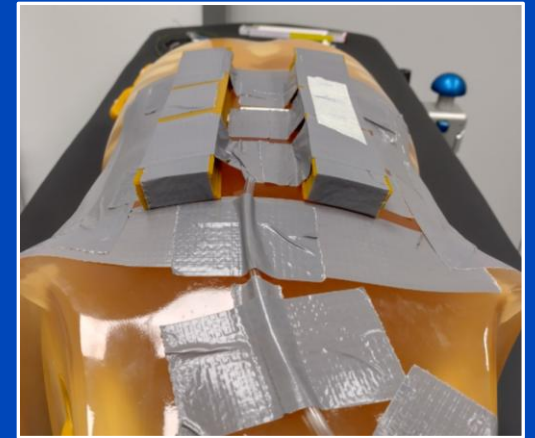
# Results

Reconstruction

Ground Truth



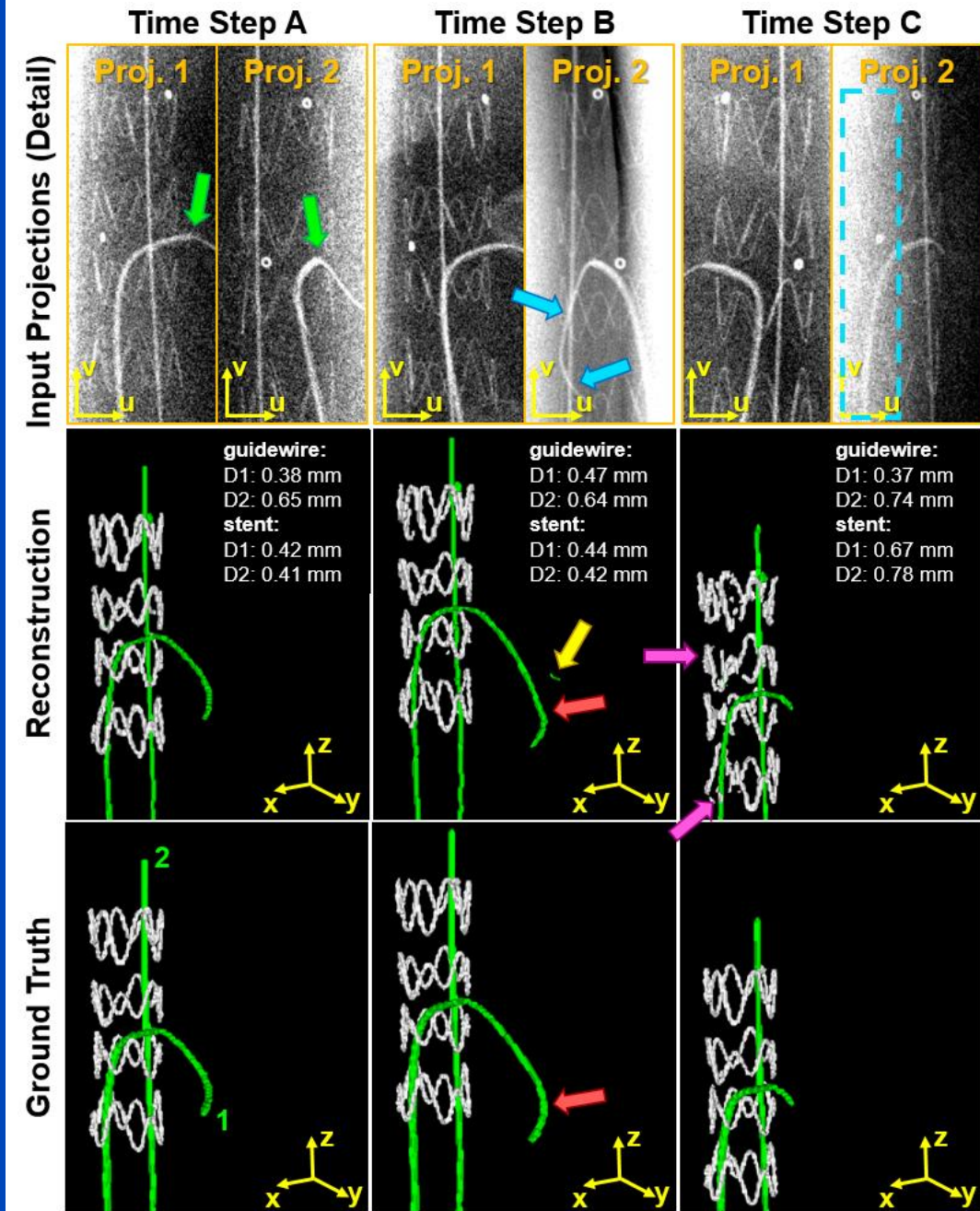
5 fps video of stop motion scan with 57 time steps.  
Sinusoidal 15 rpm motion of whole phantom with 11 mm amplitude.



Trunc phantom (with fat extension and interventional material) used for stop motion measurements.  
 $U = 100 \text{ kV}$ ,  $I = 30 \text{ mA}$ ,  $T_{\text{rot}} = 25 \text{ s}$ ,  $T_{\text{pulse}} = 20 \text{ ms}$

# Results

- **Figures of merit:**
  - $D_1$ : average distance between a skeleton of the ground truth and a skeleton of the reconstruction
  - $D_2$ : average distance between a skeleton of the reconstruction and a skeleton of the ground truth
- **Median over 57 time steps:**
  - **Guidewire:**  
 $D_1 = 0.37$  mm  
 $D_2 = 0.62$  mm
  - **Stent:**  
 $D_1 = 0.44$  mm  
 $D_2 = 0.44$  mm





# Thank You!

This presentation will soon be available at [www.dkfz.de/ct](http://www.dkfz.de/ct).

Job opportunities through DKFZ's international PhD or Postdoctoral Fellowship programs ([marc.kachelriess@dkfz.de](mailto:marc.kachelriess@dkfz.de)).

Parts of the reconstruction software were provided by RayConStruct<sup>®</sup> GmbH, Nürnberg, Germany.